Experimental modal validation of a semi-analytical method for assessing dynamic behaviour of flood gates

By

Martijn Helsdingen

[Blank page]

Experimental modal validation of a semi-analytical method for assessing dynamic behaviour of flood gates

Master Thesis CIE5060-09

By

Martijn Helsdingen

4383613

in partial fulfilment of the requirements for the degree of

Master of Science

in Hydraulic Engineering

at the Delft University of Technology

Faculty of Civil Engineering

Department of Hydraulic Engineering

Section Hydraulic Structures & Flood Risks

1st of July 2021

Thesis committee:	Dr. Ir. B. Hofland (Chairman)	TU Delft
	Dr. Ir. E. Lourens	TU Delft
	Ir. O. C. Tieleman,	TU Delft
	Ir. E. De Almeida	TU Delft

An electronic version of this thesis is available at http://repository.tudelft.nl/.

[Blank page]

Preface

In front of you lies the report that finalised my master Hydraulic Engineering at the Technical University of Delft. Three years ago, I started this journey, which will now be completed by means of the research described in this report.

I had the opportunity to investigate the validity of a newly developed semi-analytical model that predicts the dynamic behaviour of slender flood gates including an overhang. I was always fascinated by structures that enables the Dutch citizens to live in a safe and protected environment. Therefore, this topic was a perfect match for me. Thriving for a better future and putting my capabilities for the society to provide have led to the decision to start this topic.

During the execution of the experiments, I have learned a lot about approaching problems in a scientific manner. Furthermore, it taught me to break down problems into measurable schemes which on their turn lead to an answer to complex questions.

This research could not have been executed without the help of Orson Tieleman and Ermano de Almeida, who created this research line. Without them, I was not able to execute the experiments. I want to thank Orson in particular for his effort in guiding me throughout the master thesis' stages. Furthermore, a special thanks to Eliz-Mari Lourens should be noted for her help in topics that relate to her area of expertise. I also want to thank Bas Hofland for his effort to guide me through the stages for the experiments and for his expertise on this subject.

A special thanks goes out to my parents. They have always supported me to get the best out of myself and they have generated the opportunity to start an academic career at the Technical University of Delft.

Martijn Helsdingen

Delft, June 2021

Summary

The Netherlands has always been in a battle with surrounding water bodies and rivers crossing the country. One of the important water defence structures is the Afsluitdijk, which separates Lake IJssel with the Waddensea. Renovations of the discharge sluices led to new insights in the design wave forces on these flood gates. Since they have an overhang on top of them potentially large forces of standing waves are exerted on the structure. This has yet to be investigated.

A new semi-analytical model is developed to predict the dynamic response of slender gates in combination with an overhang, which are subjected to standing waves. Still little is known for these types of gates for this specific forcing type. The semi-analytical model is still in its development phase and must be validated on its performance. This thesis aims for validation of the modal calculations performed by the Semi-Analytical model for submerged gates, which include fluid structure interaction.

Experiments were executed to generate data that give insight in the modal shapes and natural frequencies of two different scaled models. The scaled models existed of a Solid Plate and a Reinforced Plate. The Reinforced Plate was equipped with two stiffeners. Both prototypes had a width of 80 cm and a height of 60 cm and where made of RVS304. The Solid Plate was designed to have most energy in its first mode, while the Reinforced Plate had its energy divided in the first three modes. The experiments took place in the flume of Stevinlab 2 at the faculty of Civil Engineering at the TU Delft. Three types of tests were performed:

- In-vacuo hammer tests were used for a dry modal analysis.
- Immersed hammer tests were used for a wet modal analysis, which gave insight in the wet modes of the plates. Different water levels were investigated: 0.3 m, 0.4 m, 0.5 m, 0.56 m and 0.6 m.
- Wave experiments were executed for further modal analysis in case of insufficient data of the wet hammer tests. These experiments used water levels of 0.56 m and 0.6 m.

In order to get reliable results on the experiments, a measurement device plan was designed. Starting point for the design was investigating the wet modes that were predicted by the SA model. Local nodes and anti-nodes were assigned to be potential locations for strain gauges and accelerometers. These spots were found using the semi-analytical predictions of the modal shapes. Together with synthetic time series of the SA model and the experiment modal analysis method Frequency Domain Decomposition (FDD) method, the performance of different measurement device plans was investigated. Eventually the Reinforced Plate was equipped with 25 strain gauges and 12 accelerometers, while the Solid Plate had 20 strain gauges and 12 accelerometers.

The experimental data obtained from the dry hammer, wet hammer and wave tests were subjected to the FDD algorithm in order to identify modes in the output data. The identified modes were compared to the predicted SA modes by means of a Modal Assurance Criterion (MAC). High MAC values indicate high correspondence between the predicted and identified modal shapes. Several types of analysis were done to get insight in the reliability of the SA

model. First, dry finite element method (FEM) modes were generated and used as input for the calculations. Secondly the identified dry FEM modes were used together with the identified natural frequencies in order to get insight in the accuracy of the SA models calculations. These set of modal shapes and natural frequencies is known as the adjusted set of dry FEM modes. It was found that for the Solid Plate all initial FEM modes correspond to the identified modes while for the Reinforced Plate several FEM modes did not show up in the data. The latter might have implied that a wrong set of input modes was used. The results of the SA model were compared to the experimental results in order to draft conclusions on the performance of the SA model in these situations. A last analysis was performed by means of using the dry modal shapes and frequencies that were found in the dry hammer experiments as input for the SA model.

The results of the analysis showed that the SA predictions of the Solid Plate had good correspondence with the experimental observations. The best results were found when the FEM generated modes were used as input of the model. The first three modes were all found with consistently high MAC values, except for a water level of 0.5 m. The relative averaged errors of the first three modes for the natural frequencies were also found to be very small, in the order of 2% - 6%. The Reinforced Plate showed a more scattered pattern. Not all modes were found for the water levels. Using a combination of strain gauges and accelerometers showed the identification of the first three modes, except for a water level of 0.56 m. The relative error of the natural frequencies turned out to be rather high. This led to analysing the data of the wave impacts as well. It was thought that these forces were larger and therefore the response of the Reinforced Plate was measured more easily. Water levels of 0.56 and 0.6 m identified all first three modes when the FEM modes were used as input. The best results for this plate were obtained by using an adjusted set of dry FEM modes as input. The averaged relative error of the first three modes for the natural frequencies was determined to be respectively 12.6% and 6.6%.

The above results had to be taken with some possible measurement mistakes. First, the accelerometers for the Reinforced Plate showed large angles of inclination, up to 18º which might indicate that accelerometers got loose from the plate. Furthermore, it was observed that the Reinforced Plate had large damping, which might have caused uncertainty in the measurements for the dry and wet modal experiments. Perhaps the most important flaw that was discovered was the loosening of the stiffeners and the U-frame from the front of the Reinforced Plate. The glue was not applied properly on the front plate, which caused the gate components to fail. Therefor no assurance could be given regarding the fully clamped boundary conditions. It was not observed when this happened as it was discovered after the experiments. This has influenced the modal characteristics of the Reinforced Plate, causing corrupt datasets.

The results and discussion conclude that the modes that play a large role in the response were detected for both the Solid and Reinforced plates. The modal shapes were predicted correctly by the semi-analytical model for both plates. Natural frequencies matched perfectly for the Solid Plate, while the Reinforced Plate showed larger errors. Due to the complexity of the semi-analytical calculations and potential experimental mistakes, it is advices to redo the experiments

for the Reinforced Plate and more complex plate geometries. Furthermore the assurance for the fully clamped boundary conditions leads to more reliable results.

Table of content

List of Abbreviations

Abbreviation	Full name
DMA	*Dry Modal Analysis*
DOF	*Degree of Freedom*
EMA	*Experimental Modal Analysis*
EOM	*Equation of Motion*
FDD	*Frequency Domain Decomposition*
FEM	*Finite Element Method*
FRF	*Frequency Response Function*
FSI	*Fluid Structure Interaction*
MAC	*Modal Assurance Criterion*
MDOF	*Multiple Degree of Freedom*
PP	*Peak Picking*
SA	*Semi-Analytical model (Tieleman et al, 2020)*
SDOF	*Single Degree of Freedom*
SVD	*Singular Value Decomposition*
WMA	*Wet Modal Analysis*

List of Symbols

Symbol	Description	Unit
A	*Area*	m^2
A_k	*Amplitude coefficient of plate mode*	-
$\alpha_{inclination}$	*Inclination angle of accelerometers*	*degree*
B_p^-	*First amplitude coefficient of fluid mode I*	-
B_p^+	*Second amplitude coefficient of fluid mode I*	-
β	*Expression for relation natural frequency*	-
c	*Damping coefficient*	*Ns/m*
C	*Damping matrix for MDOF system*	*Ns/m*
C_r^+	*Amplitude coefficient fluid mode II*	-
C_{uu}	*Correlation matrix of inputs*	-
C_{zz}	*Correlation matrix of response*	-
D_t^+	*Amplitude coefficient fluid mode III*	-
Δ	*Laplace equation*	-
E	*Matrix containing Eigenvectors of a system*	-
ε_{xx}	*Strain in x-direction*	-
ε_{zz}	*Strain in z-direction*	-
$\tilde{f}(\omega)$	*Forcing vector in frequency domain*	*N*
$f_{calibration}$	*Calibration factor for accelerometers*	ms^{-2}/V
$f_{inclination}$	*Correction factor for inclined accelerometers*	-
F	*Forcing vector*	*N*
G_{yy}	*Power Spectral Density of response displacements*	m^2/Hz
G_{xx}	*Power Spectral Density of input displacements*	m^2/Hz
$H(\omega)$	*Frequency Response Function*	*m/N*
$\tilde{H}(\omega)$	*Complex valued Frequency Response Function*	*m/N*

I	*Moment of Inertia*	mm^4
K	*Stiffness matrix*	*N/m*
k_w	*Added water stiffness*	*N/m*
k_{system}	*System stiffness*	*N/m*
L	*Length dimension*	*m.*
M	*Mass matrix*	*kg*
m_w	*Added water mass*	*kg*
m_{system}	*System mass*	*kg*
ω	*Frequency*	*Rad/s*
ω_n	*Natural frequency*	*Rad/s*
p	*Pressure*	*Pa*
$\hat{\phi}_i$	*Eigenvector corresponding to mode i*	-
Φ	*Eigenvector*	-
Φ_p^I	*Fluid mode of region I*	-
Φ_p^{II}	*Fluid mode of region II*	-
Φ_p^{III}	*Fluid mode of region III*	-
ρ	*Density*	kg/m^3
S_{zz}	*Power Spectral Density of modal coordinates*	m^2/Hz *or* $ms/^2/Hz$
S_{uu}	*Power Spectral Density of response*	m^2/Hz *or* $ms/^2/Hz$
Σ	*Matrix holding the singular values*	-
U	*Matrix holding the left singular vectors*	-
u_i	*Time series of modal coordinate i*	*mm*
V	*Voltage*	*V*
$\widetilde{w}(\omega)$	*Plate response in frequency domain*	*m*
W_k	*Plate mode*	-
$W(x)$	*Structural mode of the system*	*m*
$w(x,t)$	*Structural response of the system*	*m*

$X(\omega)$	*Response vector in the frequency domain of MDOF*	*m*
$\tilde{x}(\omega)$	*Response in frequency domain*	*m*
$\hat{x}_i$	*Eigenvector for mode i*	-
ξ	*Damping ratio*	-

1 Introduction

The Netherlands is a low-lying country that is part of the delta of several rivers, from which the Rhine and the Meuse are the most famous ones. Most economic wealth and inhabitants of the Netherlands are situated under sea level. To ensure a safety threshold, many hydraulic structures are built to prevent flooding. A large important flood defence structure is the Afsluitdijk. Its function is to regulate the water levels in lake IJssel to prevent flooding of the area around. In order to discharge the excess water from the river, several discharge sluices are installed in the dike as depicted in Figure 1. Furthermore, it creates a freshwater buffer and provides sufficient discharge into the Waddensea by means of the Stevin and Lorentz sluices.

Up to recent, these sluices were safe enough, but insights on wave induced dynamics changed the opinion about this safety. Since these sluices have a stiff concrete road over the chambers, standing wave pressure impulses may be amplified leading to an excessive increase of wave pressure on the gates. First studies show the importance of this force for the quantification of the safety threshold of the gates.

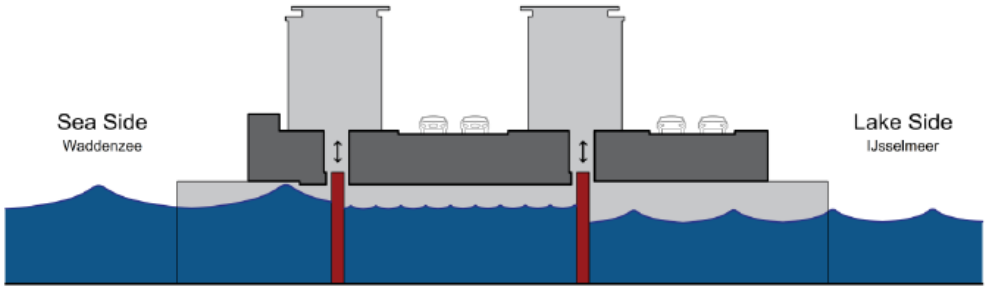

Figure 1 Side view of sluice chamber underneath the Afsluitdijk. The overhang on the sea side and lake side creates an extra pressure force acting on the gate in the case of standing waves (De Almeida, Hofland & Jonkman, 2019).

1.1 Current research

Design of hydraulic gates usually incorporates two important research lines. These are both part of the DynaHicS program funded by the Dutch government. These research lines are known to be the (1) external forcing part and (2) the resistance/internal forcing part of the gate. For both, a brief overview of current research will be given in §1.1.1 and §1.1.2.

1.1.1 Current research wave impacts

De Almeida, Hofland & Jonkman (2019) state that wave impacts may be classified into three categories: 1) breaking waves on vertical wall, 2) Overtopping waves on crest wall and 3) non-breaking standing waves on a vertical wall with an overhang. They conclude that from these three general wave impact categories the breaking waves are studied extensively. Bagnold (1939) was the first to come up with a method to find the wave impact by means of the pressure-impulse theory. In general Goda (1974) came up with a relation for calculating pressures of breaking waves on breakwaters. Cuomo et al. (2010) focused their research on vertical walls subjected to breaking waves. More recent studies from Chen et al. (2019) take the dynamic

characteristics of a gate into account as well. They come up with a method that relates the excitation frequency of a wave with that of the structure, which eventually leads to a Dynamic Amplification Factor (DAF) for the static wave impact force.

Still little is known about standing wave impacts on structures with an overhang. De Almeida et al. (2019) took the pressure impulse derived by Bagnold (1939) in combination with the pressure-impulse theory from Cooker & Peregrine (1995) to obtain a method for standing wave impacts on gates with an overhang. The study was validated using a stiff concrete structure, which potentially only approximates the real life situations were flexible gates are often implemented. Almeida & Hofland (2020) validated the new approach for low steepness standing wave impacts on gates that were equipped with an overhang. They excluded the dynamic behaviour of the gate and solely looked at the static forces due to standing wave impacts. By means of the pressure-impulse theory it was found that an additional force was acting on the structure in case of a rigid overhang. This force is best described as the impulsive load. Almeida et al (2020) also describe that the presence of air can influence the magnitude of this impulsive load. The latter was already found by Bredmose et al. (2009) and Hofland et al. (2010).

1.1.2 Current research gate dynamics

Tieleman et al. (2019) state that current design approaches are mainly based on simplified single degree of freedom (SDOF) systems. The dynamics of these SDOF system are usually predicted by means of a so-called DAF (Chen et al, 2019) which depends on the dynamic characteristics of the SDOF system. Static forces are multiplied with the DAF to obtain dynamic stresses in the structure. Kolkman & Jongeling (1996b) describe a method that looks like the DAF method of Chen et al (2019). They relate the factor of the dynamic over the static amplification comparing the excitation period by the Eigen period of the structure. They treat the structure as a SDOF mass-damp system. In real life most flood gates are acting in the 3D plane, which makes them a multiple degree of freedom (MDOF) system. Hattori & Tsujioka (1996) were the first to study the system as a MDOF and compared it to the outcomes from the SDOF systems. It was found that for breaking waves the results were closely related in terms of peak pressures. Tieleman et al (2019) state that SDOF models lack precision in case of designing 3D structures such as slender gates. They come up with a semi-analytical (SA) model based on research of Tsouvalas & Metrikine (2014). The semi-analytical model theoretically derives a solution method for a 3D deflection field of a slender structure. It makes use of modal decomposition and using boundary and interface conditions the fluid field on both sides of the gates is considered as well. Fluid structure interaction (FSI) follows from the interface conditions at the gate-fluid interface. Although more precise finite element method (FEM) packages are available, the semi-analytical model is usually preferred due to the significant reduction in computational costs. The semi-analytical model is expanded to situation where an overhang is present in the system (Tieleman, Hofland, Tsouvalas et al, 2020). The semi-analytical model of Tieleman et al. (2020) still must be validated since it incorporates some potentially crucial assumptions.

1.2 Problem statement

Concluding the above paragraph, one might identify a case which is still not available for dynamic gate design under wave loading, while examining the semi-analytical model of Tieleman et al. (2020):

It is still not known/verified whether the semi-analytical model holds for a gate geometry in combination with the presence of an overhang, entrapped air and fluid structure interaction, which is often the case for hydraulic structures in the Netherlands. The derived model is based on an analytical approach but is not tested nor validated. The model relies on assumptions that should be tested on their legitimacy.

The above statement shows that current research has a gap in terms of relevant knowledge for dynamic gate design. Although research is currently taking place, validation and improvement of the models should be examined.

1.3 Research questions

In order to manage the problem statements mentioned in §1.2, a main research question is drafted. Four sub-questions lead to the answer on the main research question. Important to notice is that the SA model relies on dry mode shapes and natural frequencies as input, which eventually lead to wet mode shapes and natural frequencies. From there the time series are obtained. Further explanation is given in Chapter 4.

Main research question:	Does the modal prediction of the semi-analytical model derived by Tieleman et al. (2020) hold for common designs such as discharge sluices in the Afsluitdijk?
Sub-question A)	Which method is suitable for finding natural frequencies and mode shapes for experimental data?
Sub-question B)	What is a suitable measurement device plan for measuring different modes correctly?
Sub-question C)	Does the semi-analytical model asses the right structural modes of the system in submerged state for two different gate designs?
Sub-question D)	Can the semi-analytical model be improved by using experimental data in the form of modal shapes and natural frequencies to represent the boundary conditions?

1.4 Research methodology

To validate and potentially improve the semi-analytical model scaled flume tests are carried out in order to create a dataset of deflections and strains of the model. This dataset is obtained via a measurement device plan containing strain gauges and accelerometers. The data from the flume tests should afterwards be translated to relevant dynamic data for validation and improvement of the semi-analytical model. This sequence can be captured in several steps that eventually lead to the desired result.

1.4.1 Experimental modal analysis algorithm

An experimental model analysis is performed for 2 specific reasons: 1) as an extra tool in the design of a measurement device plan and 2) obtain modes and natural frequencies of the scaled model during dynamic experiments in the wave flume. The experimental modal analysis is performed using Frequency Domain Decomposition (FDD). An acceleration or strain time series for every measurement point is used as input and the outputs are the different mode shapes and their corresponding natural frequencies. The implementation of the algorithm is validated by data obtained from the semi-analytical model while its output is again compared to the output of the semi-analytical model. The latter enables validation of the semi-analytical model for different circumstances.

1.4.2 Modal analysis tests

Hammer test in both dry and submerged conditions may give insight in the dynamic behaviour of the gate as well as the correctness of implementation of the experimental modal analysis. The Fluid Structure Interaction (FSI) can be investigated by comparing both hammer tests. It reveals all dynamic characteristic of the gate itself. These are the stiffness, damping, natural frequencies and mode (shapes), which give already some preliminary conclusions about the performance of the semi-analytical model.

1.4.3 Flume tests

Flume testing enables to subject the gate to scaled real life wave conditions and analyse the performance of the semi-analytical model by comparing the outcome of the tests with the prediction of the model. Different situations are investigated in terms of wave conditions. Using the displacement field of the gate enables to validate and/or improve the semi-analytical model. The displacement field is first translated to natural frequencies and their corresponding modes, which are compared to the output of the semi-analytical model afterwards.

1.4.4 Measurment devices

In the experiments different types of devices are used to obtain force fields, deflections field and incoming wave characteristics. A more detailed follow up is given in §5.1.2. An overview of the devices used in the experiments is given in Table 1. This thesis solely uses the results of the accelerometers and strain gauges. The remainder is used in for other research.

Device	Obtained data
Strain gauges	Strains that lead to a strain field of the scaled model
Accelerometers	Accelerations which lead to an acceleration field of the scaled model
Wave gauges	Measuring the incoming wave height
Pressure sensors	Measuring the pressure impulse of the incoming standing wave
Load cells	Measuring the total load acting on the gate

Table 1 Measurement devices used during the experiments

1.5 Thesis outline

This report starts with a relevant literature study about structural mechanics and dynamics, experimental modal analysis and the semi-analytical model (Tieleman et al, 2020) is elaborated. The structural mechanics partly addresses the stress-strain relation and the method for rewriting displacements of a plate to strains. This serves as a basis for incorporating the strain field and rewriting it to a displacement field. The structural dynamics part will focus on the conventional solution techniques for Multiple Degree of Freedom systems (MDOF) such as modal analysis and frequency response functions. Furthermore, it reveals the approach to obtain standard dynamic characteristics such as damping and the natural frequency. The chapter on Experimental Modal Analysis (Ch. 3) gives an insight in the different techniques and will then elaborated the most important ones for this research. The Frequency Domain Decomposition (FDD) and the Peak Picking (PP) technique are treated in detail. The literature research is finalized with a chapter about the SA model of Tieleman et al. (2020). This chapter is accompanied with Appendix C which treats the SA mode of Tieleman et al. (2019) which does not include an overhang.

Following on the literature study a chapter on the experimental tests is given, Ch. 5. This chapter treats the scaled models that are used, the location and flume of the experiments, as well as the different experiments that are executed. Important part of this chapter is about the processing and correction of the data.

The start of the analysis takes place in chapters 6 and 7. Chapter 6 treats the optimal measurement set up for both scaled models. First research is executed on the modal parameters of both plates. This is done by using the results from the SA model of Tieleman et al. (2020). The natural frequencies and mode shapes are then used for further research on the measurement plan. The approach and results are a follow up, after which the chapter is finalized with some mode plots that are generated with the measurement device plan.

Chapter 7 describes the modal analysis that is executed to quantify the modes that are identified with the modes that were predicted by the SA model. The detected modes and natural frequencies in the dry situations are also used as input for the SA model and will be analysed accordingly. The influence of the boundary conditions is on its turn modelled by using the exact dry modes, as found in the dry modal analysis for both plates, as input for the SA model. The

modal parameters that are predicted are then compared to the identified ones in order to draw conclusions.

The report is finalized by the chapters 8 and 9 with the discussion, results and recommendations.

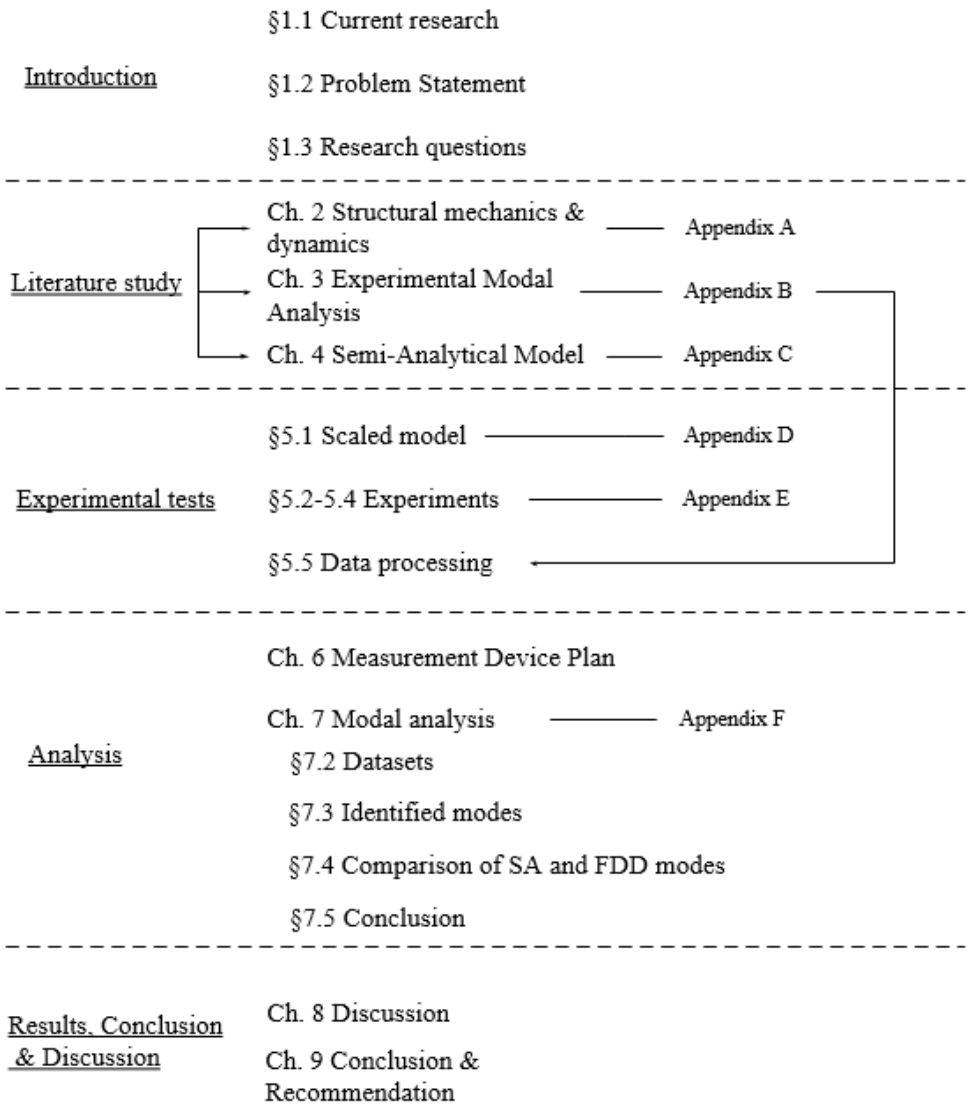

Figure 2 Thesis outline

2 Theory – Structural Mechanics and Dynamics

To describe the outcome of the experiments in a correct order, a literature study is performed. The literature that is examined serves as a base for the master thesis and the analyses that are performed. This chapter goes into the relevant available literature of Wave impacts, Structural dynamics, Experimental modal analysis and basic structural relations for rewriting measured data to useful data for analysing the experiments.

2.1 Structural mechanics

In order to obtain useful data from the different measurement devices several structural mechanical as well as dynamic relations should be used. This paragraph gives an overview of the fundamental relations that are crucial for this research.

2.1.1 Kinematical relation in structural mechanics – strains to delfections

In order to obtain the right deflections following from a strain field, one should apply the kinematical relationship that links both quantities to each other. Equation 1 gives a representation of the relationship between the strains and the displacements (Hartsuijker, 2001).

$$\varepsilon_x = a * \frac{d^2w}{dx^2} \tag{1}$$

Rewriting this relation gives an expression for the deflection with a strain field as input.

$$w(x) = \frac{1}{a}\iint \varepsilon(x)dxdx + Ax + B \tag{2}$$

In which A and B are integration constants that can be solved using the boundary conditions and a is the distance from the centre of mass towards the locations of the measured strain. The strain field ε(x) follows from measurements and can be numerically integrated.

2.1.2 Stress in a plate

Stresses in a steel plate can be either directly obtained from strains or a deflection field. These are directly linked to each other according to relation 3. Equations 3 and 4 give handholds for translating both quantities to a stress field (Hartsuijker, 2001).

$$\kappa = -\frac{d^2w}{dx^2} \rightarrow M = EI\kappa \rightarrow \sigma = \frac{M * a}{I} \tag{3}$$

$$N = EA\varepsilon \rightarrow \sigma = \frac{N}{A} \tag{4}$$

2.2 Structural Dynamics

This paragraph serves as a basis of structural dynamics quantities and theories such as Fluid Structure Interaction (FSI), Damping and Natural Frequencies of a system. It gives a first insight into these phenomena and for the natural frequencies it gives a handheld for the expected outcomes of the future analysis.

2.2.1 Fluid structure interaction

Several important dynamic characteristics are adjusted in a situation where the gate is submerged in water. The natural frequency of a system depends on both the mass and the stiffness. Due to added water effects the stiffness might significantly increase and therefore the influence on the natural frequency is significantly. Kolkman & Jongeling (1996a) approach the added water mass as a problem in which the moving gate is displacing and accelerating water particles that are in contact with it. Kolkman & Jongeling (1996a) use the velocity potential of every water particle and assume that the Laplace equation holds (eq. 5)

$$\Delta\Phi = 0 \qquad 5$$

They reason that the velocities of the water particles, and therefore the velocity potential, are in phase with the velocity of the gate. This leads to an expression of the exerted pressure from the water particle on the gate, which after integration over the total area of the gate gives the added water mass.

$$p = \rho \frac{d\Phi}{dt} + C \qquad 6$$

Wendel (in Kolkman & Jongeling, 1996a) solved the added water mass problem for different structure geometries and different direction of vibration. For a two-dimensional rectangle he comes up with an equation of the added water mass as given in eq. *7*.

$$m_w = 1.51 * \rho\pi a^2 L \qquad 7$$

In which:

ρ = Density of the fluid
a = Height of the structure under water
L = Width of the structure.

2.2.2 System damping

Damping of a system can be obtained via multiple methods, either via the time or frequency domain. Experimental research executed in this master thesis allows the following relevant methods:

1. Dimensionless damping ratio obtained from the time series of the structure.

2. Damping obtained from the width of the peaks of the singular values in the frequency domain(Brincker, Ventura, & Andersen, 2001).

The damping can be obtained from peaks in the displacement time series. Using the amplitudes (u_i) of certain locations on the gate and the measured decay (u_{i+n}) one can obtain the damping of the system (Little & Mann, 2019).

$$\zeta = \frac{\delta}{\sqrt{(2\pi)^2 + \delta^2}}; \quad \delta = \frac{1}{n}\ln\left(\frac{u_i}{u_{i+n}}\right) \tag{8}$$

2.2.3 Natural frequency of a dynamic system

In case of a simple Single Degree of Freedom System (SDOF), a mass-spring system, one can compute the natural frequency of the SDOF using equation *9* (Metrikine, n.d.). The natural frequency of the system determines to a great extend the dynamic behaviour of the structure that is subjected to a dynamic force with a certain period.

$$\omega_n = \sqrt{\frac{k_{system} + \sum k_w}{m_{system} + \sum m_w}} \tag{9}$$

In which:

k_{system} = Total stiffness of the system
k_w = Added water stiffness
m_{system} = Total mass of the system
m_w = Added water mass.

In case of a Multiple Degree of Freedom System the system contains more natural frequencies corresponding to the number of degree of freedoms. Performing an Eigenvalue analysis of the multiple equations of motion lead to a set of frequencies that belong to the system(Spijkers, Vrouwenvelder, & Klaver, 2005).

2.3 Dynamics of Systems

This paragraph serves as an insight in the different solutions techniques available in the field of structural dynamics. The most well-known techniques for both a MDOF and Continuous systems are treated. The MDOF strategies will be discussed in more detail since they serve as the basis for the Experimental Modal Analysis strategies which are the core of the data analyses in order to find the validity of the semi-analytical model. The paragraph will kick off with some basic fluid structure interaction and on how to obtain damping from a dataset.

2.3.1 Continuous systems

In case of a continuously distributed system, it is classified as a continuous model. These models can be either of one-dimensional nature or may consist of more dimensions. A one-dimensional problem is defined by the fact that deflections depend, besides time, on one space

coordinate only (personal communication, 2019). Spijkers et al. (2005) describe a derivation of the equations of motion (EOM) by means of a balance of forces in sections of the system. The list below gives an overview of relevant EOM's (Spijkers et al., 2005).

- Euler-Bernoulli Bending beam $$\rho A\frac{\partial^2 w}{\partial t^2} + EI\frac{\partial^4 w}{\partial x^4} = f(t)$$
- Beam on visco-elastic soil $$\rho A\frac{\partial^2 w}{\partial t^2} + \frac{\partial^2 w}{\partial x^2}\left(EI\frac{\partial^2 w}{\partial x^2}\right) + kw + c\frac{\partial w}{\partial t} = f(t)$$
- Bending plate (Tieleman et al, 2019) $$\rho\frac{\partial^2 w}{\partial t^2} + D\left[\frac{\partial^4 w}{\partial x^4} + \frac{\partial^4 w}{\partial x^2 \partial z^2} + \frac{\partial^4 w}{\partial z^4}\right] = f(t)$$

Using boundary conditions, the equations can be solved for a given geometry and situation.

When solving continuous systems often a modal analysis is used. This analysis states that the deflections of a system can be described as the multiplication of their modes with a certain amplitude which varies in time. In theory an infinite number of modes can exist in a structure, that must be summed to obtain a final result.

Spijkers et al. (2005) describe that for a continuous system one can separate the unknown displacement into a time and space dependent part, as given in equation *10*.

$$w(x,t) = \hat{x}(x)A(t) \qquad 10$$

In which $\hat{x}(x)$ is defined as the structural mode of the system and A(t) as a time related amplitude function. Multiplying both will eventually lead to a solution for the displacement in both the time and space domain. Spijkers et al. (2005) describe a general solution for the space domain of a Euler-Bernoulli bending beam, that can be obtained via solving the space dependent part of the solution (eq. *11*).

$$W(x) = Acosh(\beta x) + Bsinh(\beta x) + Ccos(\beta x) + Dsin(\beta x) \qquad 11$$

$$\beta^4 = \frac{\rho A\omega^2}{EI} \qquad 12$$

In which A, B, C and β can be found using the boundary conditions and D is found as a ratio of respectively A/D, B/D and C/D. Since β has infinite solutions, we also find that the corresponding normal modes has infinite solutions.

The time dependent part A(t) is in the form of an imaginary exponential function: $e^{i\omega t}$ or $\sin(\omega t)$.

2.3.2 Multiple Degree of Freedom systems

Continuous systems can be discretized in a grid with several degrees of freedom. These so called Multiple Degree of Freedom (MDOF) systems can be solved using different types of strategies. The relevant strategies are given in the coming paragraphs and are known to be:

1. Modal domain (Modal decomposition)
2. Frequency domain (Frequency Response Function)

2.3.3 Modal domain

Solution techniques that make use of modal decomposition are well suited for problems that comprise linear MDOF systems. The main idea is that the response of a system exists of a summation of different response shapes in time, that can be summed to obtain the total response of the system(Spijkers et al., 2005). This paragraph will first treat the definition of modes and how they can be obtained, after which the modal analysis solution technique is treated.

Modes

Spijkers et al. (2005) describe the method to obtain eigenvectors of a MDOF. The vectors can be obtained by performing an Eigenvalue problem of a MDOF equation of motion, neglecting the damping. This approach gives the natural frequencies and the corresponding Eigenvectors (equivalent for mode shape) of the system. Knowing the modes of a MDOF system is of great importance. Resonance may occur when loading frequencies are approaching the natural frequencies of a system. Insight in these natural frequencies is therefore good practice and should always be considered when designing dynamically loaded structures.

In case of a mode shape and natural frequency extraction from experimental data the Frequency Response Function provides an adequate approach (Schwarz & Richardson, 1999). This is treated in §2.3.4 and a graphical representation of the operational deflection shape extraction from the FRF plot is given in Figure 3. Schwarz & Richardson (1999) further describe a mode as the shape of the structure that dominantly vibrates when forcing the structure near the natural frequency of the mode.

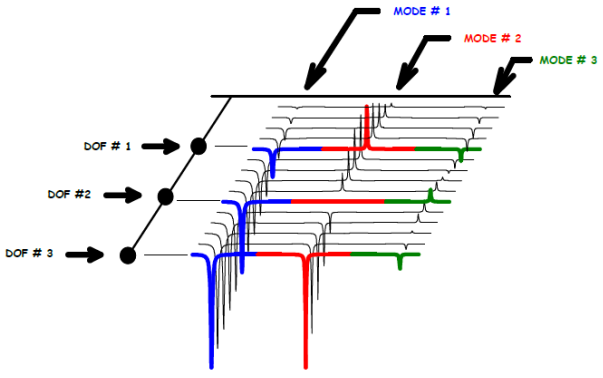

Figure 3 Graphical representation of operational mode shapes extracted from the response plotted in the frequency domain for different degrees of freedom(DOF 1, 2 and 3) of a structure (Avitabile, 2001)

Modal analysis

Spijkers et al. (2005) state that a vibration pattern can be decomposed into a set of individual vibration patterns that, when summed, lead to the total vibration pattern in time.

$$x(t) = \sum \hat{x} u_i(t) = \boldsymbol{E} u(t) \qquad 13$$

In which:

$\hat{x}$ = Mode shape / Eigenvector for mode i
$u_i(t)$ = Modal coordinate time series corresponding to mode i

This method assumes a displacement vector that can be split up into a matrix containing the Eigen vectors (modes) and a time dependent deflection vector. For this situation, the equation of motion looks as depicted in equation *14*.

$$E^T M E \underline{\ddot{u}} + E^T K E \underline{u} = E^T \underline{F}(t) \qquad 14$$

Spijkers et al. (2005) state that the system now only contains a set of fully uncoupled linear equations. This system can therefore be treated as different SDOF systems for which u(t) can be solved. Solving u(t) leads eventually to a solution of x(t). The vector u(t) refers to the modal coordinates of the system. Each solution of the equation is multiplied with the modes shape corresponding to that SDOF to enable a generation to nodal coordinates again.

For this method it is crucial to explore which modes are acting in a vibration pattern of the system. They serve as an input and influence the outcome directly. Schwarz & Richardson(1999) state that a mode is defined by a natural frequency, damping and a mode shape.

2.3.4 **Frequency Response Function**

Performing a Fourier Transformation on the time series for either deflections or forces results in a representation of the time series in the frequency domain.

$$M\ddot{x}(t) + C\dot{x}(t) + Kx(t) = F(t) \qquad 15$$

$$\tilde{f}(\omega) = \int_{-\infty}^{\infty} f(t) e^{-i\omega t} dt \qquad 16$$

$$\tilde{x}(\omega) = \int_{-\infty}^{\infty} x(t) e^{-i\omega t} dt \qquad 17$$

Substituting equations *15* and *16* into an equation of motion gives an steady state response, as depicted in equation *18* (Katsikadelis, 2020). This is a rather simple expression for the frequency dependent displacements (x(ω)).

$$\tilde{x}(\omega) = \frac{1}{-\omega^2 M + i\omega C + K}\tilde{f}(\omega) \qquad 18$$

The relation between the input (f(ω)) and the output (x(ω)) is called the Frequency Response Function(FRF) (Schwarz & Richardson, 1999). In case of a MDOF system the FRF matrix, denoted as H(ω) consists of entries that link the input at a certain point to the response of another point due to the impact at that particular point. For MDOF systems equation *18* can be rewritten to equation *19*.

$$X(\omega) = H(\omega)F(\omega) \qquad 19$$

The sizes of the vectors and matrices depend on the number of Degrees of Freedom (DOF). Every DOF resembles an entry in the complex displacement vector X(ω). DOF's can be linked to the locations of the measurements, called a spatial distribution (Schwarz & Richardson, 1999).

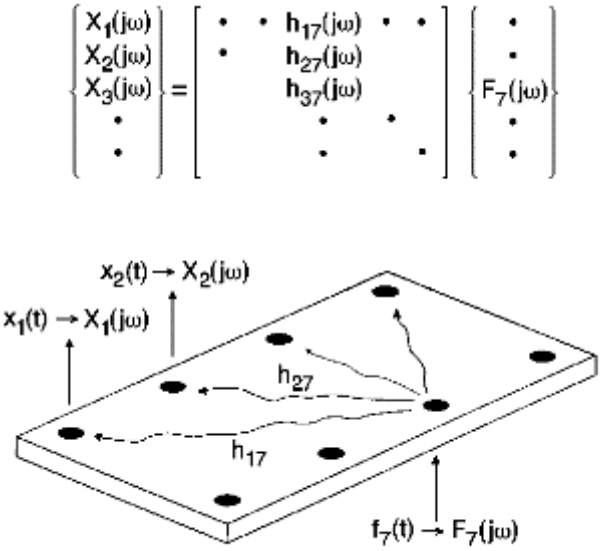

Figure 4 Representation on how to obtain a FRF via experiments (Schwarz & Richardson, 1999)

The response of different DOF's can easily be analysed by plotting the response of that DOF as a function of the frequency. Schwarz & Richardson(1999) describe that every peak in a spectral density plot of a DOF represents a mode. Local peaks refer to natural frequencies relating to the frequency observed at that peak.

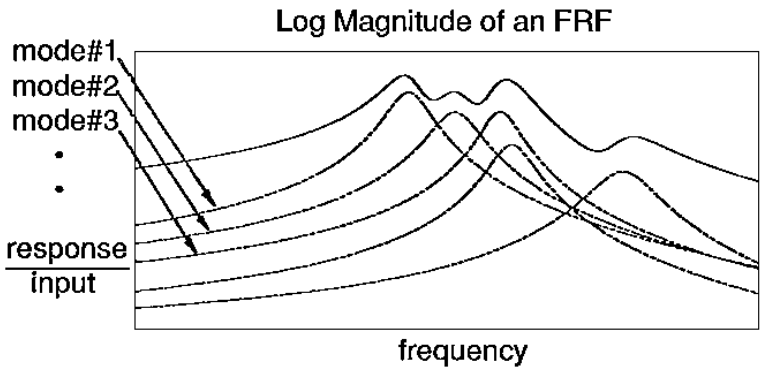

Figure 5 Plot of response as a function of frequency for different DOF's of a system, which represent the different modes of that system (Schwarz & Richardson, 1999)

3 Theory – Experimental Modal Analysis

The field of Experimental Modal Analysis (EMA) is developed to give insight in dynamic quantities such as mode shapes, natural frequencies, damping etc. of civil structures. EMA techniques provide an adequate solution. The inputs (forces) and outputs (response) are measured to find an optimal relationship between the two in the form of a Frequency Response Function. The different methods that are available will be treated in section 3.1, while two specific relevant methods are highlighted and treated in more depth in 3.2 and 3.3. The experiment executed in this thesis contain only data from the response of the structure, the Peak Picking method and Frequency Domain Decomposition are therefore relevant for this thesis and highlighted.

3.1 Different methods of Experimental Modal Analysis

Experimental modal analysis techniques can be subdivided into two main groups:

1. Input – output methods
2. Output only methods

For both groups it holds that there are methods that can be analysed in the time or frequency domain.

Maia & Silva (2001) describe several Input-Output methods. The list below gives an overview of the different EMA using Inputs and Outputs in the time domain. The overview is purely informational and will not be used in the remainder of this thesis.

- ARMA model;
- Complex exponential model;
- Least squares complex exponential;
- Polyreference complex exponential;
- Ibrahim time domain method;

Cunha & Caetano (2006) elaborate that input-Output methods in the frequency domain are mainly based on the Frequency Response Function. They state that depending on the number of degree of freedoms extra actions should be carried out to obtain a proper fit of the measured FRF and the theoretical FRF. Furthermore, SDOF system often do not need an extra analysis and can be fitted directly. According to Cunha & Caetano (2006) MDOF systems need different methods for the fit between the theoretical and measured FRF to hold for a large range of frequencies. They describe the rational fraction polynomial (RFP), complex exponential frequency domain (CEFD) and the Polyreference frequency domain (PRFD).

Besides the Input-Output methods some output only modal analysis methods are developed as well. The huge advantage of these methods is that one only needs to measure the response of a structure whereas the input is assumed to be an excitation of a zero-mean Gaussian white noise(Cunha & Caetano, 2006). They can be divided into two groups in which the solution is either based in the time or frequency domain. The frequency domain methods are all relying on the fact that a response time series is translated to the frequency domain, after which the spectral

density is calculated, as can be observed from Figure 6(Cunha & Caetano, 2006). From this point several methods with each their own reasoning use these spectral densities as an input to calculate the modal parameters. Ewins (1984) and Ranieri & Fabbrocino (2014) state that the most basic method is the Peak Picking (PP) method, which is elaborated in §3.2. This method was later improved by means of a singular value decomposition (SVD) of the Power Spectral Density (PSD) functions, which is known as the Frequency Domain Decomposition (§3.3) from Brincker, Zhang & Andersen (2001). Figure 6 gives an overview of both the time and frequency-based techniques.

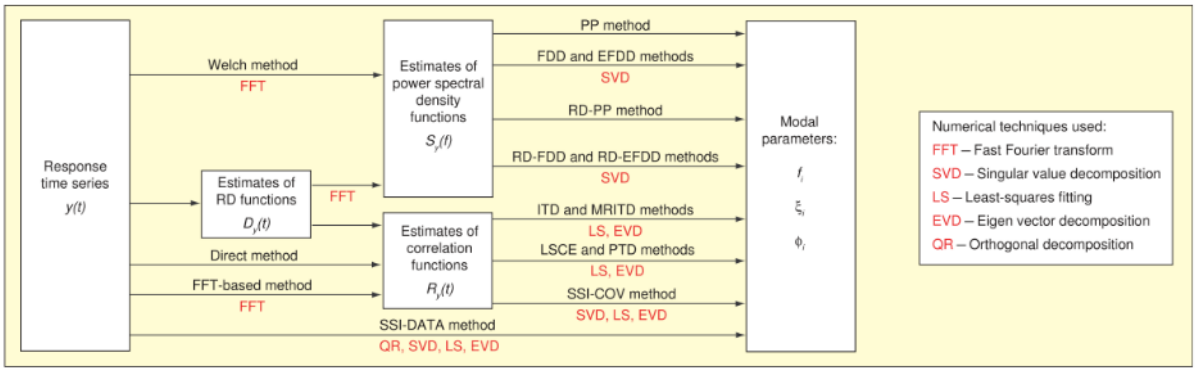

Figure 6 An overview of Output-only modal identification methods. The scheme is divided into two parts: 1) Methods for translating a time series into the desired power spectral density or correlation functions and 2) methods that generate modal parameters.(Cunha & Caetano, 2006)

3.2 Output only Frequency domain method – Peak Picking

Ranieri & Fabbrocino (2014) state that perhaps the most general output-only method in the field of Experimental Modal Analysis is the Peak Picking method (PP). Felber (1993) elaborates methods for extracting natural frequencies and mode shapes using this method. The reader is referred to his dissertation for a detailed elaboration of the method. Naderpour & Fakharian (2016) state that the PP assumes, as all the other output-only EMA's, an input of Gaussian white-noise. They state that the method is based on the characteristic of the FRF that peaks in this plot are observed near natural frequencies. Also, when the force is assumed to be a Gaussian white noise input, the FFT of the data at a sensor location can be taken as an equivalent of the FRF of the data at that location.

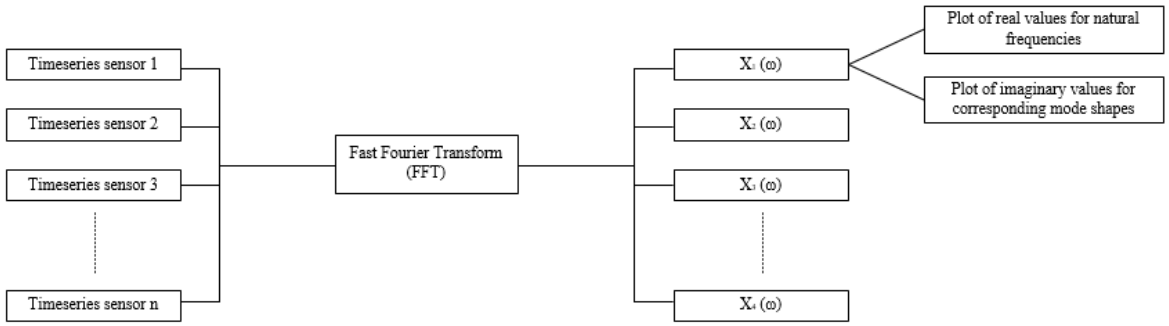

Figure 7 Peak Picking Method route for obtaining the natural frequencies from the real part of the FFT and the mode shapes from the imaginary part of the FFT.

The FRF of a system also holds information on the mode shapes. Zimmerman et al (2008) give a method for retrieving operational shapes by means of the PP method. Avitabile (2001) states that the FRF is a complex valued matrix from which the real values denote the natural frequencies, and the complex values can be used for the mode shape. He reasons that for every frequency that holds a peak in the FRF plot of the real values, the corresponding imaginary values give the amplitude of the mode shape of a particular sensor. This is best visualized in Figure 8 from Avitabile (2001).

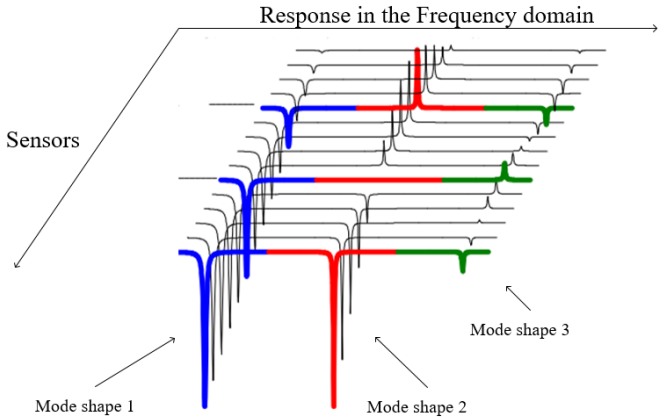

Figure 8 Visualization from Avitabile (2001) on how to retrieve the mode shapes from the imaginary part of the FRF plot of all sensors.

3.3 Output only Frequency domain method – Frequency Domain Decomposition

The PP method was improved by Brincker, Zhang, et al. (2001) by means of performing a SVD on the PSD of the decomposed SDOF systems. This method is the Frequency Domain Decomposition(FDD). Brincker, Zhang, et al. (2001) state that using this method may overcome some major drawbacks of the Peak Picking method:

1. Natural frequencies can only be detected for well separated frequencies, this problem is tackled when using the Frequency Domain Decomposition.
2. Damping estimation is highly uncertain in the Peak Picking method.
3. The frequency resolution limits the estimates in the PP method

Important to note is that this method also assumes a Gaussian white noise as input for the forcing. Results are exact when this input is achieved but might deviate when this is not the case. Nevertheless Brincker, Zhang, et al. (2001) state that the results are more precise using this method compared to the Peak Picking method in the situation when the assumptions are not met.

Using the PP method one can detect solely well separated modes directly from the PSD easily. Brincker, Zhang, et al. (2001) comes with a method to tackle this drawback. The FDD method first generates a spectral density matrix by performing a FFT on the measured data. It provides an additional step to be able to extract closely neighbouring natural frequencies as well. Furthermore, the FDD approach gives mode shapes as a result, where the PP method solely

gives the operational deflection shapes. In the FDD method the spectral density matrix is subjected to a singular value decomposition (SVD) which decomposes the spectral matrix into several auto spectral matrices. These auto spectral matrices each represent a SDOF of the system. The problem is translated from a MDOF to a set of SDOF's. The singular values of the SVD analysis are stored in the auto spectral matrices and the peaks in their plot represent the natural frequencies (see Figure 9). The left singular vectors, which is a residue of the SVD, hold information about the mode shapes. Left singular values belonging to a peak singular value give the corresponding mode shape of the system.

3.3.1 Theoretical basis and Assumptions

Brincker, Zhang, et al. (2001) describe a theoretical basis of the FDD which is elaborated in this paragraph. They start with the fact that a PSD of the measured output can be written as in equation *20*.

$$G_{yy}(j\omega) = \bar{H}(j\omega)G_{xx}(j\omega)H(j\omega)^H \qquad 20$$

In which:

G_{yy} = PSD of the response
G_{xx} = PSD of the inputs
H^H = Transpose of the FRF matrix.
$\overline{H}$ = Complex conjugate of the FRF matrix

This equation can be simplified by taking the assumptions listed below. Assuming a forcing that consists of Gaussian white noise with a zero mean the PSD of the input can be simplified to a matrix which is proportional to the identity matrix. This can be done since the forcing inputs are Gaussian white noise. Assuming this will lead to equation *21* which states that the PSD of the outputs is proportional to the matrix $H(j\omega)H(j\omega)^H$. This directly implies that the PSD of the response holds the modal parameters.

$$\tilde{G}_{yy} \propto \tilde{H}(j\omega)\tilde{H}(j\omega)^H \qquad 21$$

Assumptions:

1. Input forces should cover a broad spectrum of frequencies.
2. Input forces should act over the total surface area.
3. Input forces should be uncorrelated.
4. Input forces should have similar amplitudes.

Decomposition of the Response PSD

The general idea is to decompose the PSD of the response into several spectral densities that each belong to a SDOF using a SVD. The starting points of this decomposition lies in the correlation of two vectors. Brincker & Zhang (2009) and the master thesis of Ogno (2013) describe a method for the decomposition of the spectral matrix using a uncorrelated input. This

is elaborated in equations *22 – 26*. The correlation matrix C_{uu} is rewritten to a Power Spectral Density matrix using the relations below. Using the modal coordinates $\mathbf{u}(t) = \mathbf{\Phi z}(t)$ this leads to a relation as given in eq. *22 - 24*.

$$\boldsymbol{C}_{uu}(\tau) = E\{\boldsymbol{u}(t)\boldsymbol{u}(t-\tau)^T\} \quad 22$$

$$\rightarrow \boldsymbol{C}_{uu}(\tau) = \Phi E\{\boldsymbol{z}(t)\boldsymbol{z}(t-\tau)^T\}\Phi^T \quad 23$$

$$\rightarrow \boldsymbol{C}_{uu}(\tau) = \Phi C_{zz}(\tau)\Phi^T \quad 24$$

In which C_{zz} is the correlation of the response vectors in modal coordinates. Performing a FFT on the correlation matrix one can find a PSD of the responses, which leads to a relation as given eq. *25*. The correlation and PSD are linked to each other via the Wiener-Khinchin Theory.

$$\tilde{S}_{uu}(\omega) = \Phi\tilde{S}_{zz}(\omega)\Phi^T \quad 25$$

The decomposition is finalized by taking the SVD of the PSD $S_{uu}(\omega)$ and relate the outcome to equation *25*. Equation *26* gives the final relationship that denotes the decomposition of the PSD by performing a SVD.

$$\tilde{S}_{uu}(\omega) \propto \tilde{H}(\omega)\tilde{H}(\omega)^H = U\Sigma U^T \quad 26$$

In which:

U = Matrix holding the left singular vectors
Σ = Diagonal matrix holding the singular values

When an SVD is performed for every individual frequency in a dataset the singular values and left singular vectors are stored in a matrix for which each entry represent a frequency.

Brincker, Zhang, et al. (2001) use the output of the SVD as an identification tool for the modal parameters. Depending on the rank of S_{uu} one might use one or multiple rows of the singular value matrix. Specific peaks of this plot correspond to the natural frequencies. Using a matrix that has a rank of 2 or higher, one can find closely located modes by taking multiple rows of the singular value matrix into account.

The mode shapes are found by examining the corresponding column of the left singular value matrix (Brincker, Zhang, et al., 2001).

$$U_{i,1} = \hat{\phi}_i \quad 27$$

Brincker, Zhang, et al. (2001) state that in case of closely situated modes one should take the second column of the left singular value matrix into account as well. They write that the first

vector is a good measure for the strongest mode in the region while the second vector denotes the mode shape of the second mode.

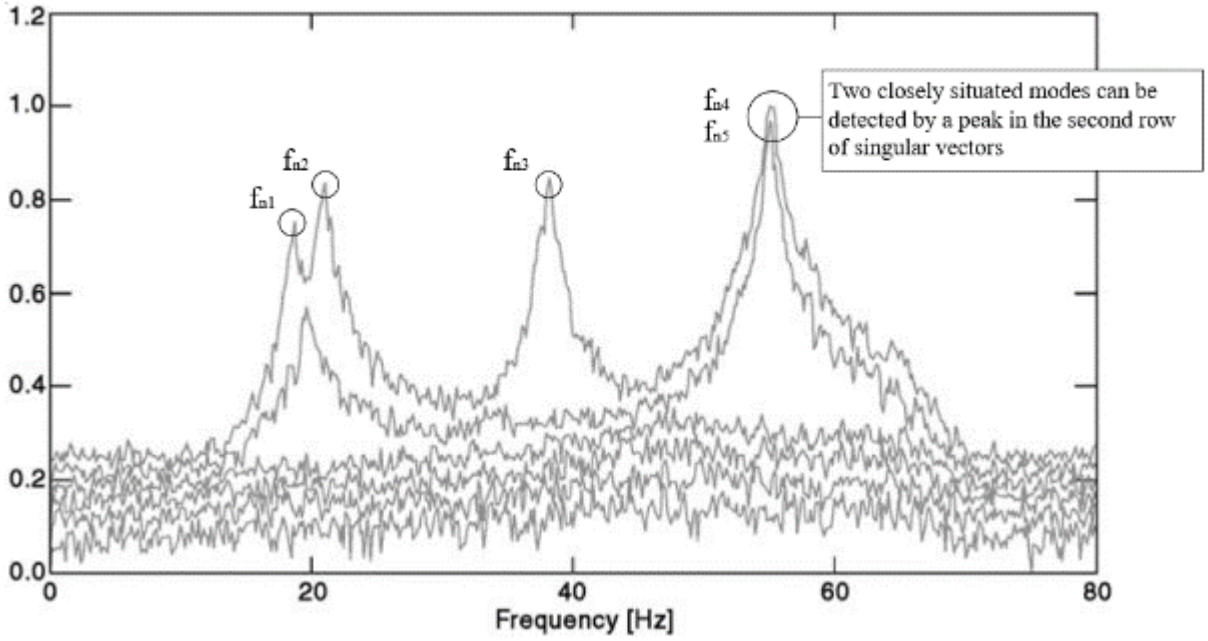

Figure 9 Plot of the singular value matrix obtained via a SVD on the PSD of the responses. The 4th and 5th mode are closely situated to each other which can be seen in the peak of the second singular vector row (Brincker, Zhang, et al., 2001)

3.3.2 Implementation of the FDD algorithm

Based on Brincker, Zhang, et al. (2001) the FDD algorithm can be divided into several parts that form the total algorithm. Every part is discussed in the coming paragraphs. The main topics that can be divided are:

1. Generate a dataset that consists of time series of every measurement location.
2. Segmentation of the dataset and perform Fast Fourier Transformation into the frequency domain.
3. Singular Value Decomposition of the segmented dataset.
4. Plot Singular values and detect natural frequencies.
5. Plot corresponding left singular matrix to obtain the mode shapes.

Time series

Following the FDD method of Brincker, Zhang, et al. (2001) the time series that act as input of the experimental modal analysis follow from experiments that are executed. They should at least fulfil the requirement that loading is white noise (Brincker, Zhang, et al., 2001).

The time series as an input has the form of a matrix d [m x n] with on the vertical entries the different measurement locations and on the horizontal entries the time series.

$$d = \begin{bmatrix} d_{1,t0} & \cdots & d_{1,tn} \\ \vdots & \ddots & \vdots \\ d_{n,t0} & \cdots & d_{n,tn} \end{bmatrix}$$

Segmentation and Fast Fourier Transform

A FFT is performed to transform the time series into the frequency domain from which the remained of the algorithm will act. Segmentation of the data can be useful to increase the rank of the PSD S_{dd}. Brincker et al. (2003) describe that a dataset should contain multiple forcing as input. This can be obtained by merging multiple different experimental datasets as segments. The new S_{dd} is now obtained by a summation of the averaged segments, multiplied by their conjugate (Lourens, 2020). Furthermore Lay (2012) lay denotes that the rank determines the number of non-zero singular values. Incorporating equation 28 leads to an increase in the rank of the matrix(Lourens, 2020).

$$S_{dd} = \tilde{d}_1(\omega)\tilde{d}_1^H(\omega) + \cdots + \tilde{d}_n(\omega)\tilde{d}_n^H(\omega) \qquad 28$$

Singular Value Decomposition and results

Brincker, Zhang, et al. (2001) elaborate the finishing part of the FDD algorithm focuses on the singular value decomposition of the spectral density matrix. They state that the output of this decomposition is a diagonal matrix containing the singular values of each measurement location of each point in the frequency domain, leading to a [m x m x k] matrix. In which m is the number of measurement points in space and k is the number of measurement points in the frequency domain. The left singular vector U is also a result of the decomposition and exists of vectors representing the modal shapes for every singular vector per point in the frequency domain. U is therefore a [m x m x k] matrix as well. Where the first column is associated with the mode shape of the first singular vector from S and so on. A graphical representation of the singular value plot is given in Figure 10.

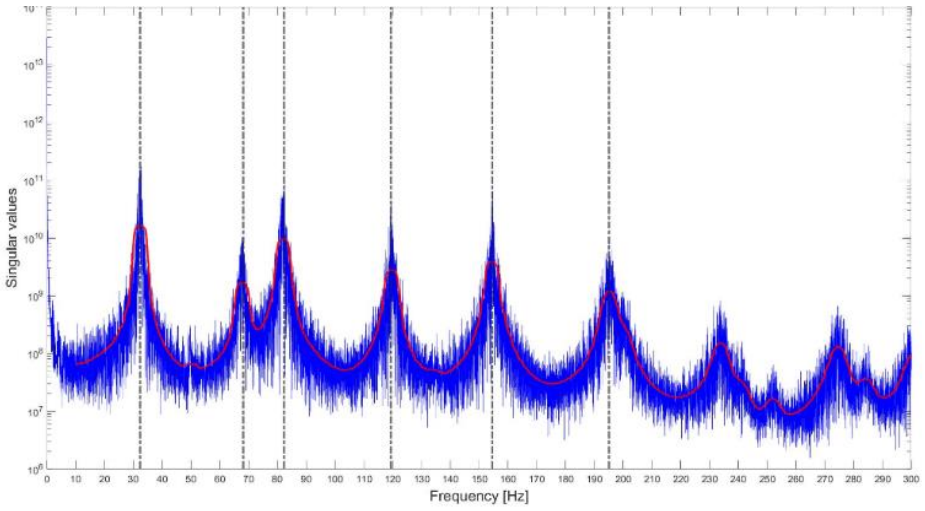

Figure 10 Graphical representation of singular values as an outcome of the frequency domain decomposition

3.4 Modal Assurance Criterion (MAC)

Pastor et al. (2012) state that the MAC is one of the tools that is often used to quantitatively compare two modes. High MAC values correspond to modes that are much alike while low MAC values denote that examined modes are different from each other. It can be used to identify different modes from one dataset to examine whether all the detected mode shapes belong to different modes, whereas it can also be used as a tool to examine whether the modes that are found from a dataset correspond to the expected modes from other models.

The MAC is calculated by comparing two vectors and take their normalized scalar product (Pastor et al., 2012). This yields into a formulation as given in equation *29*.

$$MAC(A,B) = \frac{|\{\phi_A\}^T\{\phi_B\}|^2}{(\{\phi_A\}^T\{\phi_A\})(\{\phi_B\}^T\{\phi_B\})} \qquad 29$$

In which:

φ_A = Mode shape vector from FDD
φ_B = Mode shape vector from FEM or other model
MAC(A,B) = Modal assurance criterion value for mode shape vectors A and B

In case of orthogonal modes a MAC matrix has solely diagonal values. This will be the case for individual modes as well. Figure 11 gives a representation of a MAC matrix that is a result of one of the experimental analyses. It can be seen clearly that a diagonal matrix is obtained, meaning that the modes are orthogonal.

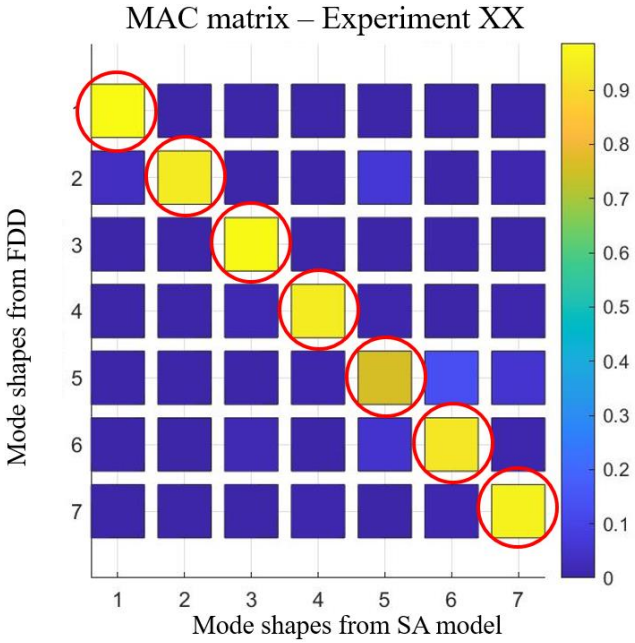

Figure 11 Example of a MAC matrix obtained from the experiments. Yellow squares denote high MAC values, Orthogonal matrices are marked with red circles and denote that modes correspond to each other.

4 Theory - Semi-analytical model (Tieleman et al., 2020)

Tieleman et al (2020) derived a semi-analytical to predict gate vibrations in a fluid, which will be treated here. The problem is split up into a structural part and a fluid part that are each treated separately, after which a coupling is made using interface conditions. Figure 12 gives an overview of the examined problem.

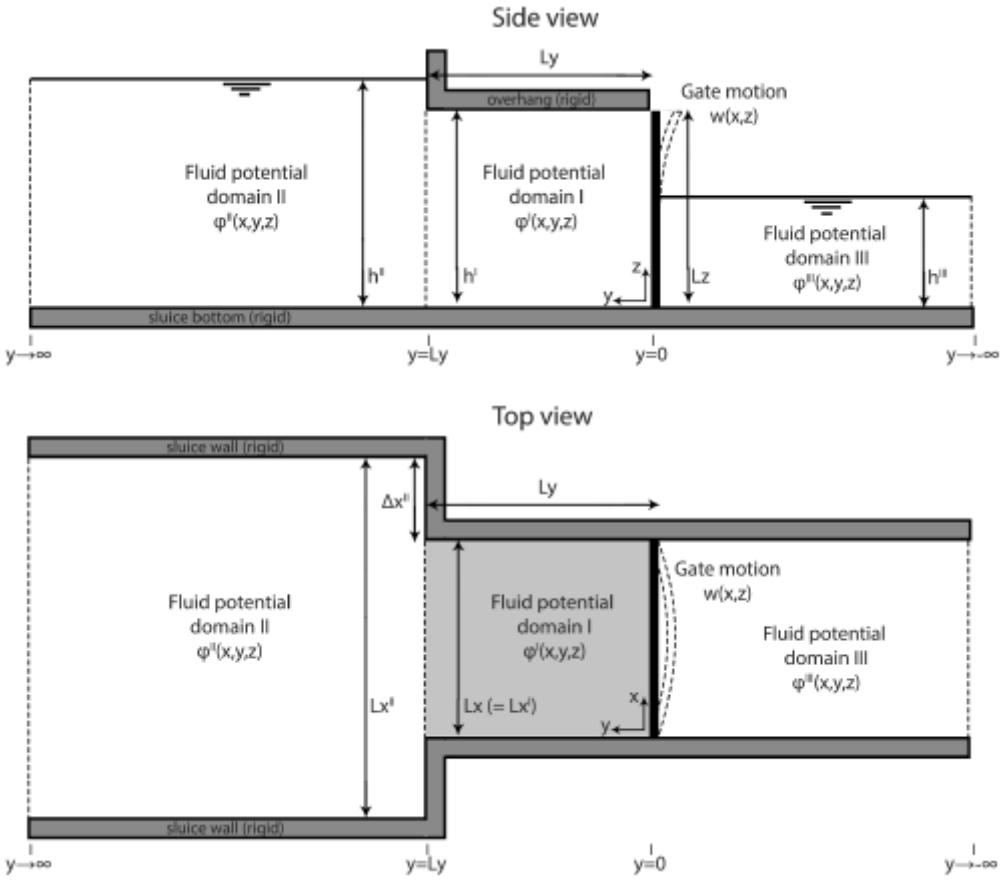

Figure 12 Problem under consideration (Tieleman et al, 2020)

The derivation is based on the assumption that the vertical thin plate is homogeneous and isotropic. The result is a 3-dimensional solution for the bending gate vibrations. the corresponding equations of motion for both the structure and the fluid can be found in appendix B.

Tieleman et al. (2020) use the technique of separation of variables for both the structural and fluid part for both the x- and z-direction. This leads to the following expansions in the frequency domain. In which $W_{x,k}$ denotes the plate modes and Φ the fluid modes.

$$\widetilde{w} = \sum_{k=1}^{\infty} A_k(\omega) W_{x,k}(x,z) \qquad 30$$

$$\tilde{\phi}^{I}(x,y,z,\omega) = \sum_{p=1}^{\infty} \left(B_p^{-}(\omega) e^{-ik_{y,p}^{I}(L_y - y)} + B_p^{+}(\omega) e^{-ik_{y,p}^{I} y} \right) \Phi_p^{\mathrm{I}}(x,z) \qquad 31$$

$$\tilde{\phi}^{II}(x,y,z,\omega) = \sum_{r=1}^{\infty} \left(C_r^{+}(\omega) e^{-ik_{y,r}^{II}(L_y - y)} \right) \Phi_r^{\mathrm{II}}(x,z) \qquad 32$$

$$\tilde{\phi}^{III}(x,y,z,\omega) = \sum_{r=1}^{\infty} \left(D_t^{+}(\omega) e^{-ik_{y,t}^{III}(-y)} \right) \Phi_t^{\mathrm{III}}(x,z) \qquad 33$$

Tieleman et al. (2020) describe a solution technique that makes use of interface conditions between the different regions. The result is a set of three equations that each has an unknown modal coefficient, which relates to each of the three regions. The unknowns that are present in this problem definition are A_k, B_p^{-}, B_p^{+}, C_r^{+}, D_t^{+}.

Applying the first interface conditions leads to two equations as given in equation *34* & *35*. The details about the calculation are not treated in this report. The first interface conditions enhance the interface between fluid regions 1 and 3 with the gate. Tieleman et al. (2020) give the following relations:

$$\sum_{k=1}^{\infty} A_k \left(I_l \delta_{kl} - \sum_{t=1}^{\infty} \frac{\rho_f \, \mathrm{i}\omega^2 \, T_{k,t} T_{l,t}}{k_{y,t} \Delta_t} \right) + \sum_{p=1}^{\infty} B_p^{-} \left(-\rho_f \, \mathrm{i}\omega \, Q_{l,p} \, e^{-\mathrm{i}k_{y,p}^{I} L_y} \right) + \sum_{p=1}^{\infty} B_p^{+} \left(-\rho_f \, \mathrm{i}\omega \, Q_{l,p} \right) = F_l \qquad 34$$

$$T_{k,t} = \iint_S \Phi_t^{III}(x,z) \, W_k(x,z) \, dx \, dz$$

$$\Delta_t = \iint_S (\Phi_t^{III}(x,z))^2 \, dx \, dz$$

$$Q_{l,p} = \iint_S \Phi_p^{I}(x,z) \, W_l(x,z) \, dx \, dz$$

$$F_l = \iint_S \tilde{f}_e(x,z) \, W_k(x,z) \, dx \, dz$$

$$I_l = \rho_s \, (\omega_l^2 - \omega^2) \, \Gamma_l$$

$$\Gamma_l = \iint_S W_l^2(x,z) \, dx \, dz$$

$$\sum_{k=1}^{\infty} A_k \left(\omega\, Q_{k,q}\right) + \sum_{p=1}^{\infty} B_p^- \left(k_{y,p}^I e^{-\mathrm{i}k_{y,p}^I L_y} \Delta_q \delta_{pq}\right) + \sum_{p=1}^{\infty} B_p^+ \left(-k_{y,p}^I \Delta_q \delta_{pq}\right) = 0 \qquad 35$$

$$Q_{k,q} = \iint_S \Phi_q^I(x,z)\, W_k(x,z)\, dx\, dz$$

$$\Delta_q = \iint_S \Phi_q^{I\,2}(x,z)\, dx\, dz$$

The second interface conditions are applied on the fluid regions I and II and, as was the case for the first method, orthogonality on the fluid modes. The result is given in equation *36*.

$$\sum_{p=1}^{\infty} B_p^- \left(\frac{\rho_f^I}{\rho_f^{II}} \Delta_p \delta_{pq} + k_{y,p}^I \sum_{r=1}^{\infty} \frac{R_{r,q} R_{r,p}}{k_{y,r}^{II}\, \epsilon_r}\right) + \sum_{p=1}^{\infty} B_p^+ e^{-\mathrm{i}k_{y,p}^I L_y} \left(\frac{\rho_f^I}{\rho_f^{II}} \Delta_p \delta_{pq} - k_{y,p}^I \sum_{r=1}^{\infty} \frac{R_{r,q} R_{r,p}}{k_{y,r}^{II}\, \epsilon_r}\right) = 0 \qquad 36$$

$$R_{r,q} = \iint_{S_w} \Phi_q^I(x,z)\, \Phi_r^{II}(x,z)\, dx\, dz$$

$$R_{r,p} = \iint_{S_w} \Phi_p^I(x,z)\, \Phi_r^{II}(x,z)\, dx\, dz$$

$$\epsilon_r = \iint_{S_w} \Phi_r^{II\,2}(x,z)\, dx\, dz$$

Tieleman et al. (2020) state that solving all equations at once, opens the opportunity to solve the unknowns that are left in the equations. The system of equation can be solved numerically with a truncation of modes that are considered.

Figure 13 gives a roadmap to obtain a solution that fully depends on the structural modes only.

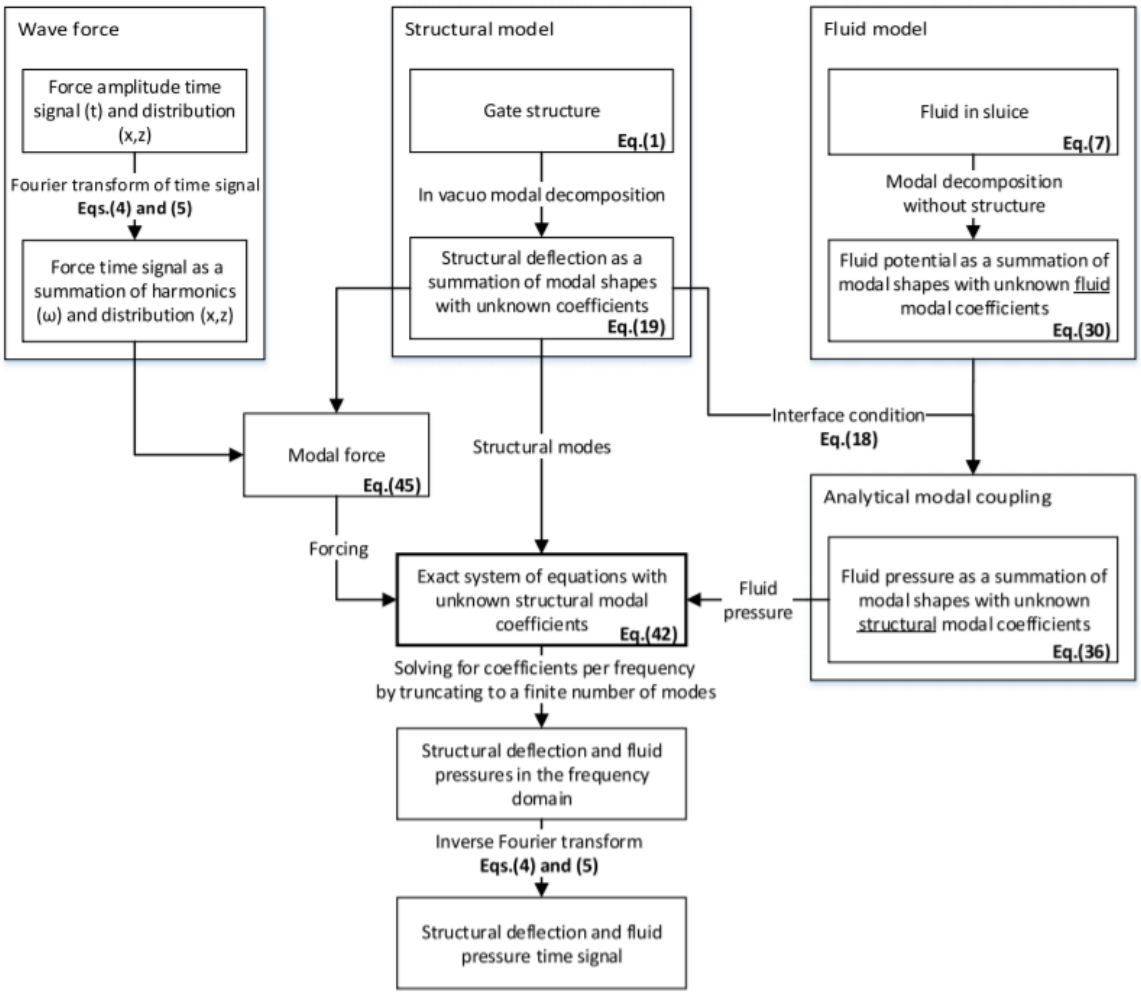

Figure 13 Roadmap for deflections for immersed vertical gate (Tieleman et al, 2019)

5 Experimental tests

This chapter focusses on the different experiments that are executed. Figure 14 gives a schematic workflow which ultimately leads to a desired output of the different tests that are executed. The structure of this chapter is such that all experiments and their set up are briefly explained.

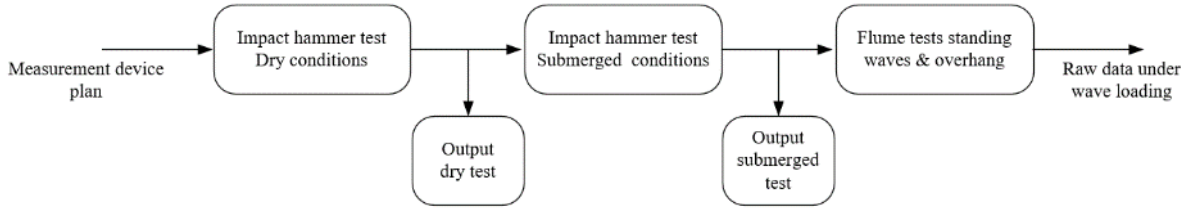

Figure 14 Workflow of experiments to derive at required data for validation of the semi-analytical model

The tests can be divided into three experiments:

- Dry Modal Analysis test
- Wet Modal Analysis tests in submerged conditions and
- Flume tests with both regular and irregular wave impacts.

The desired output is a time series of strains and accelerations for different points on the scaled model. The goal of these experiments is to validate the SA model derived by Tieleman et al. (2020) for assessing dynamic response of slender flood gates. Using the dry and wet modal analysis gives insight in the modal parameters of the structure, while the wave experiments give insight in the modal parameters as well as time series. The latter is not treated in this thesis, but the experiments are used for modal analysis purposes as well.

5.1 Scaled model

The scaled model enhances two parts: 1) The flume and 2) the scaled model gate. Both will be treated in detail in this paragraph.

5.1.1 Flume

The flume is located at the faculty of Civil Engineering at the Technical University of Delft. It is housed at the Stevin lab 3.

The flume has the following dimensions:

- Width = 0.8 m
- Depth = 1.0 m
- Length = 42.0 m

Mind that the height of the flume is not the same as the water depth that can be reached. The height is somewhat larger. A wave maker that is installed in the flume is able to generate waves

for experimental studies, such as wave impacts and/or dynamic response of structures due to wave impacts.

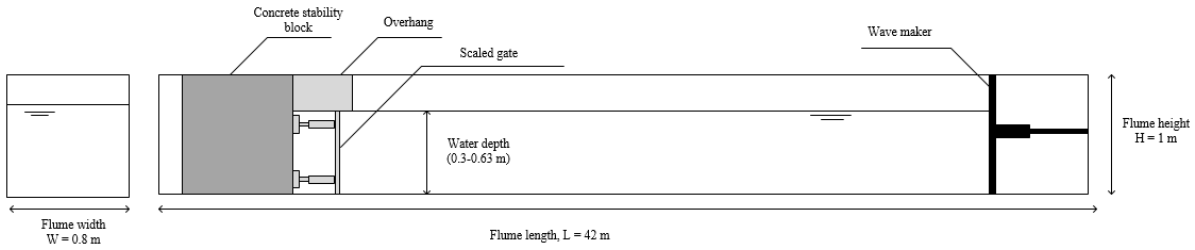

Figure 15 Schematic side(Right) and front(Left) of the flume at the TU Delft. The locations of the Wave maker (Right) and Scaled model gate (Left) given.

Multiple experiments are performed using a set of both regular and irregular waves. An overview of the experiments and the desired outcome is treated in §5.2.3.

5.1.2 Measurement devices

Strain gauges and accelerometers are used on both gates to obtain a time series that contains both strains and accelerations. Using two datasets enhances the reliability of the outcome by validation of the outcome by using both datasets. Another reason for using both devices is that for the Reinforced Gate the strains in the field between the stiffeners are predicted to be rather low, based on the SA model.

Measurement device	Measuring frequency
Strain gauge	5000-10.000 Hz
Accelerometer	5000-10.000 Hz

Table 2 Overview of measurement devices and their sampling frequency

To assess the right modes, it is crucial that the devices are installed on the right locations on the gate. Chapter 6 elaborates the procedure of designing the set up plan. Figure 28 gives an overview of the measurement device plans of both the Reinforced and the Solid Plates.

5.1.3 Scaled model gate

Two types of gates are examined to guarantee a broad base for the validation of the semi-analytical model:

- Solid plate
- Reinforced plate

The solid plate acts as a basic configuration and the Reinforced plate represents a more realistic gate design. The latter is designed in such a way that during a wave impact, multiple modes are triggered. Figure 16 gives an overview of the gates including the location of the load cells and the pressure sensors. The systems' dynamic characteristics such as modes and natural frequencies are elaborated in §6.1. This paragraph also mentions the expected modes that are triggered for both gates, based on the SA analysis. The solid plate is expected to have most energy in mode 1, while the Reinforced Plate has most energy in mode 1,2 and 3. The largest

natural frequencies observed are 216 Hz (dry) and 132 Hz (wet). The measurement frequency will take this into consideration as well, where the Nyquist frequency determines the largest possible frequency that can be measured.

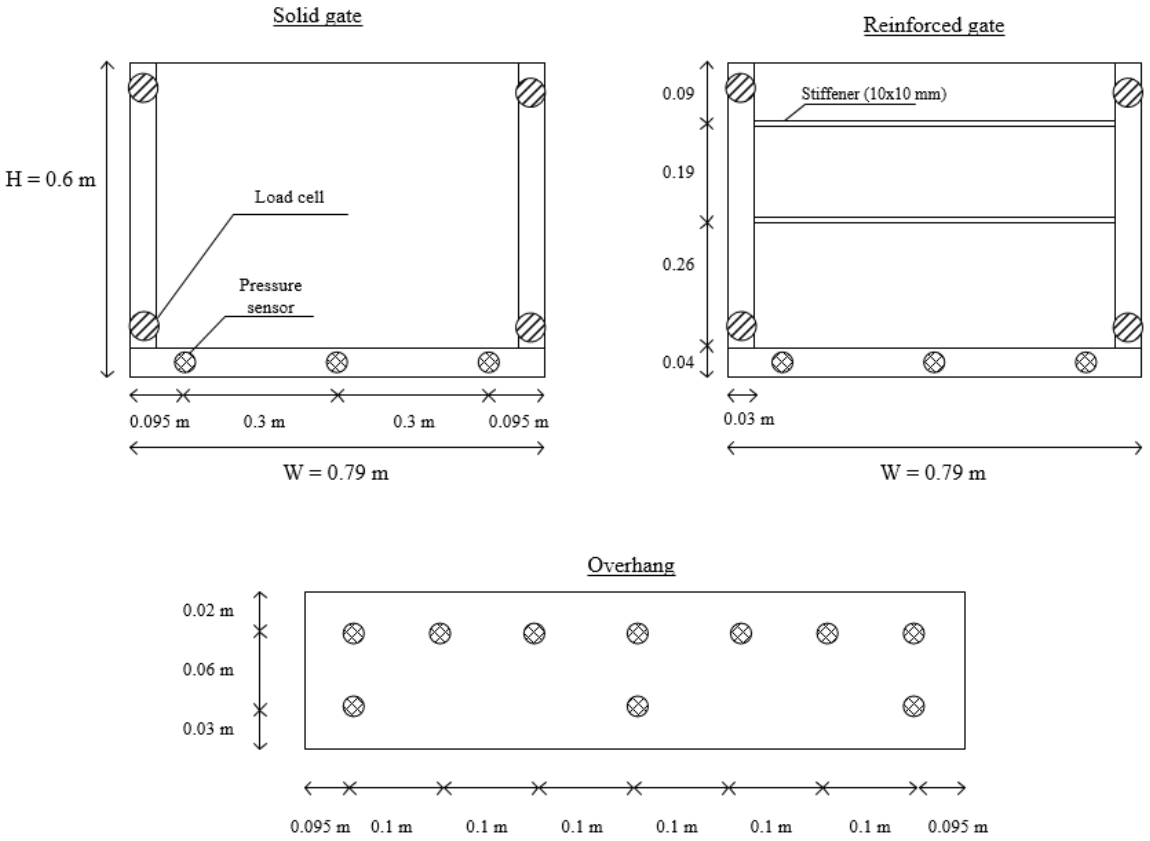

Figure 16 Schematic front view of the solid and reinforced gates including dimensions and locations of pressure sensors and load cells (top) and the location of the pressure sensors in the overhang(bottom).

5.2 Experiments

Experiments are executed in order to facilitate an experimental modal analysis in the form of a Frequency Domain Decomposition. The experiments serve different purposes which are visualized in Figure 17. The different tests that are executed are:

- Dry hammer tests - Dry Modal Analysis (§5.2.1)
- Wet hammer tests - Wet Modal Analysis (§5.2.2)
- Regular wave impacts - Wet Modal Analysis (§5.2.3)

A total overview of the executed experiments including their experiment ID is given in appendix E.

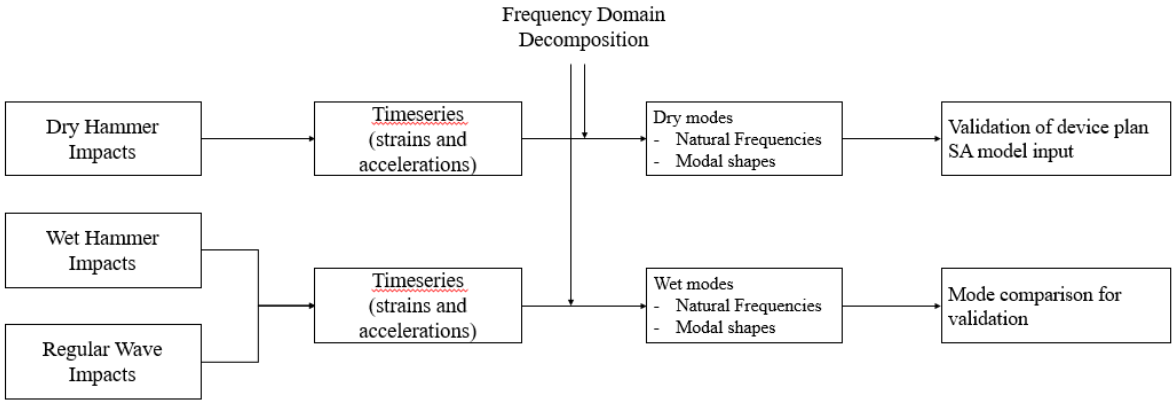

Figure 17 Workflow for different experiments and the use of their results in the different types of analyses

5.2.1 **Hammer test in dry conditions**

Dry hammer tests are executed in the situation where the gate in mounted on the concrete block, which provides stabilization of the total system, without the presence of water. Using an impact hammer, random points of the gate are subjected to an impulse. Dry hammer tests are performed for multiple reasons:

1. Validation of the measurement plan
2. Obtaining the dry structural modes of the scaled models for input in SA model
3. Obtaining the dry natural frequencies of the scaled models for input in SA model.

The structural dynamic characteristics of the system that are retrieved at these tests serve as a first validation for the semi-analytical model. The SA model uses the dry characteristics as an input, which are therefore relevant to know for the two different scale models.

Besides a dry modal analysis, single hammer impacts are also performed for eight different points on the scaled models. By analysing these datasets the damping of the system can be retrieved. The different locations of the single impacts are elaborated in Figure 18.

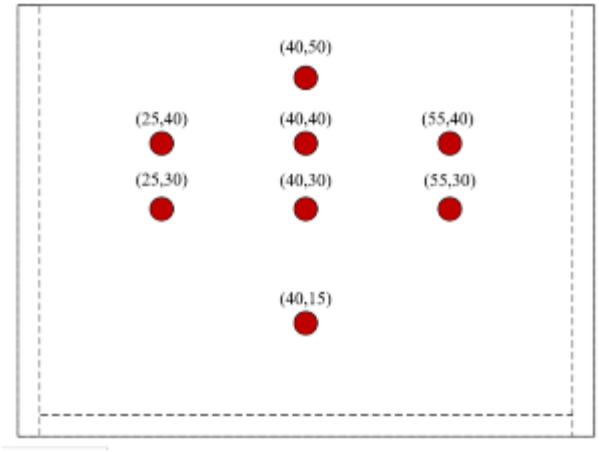

Figure 18 Locations of single hammer impacts

5.2.2 Hammer test in submerged conditions

Goal of the submerged hammer tests is to retrieve all wet natural frequencies and mode shapes of the gate, which are compared to the SA prediction. This serves as a validation step for the SA model in submerged conditions. These experiments give insight in submerged modal shapes and corresponding natural frequencies. These shapes and frequencies are then compared to the prediction of the semi-analytical model to validate the performance of the model.

Gate	Test ID	Test number	Waterlevel	Frequency
Solid plate	Wet Modal Analysis	004-006	0.30 m	5000 Hz
Solid plate	Wet Modal Analysis	007-009	0.40 m	5000 Hz
Solid plate	Wet Modal Analysis	010-012	0.50 m	5000 Hz
Solid plate	Wet Modal Analysis	013	0.60 m	5000 Hz
Reinforced plate	Wet Modal Analysis	001-003	0.30 m	5000 Hz
Reinforced plate	Wet Modal Analysis	006-011	0.40 m	5000 Hz
Reinforced plate	Wet Modal Analysis	012-017	0.50 m	5000 Hz
Reinforced plate	Wet Modal Analysis	019-024	0.56 m	5000 Hz
Reinforced plate	Wet Modal Analysis	028-030 & 034-036	0.60 m	5000 Hz
Reinforced plate	Wet Modal Analysis	031-033	0.63 m	5000 Hz

Table 3 Overview of Wet Modal Analysis experiments and corresponding water levels

5.2.3 Flume tests under wave loading

To simulate standing wave impacts, regular waves are generated by a wave maker. The results of these experiments will serve as back up for the situation that submerged hammer tests are not sufficient. Regular wave tests consist of 100 and were executed for three water levels: 1) 0.56 m, 2) 0.60 m and 3) 0.63 m. Table 4 gives an overview of the wave conditions during the different wave tests. The coding also includes the different water levels for which the experiments is executed, this number is replaced by ## in Table 4.

Test ID	Wave height (H_0)	Wave period (T_0)	Wave length (L_0)	Skewness (S_0)	Water level [m]
AS##R	0.06 m	1.30 s	2.64 m	0.023	0.56, 0.60, 0.63
BS##R	0.08 m	1.60 s	3.99 m	0.020	0.56, 0.60, 0.63
CS##R	0.10 m	1.30 s	2.64 m	0.038	0.56, 0.60, 0.63
DS##R	0.10 m	1.60 s	3.99 m	0.025	0.56, 0.60, 0.63
ES##R	0.10 m	2.00 s	6.24 m	0.016	0.56, 0.60, 0.63

Table 4 Wave conditions for different Regular Wave tests

5.3 Data processing

Raw datasets are retrieved from the experiments described in §5.2 - §5.2.3. This data is processed in order to work with zero-mean and calibrated datasets that represent real values for strains and accelerations rather than voltages. Both measurement devices are treated in this paragraph. All data is collected and processed in the MP3 software package. This program is developed for the collecting data from strain gauges during experiments. It is also possible to collect data from other measurement devices and store them in large datafiles. MP3 enables the

user to either retrieve raw data or filtered data in .csv files. Filtered data is already calibrated whereas raw data contains solely voltages.

5.3.1 **Processing of strain gauges**

Strain gauges are delivered with standard calibration and scaling factors. The data coming from these gauges is therefore already filtered in the output files. The MP3 program is specially designed for these measurement sensors. Processing the strain data therefore only consists of averaging the dataset to a zero-mean as well as detrending the dataset using Matlab. Figure 19 gives an example from a raw dataset obtained during the tests and the same dataset after processing.

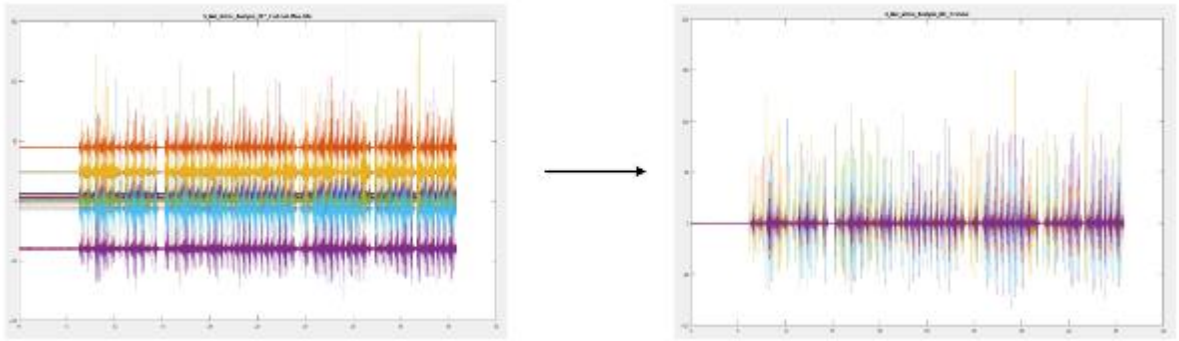

Figure 19 An example of a processed data set for strain gauges. Left: raw data, right: processed data (zero-mean and detrend)

5.3.2 **Processing of accelerometers**

Acceleration data is collected as raw data and contains voltages only. Processing these voltages to accelerations comprises several steps:

1. Calibration factors of the accelerometers and their amplifiers
2. Correction factors for possible inclination angles
3. Averaging to zero mean values and detrending.

Calibration factors are obtained via conventional methods. The voltages for both +1g and -1g are measured for every individual accelerometer-amplifier pair in the direction perpendicular to the accelerometer itself. These datasets are then used to calculate acceleration per voltage.

$$f_{calibration} = \frac{9.81\frac{m}{s^2} - \left(-9.81\frac{m}{s^2}\right)}{V_{+1g} - V_{-1g}} \qquad 37$$

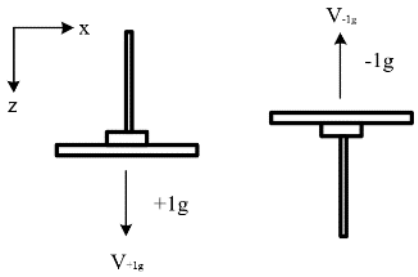

Figure 20 Accelerometer position for +1g and -1g voltage retrieval during calibration

Possible tilt correction of the accelerometers is included in the data processing as well. The voltage for 0 g is taken as the average voltage from the calibration. The actual voltage at the start of each measurement is taken to calculate the inclination angle of each accelerometer. Figure 21 gives a visual impression on how the correction factor for the inclination is calculated.

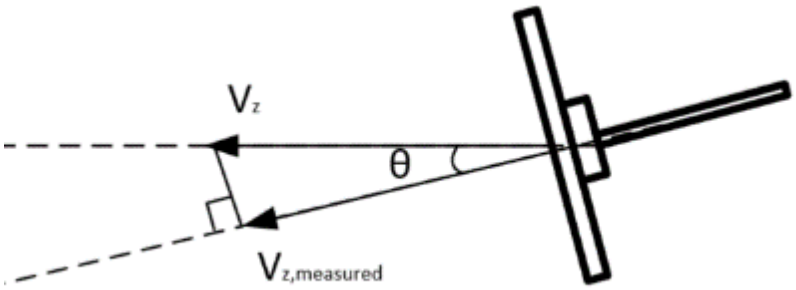

Figure 21 Visual presentation of geometry of an inclined accelerometer with the measured value and the actual value of the acceleration.

$$\alpha_{inclination} = \frac{\Delta\alpha}{\Delta V} * \left(V_{0g} - V_{t=0}\right) ; \frac{\Delta\alpha}{\Delta V} = \frac{\alpha_{+1g} - \alpha_{-1g}}{V_{+1g} - V_{-1g}} \quad 38$$

$$f_{inclination} = 1/\cos(\alpha_{inclination}) \quad 39$$

In which dα/dV is 180 degrees divided by the difference in voltage for 1g and -1g. Multiplying this value by the difference in voltage measured and the 0 g voltage, one can obtain the inclination angle of the accelerometer. The correction factor is then obtained via the cosinus of that inclination angle. Detrending the data and taking the zero-mean of the total dataset and subtract that from every measurement point gives the processed dataset.

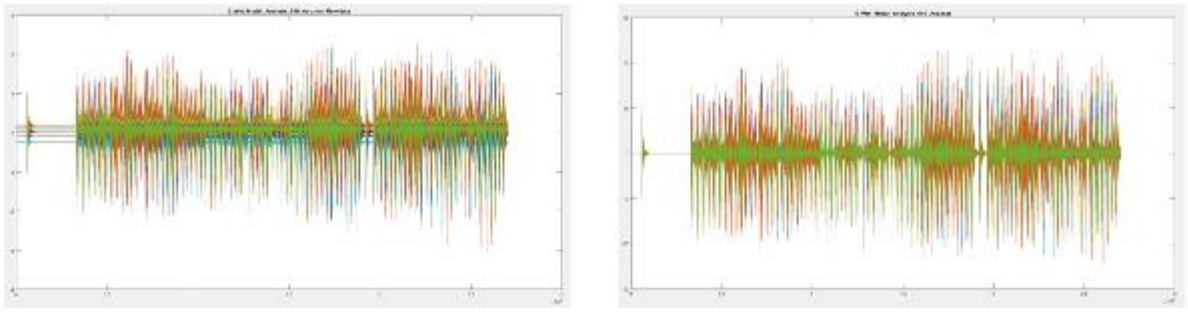

Figure 22 An example of a processed data set for accelerometers. Left: raw data, right: processed data (calibrated, inclination correction, zero-mean and detrend)

6 Measurement device plan

To obtain reliable results a measurement device plan is designed. The plan should be designed such that all the possible modes, that are acting during the experimental tests, are detected. This chapter will focus on the design process, with first a system analysis of the two plates to predict which modes will act, including the mode shapes. The predicted modes will lead to different potential measurements plans which will be tested on their performance, the results will eventually lead to an optimal measurement plan. This plan is elaborated in §6.3.

6.1 System research

System identification of the Solid and Reinforced plate focusses on two main modal subjects for different situations. This results in a set of natural frequencies and modes that should be detected by the measurement device plan. The three main modal subjects are:

1. Natural frequencies
2. Mode shapes
3. Mode contribution to the total response

This paragraph is divided into subparagraphs that focus on these dynamic quantities.

6.1.1 Natural frequencies

Both a dry and immersed analysis are executed in the SA model and a total of 8 natural frequencies for both situations are obtained. Table 5 and Table 6 give an overview of the values of these frequencies.

Table 5 Frequencies of dry modes computed by semi-analytical model

Solid Plate	f_1	f_2	f_3	f_4	f_5	f_6	f_7	f_8
Dry	34.5	74.1	87.7	129.5	162.3	167.6	210.6	216.1
Wet (0.6 m)	14.1	35.4	43.3	70.7	90.7	94	124.9	131.8

Table 6 Frequencies of wet modes computed by semi-analytical model

Reinforced Plate	f_1	f_2	f_3	f_4	f_5	f_6	f_7	f_8
Dry	84.3	95.1	135.9	169.9	183.8	207.9	216	-
Wet (0.6 m)	23.2	35.1	57.3	60	75.5	95.7	107.9	-

6.1.2 Modes

The mode shapes for both the solid and reinforced plate are given in Figure 23. Both symmetrical and asymmetrical modes are detected, which indicates that all modes are triggered.

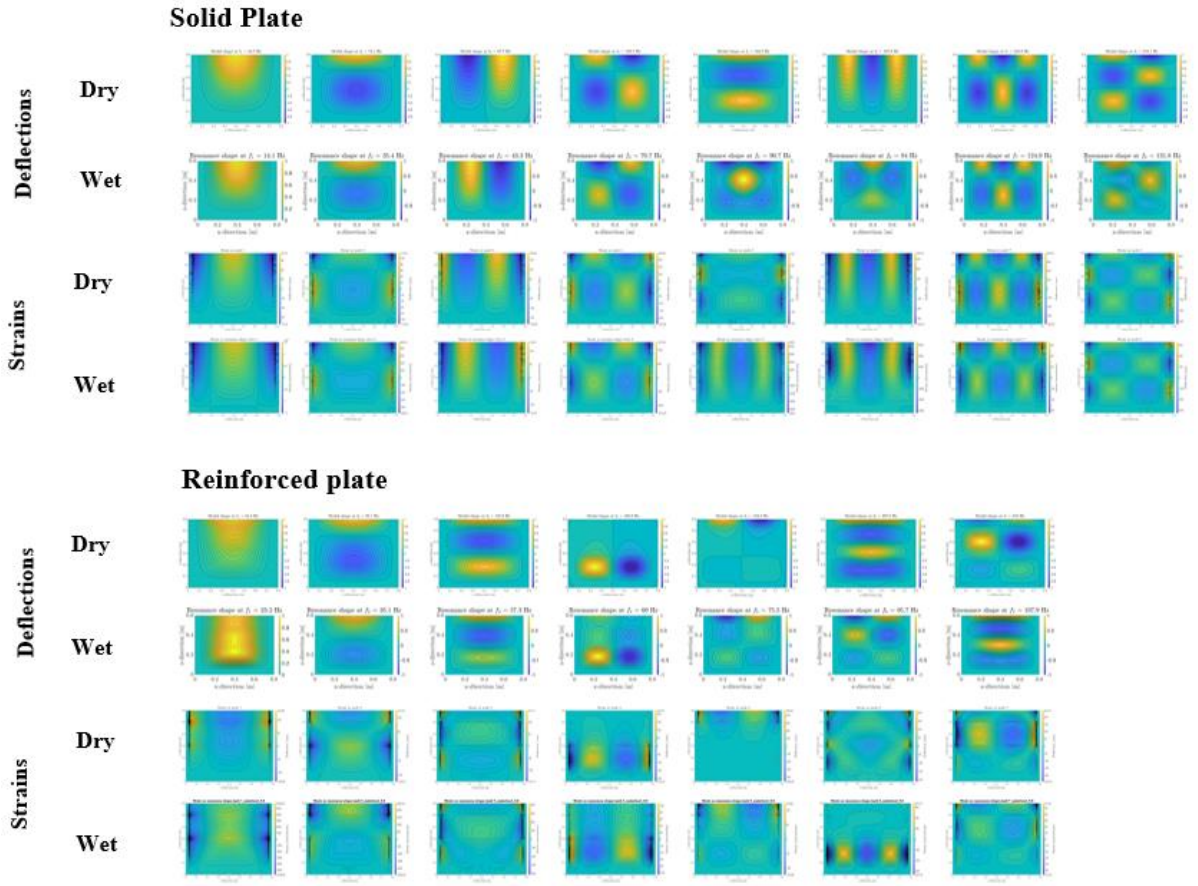

Figure 23 Total overview of all modes (dry & wet) for both the solid and reinforced plate. Wet modes are taken at a water level of 0.6 m.

6.1.3 **Mode contribution**

With the SA model, the contribution of each mode to a time series and/or maximum deflection field can be calculated. This information is relevant in order to validate whether the high contribution modes are identified in the analyses of chapter 7. Figure 24 gives an overview of the mode contribution for both the Solid Plate and the Reinforced Plate. It can be observed that for the Solid Plate most energy is put into the first mode. The Reinforced Plate divides most of the energy input in the first three modes (no. 1, 2 and 3).

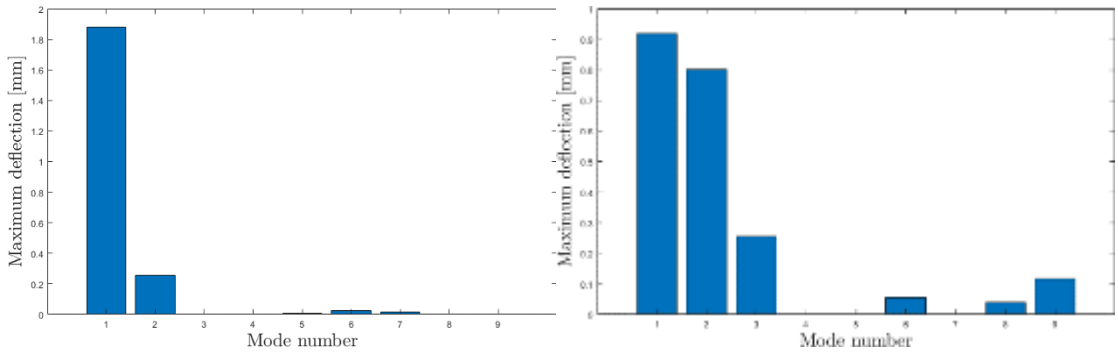

Figure 24 Mode contribution of the maxima of all timesteps. Left: Solid Plate, right: Reinforced Plate.

6.2 Approach design measurement plan

Several steps have been taken to obtain an optimal measurement plan, as is described in §6.3. The designs were limited to 25 strain gauges for every plate and 12 accelerometers. The list below gives an overview of the steps that were taken:

1. Locate the nodes and antinodes of the important modes.

   Sensors are preferably located on these locations in order to guarantee a clear mode identification.

2. Determine the number of strain gauges and accelerometers for every plate.

   The number of strain gauges and/or accelerometers depends on the number of nodes and anti-nodes in the plate.

3. Test several set ups with synthetic data from the SA model.
4. Compare the results of the FDD and SA for different set ups.

The Solid Plate has a gentle shape for both the strain and deflection field of all modes. Locating both accelerometers and strain gauges on the nodes as well as on the anti-nodes of the corresponding fields already gives a first impression on the number of devices that are needed. The same holds for the Reinforced Plate. After determining the potential locations of each measurement device, the exact locations were determined by analysing synthetic data form the SA model and compare the outcome with that of the FDD for different set ups.

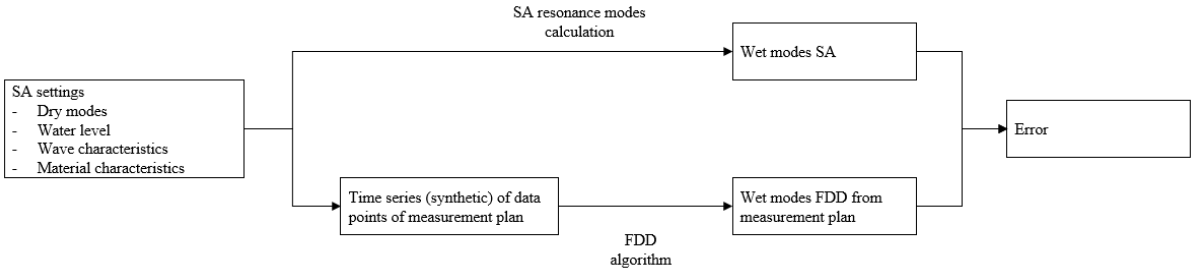

Figure 25 Workflow for obtaining error of potential measurement device plans.

Every potential set up was tested on its performance using synthetic data from the SA model. This served two goals:

1. Testing the performance of the set ups using the absolute error between the synthetic data (FDD algorithm) and SA result.
2. Testing the correctness of implementation of the FDD algorithm.

Figure 26 gives the results from one of the examined set ups for the Solid Plate, while Figure 27 gives results for the Reinforced Plate. Both figures consist of the first four modes of the gate, with 1) Strain or acceleration field from the synthetic data in combination with a FDD analysis, 2) Strain or acceleration field from the SA model and 3) the absolute error between the two. The value of the error is given in Table 7.

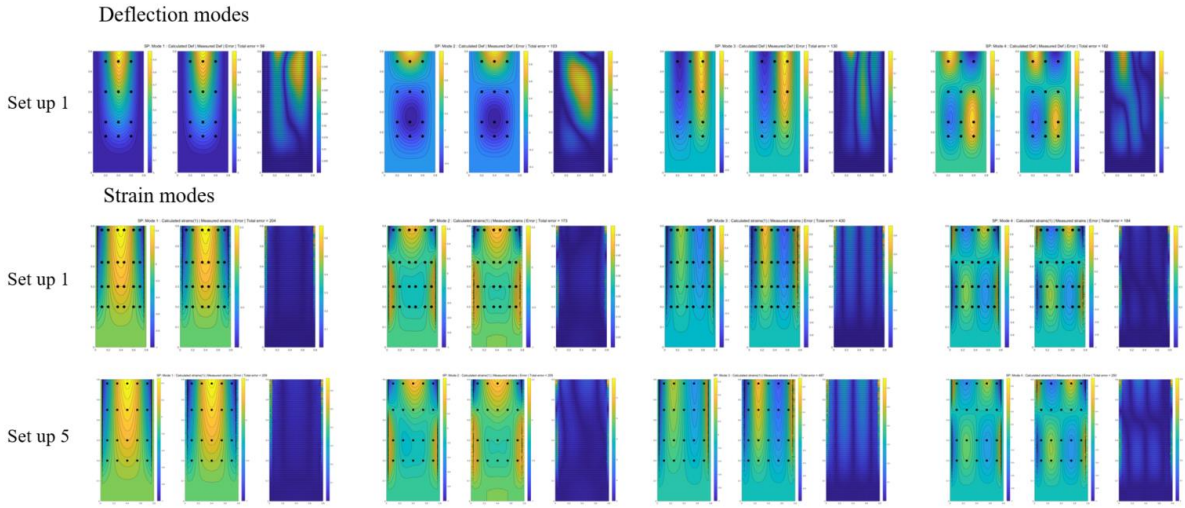

Figure 26 Deflection and strain modes for the Solid Plate calculated using the SA model and FDD analysis using synthetic SA time series. Every mode consists of three figures: 1) FDD mode from synthetic SA data, 2) Predicted mode from the SA model and 3) The error between the two for every data point. Blue denotes small amplitudes(negative) while yellow denotes large amplitudes(positive)

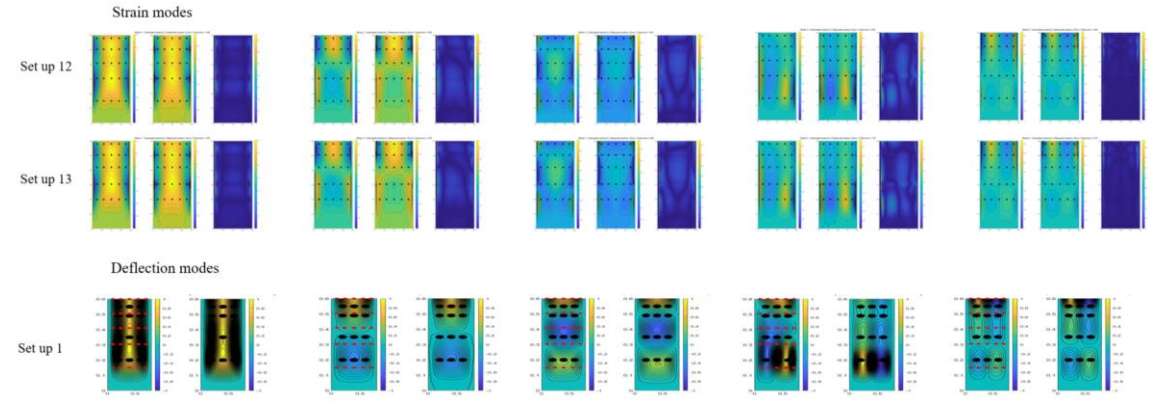

Figure 27 Deflection and strain modes for the Reinforced Plate calculated using the SA model and FDD analysis using synthetic SA time series. Every mode consists of three figures: 1) FDD mode from synthetic SA data, 2) Predicted mode from the SA model and 3) The error between the two for every data point.

Solid Plate	**Mode 1**	**Mode 2**	**Mode 3**	**Mode 4**	**Mode 5**
Strain Set up 1	204	173	430	184	415
Strain Set up 5	209	205	487	250	423
Reinforced Plate					
Strain Set up 1	352	525	641	661	202
Strain Set up 4	370	472	649	712	212

Table 7 Absolute errors per strain mode for different set ups.

6.3 Optimal measurement plan

The most optimal plan is given in Figure 28. Regarding the reinforced plate, it is useful to measure the strains on the stiffeners as well. These locations give relatively large strains which might be measured easily.

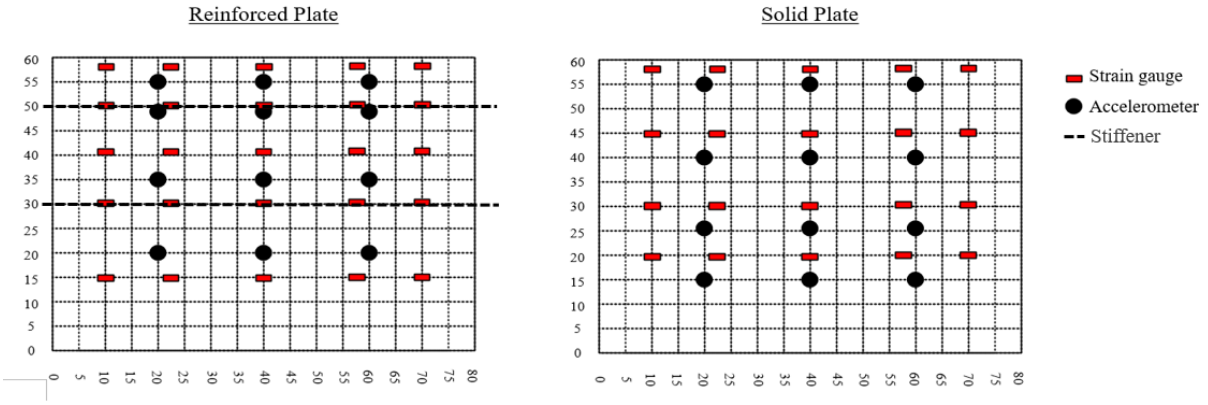

Figure 28 Measurement set up for strain gauges and accelerometers for both the Reinforced and Solid plates

6.3.1 Identified frequencies

Both set ups were analysed by means of synthetic data from the SA model and afterwards the results were compared to each other. The frequencies of both analyses should in principle be the same if both methods work accordingly. Graph 1 gives an overview of both the frequencies from the SA model as well as from the EMA for both the dry and wet situation and the Reinforced (RP) and Solid Plate (SP). The dots denoted the prediction of natural frequencies by the SA model while the crosses are the identified values using the FDD algorithm. The graph shows clearly that the EMA is able to detect natural frequencies in a high level of detail.

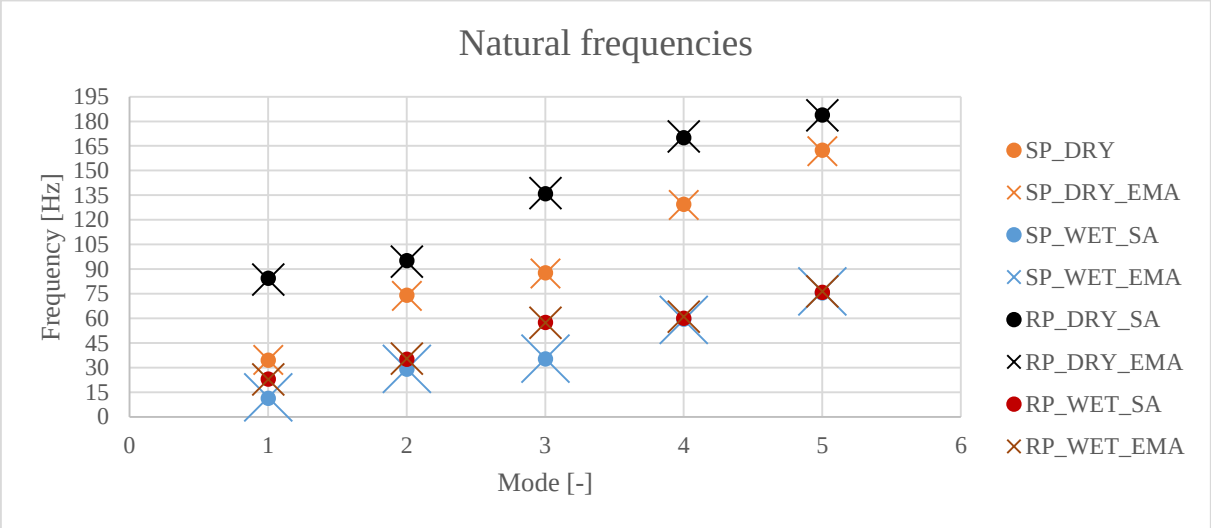

Graph 1 Overview of the first 5 natural frequencies detected by the EMA together with the results from the SA for both the solid and reinforced plate in dry and wet conditions.

6.3.2 Identified modes

The corresponding detected modes for the first five frequencies show a good correspondence with the outcome of the Semi-Analytical model in Figure 23. Both the natural frequencies and modal shapes are predicted correctly. The results for the mode shapes of the Solid Plate are visualized in Figure 29.

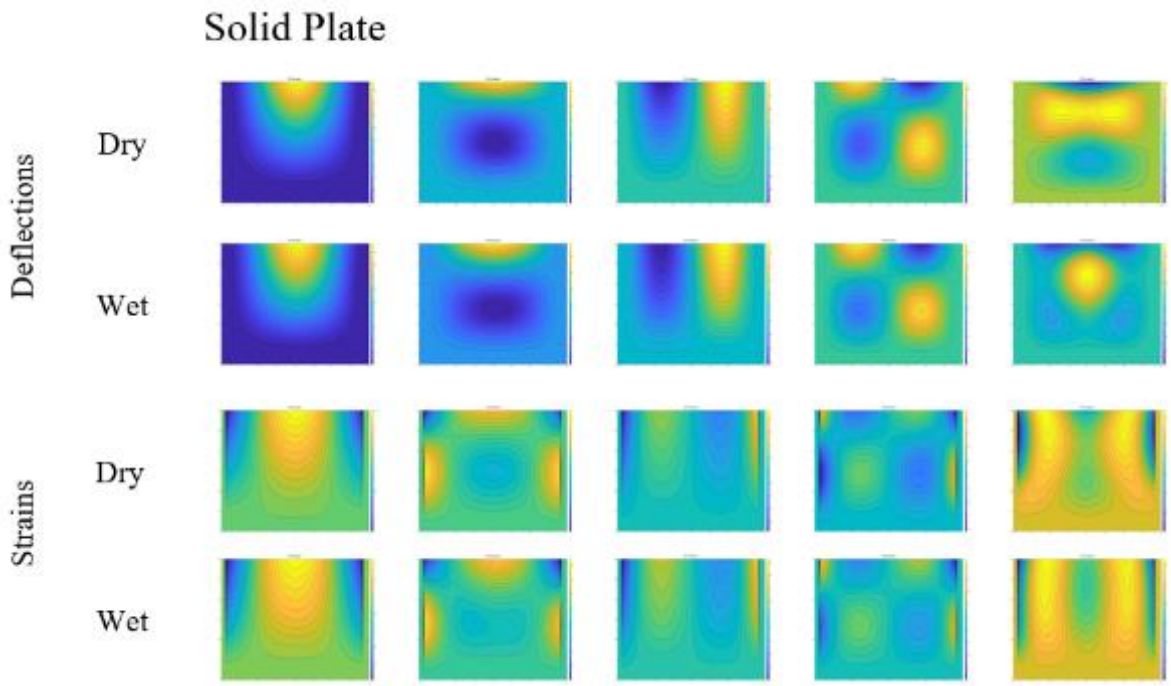

Figure 29 Overview of the first five detected modes of the Solid Plate from the Experimental Modal Analysis. They show good correspondence with the outcome of the Semi-Analytical model.

6.4 Conclusion

The measurement device plan was designed by taking several principles into consideration:

1. Strains/Acceleration should be large enough to be measured.
2. Strain gauges should also detect zero-crossings to give a well interpolated strain field of the modes.
3. Strain gauges and accelerometers should at least be able to detect the first three modes for the Solid Plate and the first five modes for the Reinforced Plate.
4. The required sensors should meet the number of sensors available, taking some spare ones into consideration.

The device plan was designed by means of the above 4 principles together with a synthetic dataset obtained from the SA model.

An optimal measurement plan was found for both plates. It was directly observed that for the Reinforced Plate, although smaller, the strain gauges should be placed in x-direction rather than z-direction. The strain field of the strains in z-direction had many local peaks that could only be detected with a large number of sensors. The strain field of the strains in x-direction was more gentile and had mild slopes and relatively small number of local peaks. The Solid Plate was easier to measure in all modes observed, due to the absence of local peaks.

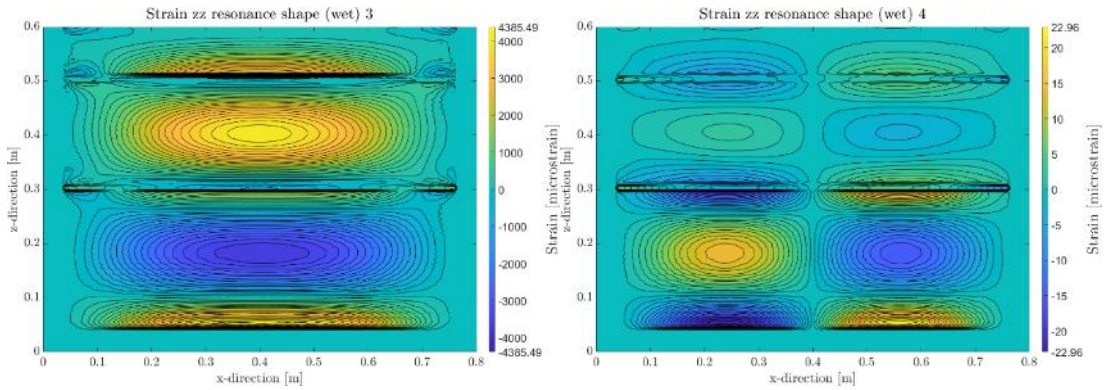

Figure 30 Resonance shapes for mode 3 and 4 in terms of strains in the z-direction. Local peaks are observed, especially at the stiffeners.

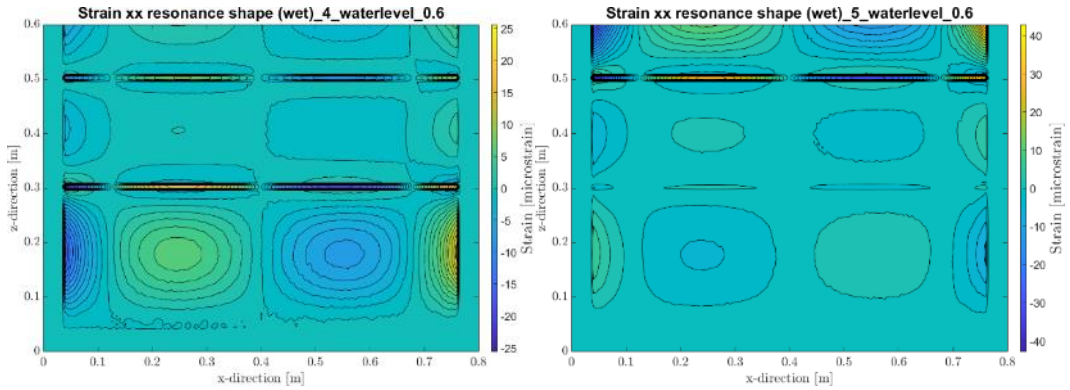

Figure 31 Resonance shapes for mode 3 and 4 in terms of strains in the z-direction. Local peaks are limited to the stiffeners only.

Close to the boundaries in x-direction, large peaks were observed in the strain field, which had to be grabbed by adding a set of strain gauges near these boundaries. This was not the case for the accelerometers, which therefore only needed to be placed on relevant nodes and antinodes.

Several measurement plans were analysed using the synthetic time series of the SA model. The outcome for different modes were compared with the prediction of the SA model and the smallest error was taken as the most optimal set up. A hard condition was that at least the first five modes should be detected. The final design for the Solid Plate consisted of 20 strain gauges and 12 accelerometers. The Reinforced Plate was equipped with 25 strain gauges and 12 accelerometers. The optimal measurement device plans, following from of these analyses, are given in Figure 28.

7 Modal analysis

This chapter focusses on the analyses for both the dry and wet modes and frequencies. Both will be treated extensively for the Solid Plate and the Reinforced Plate. First an approach of the different analyses is treated after which an overview of the data will be given, including the names of the datasets. Thereafter, the dry modes and wet modes for both the Solid Plate and Reinforced Plate are treated. This serves as a basis for the comparison between the identified modes and frequencies with the SA model. The chapter will be finalized with a conclusion and a reflection on the results.

7.1 Approach of validation analyses

The types of analyses serve several goals for validating the SA model. The SA model uses dry modes as input for the calculation of the submerged modes and corresponding response. By default, the dry modes are generated by a FEM software package such as ANSYS. In this light a dry modal analysis is performed in order to verify the dry modes. This serves several goals:

- The set of input dry modes can be adjusted in order to validate the SA model for the identified modes.
- Input of the modal shapes that are found can be used to represent boundary conditions.

The first point uses an assumption that the FEM modes that are not identified, do not play a role in the response of the structure. This is a large assumption and should be treated as such.

The wet modal analysis experiments serve the need to validate the results from the SA model. The mode shapes are identified by means of the FDD algorithm while using the experimental data from §7.2. Several wet modal analyses are used for a reliable validation of the mode prediction by the SA model. These analyses all relate to different input modes of the SA model. Figure 32 gives an overview of the different types of analysis and their workflow. The following paragraphs elaborate the results retrieved from the different analyses:

- §7.4.2: FEM modes (Default)
- §7.4.3: Adjusted set of FEM modes with the modes that are identified during the dry modal experiments. This set had updated frequencies that corresponds to the results of these experiments but take the FEM mode shapes into account.
- §7.4.4: The dry modal shapes and natural frequencies obtained from the dry modal experiments.

Regarding bullet two, using a reduced updated set of FEM modes, normal practice prescribes to calibrate the FEM model in order to represent the real situation. This is out of the scope of this master thesis. Instead, the identified FEM modes are used in combination with updated natural frequencies.

All analyses are subjected to a MAC analysis to give a scientific basis on the identified modes. The performance in terms of natural frequencies is expressed in percentual deviation of the

identified modes with respect to the SA predictions. As an additional step the cumulative error is calculated to quantify.

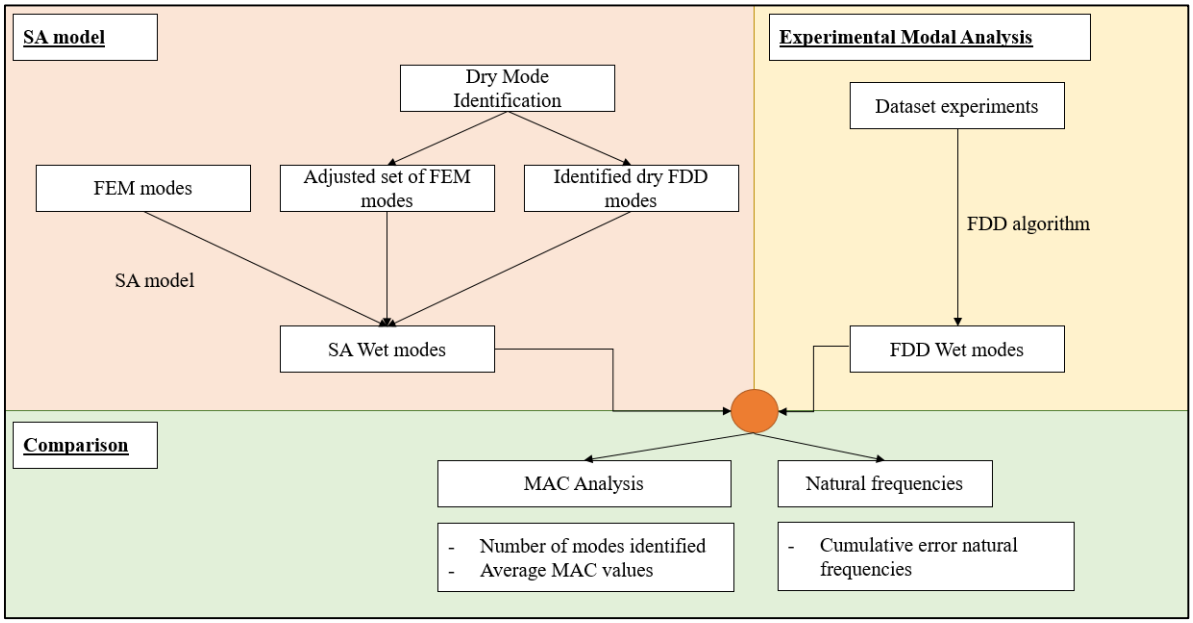

Figure 32 Overview of different analyses.

7.2 Datasets

The datasets that are used for the Solid Plate include the dry and wet modal experiments. The Reinforced plate also includes Regular Wave Impact datasets due to its potentially high damping, which makes it difficult to detect modes with a relatively small impulse during hammer impacts. Table 8 gives an overview of the datasets that are used, including the measurement device that was observed. Important to note is that all datasets that are executed under a water level, are merged into a large dataset. This increases the accuracy of the experiments for the FDD analysis. All data is processed using the techniques as described in §5.3.

Plate	Water Level [m]	Experiment ID	ID included	Device
Solid Plate		3_Dry_Modal_Analysis_008		AM
Solid Plate		3_Dry_Modal_Analysis_009		AM
Solid Plate		3_Dry_Modal_Analysis_010		AM
Solid Plate	0.3	5_Wet_Modal_Analysis_004 – 006	4, 5, 6	AM
Solid Plate	0.4	5_Wet_Modal_Analysis_007 – 009	7, 8, 9	AM
Solid Plate	0.5	5_Wet_Modal_Analysis_010 – 012	10, 11, 12	AM
Solid Plate	0.6	5_Wet_Modal_Analysis_013	13	AM
Solid Plate	0.56	5_Wet_Modal_Analysis_016 – 018	16, 17, 18	AM
Reinforced Plate		3_Dry_Modal_Analysis_033		AM
Reinforced Plate		3_Dry_Modal_Analysis_034		AM
Reinforced Plate		3_Dry_Modal_Analysis_035		AM
Reinforced Plate	0.3	5_Wet_Modal_Analysis_001 – 003	1, 2, 3	AM & SG

Plate	Water Level [m]	Experiment ID	ID included	Device
Reinforced Plate	0.4	5_Wet_Modal_Analysis_005 – 010	5, 6, 7, 8, 9, 10	AM & SG
Reinforced Plate	0.5	5_Wet_Modal_Analysis_012 – 017	12, 13, 14, 15, 16, 17	AM & SG
Reinforced Plate	0.56	5_Wet_Modal_Analysis_019 – 027	19, 20, 21, 25, 26, 27	AM & SG
Reinforced Plate	0.6	5_Wet_Modal_Analysis_028 – 036	28, 29, 30, 34, 35, 36	AM & SG
Reinforced Plate	0.56	6_Regular_Wave_Impact_005 – 009	5, 6, 7, 8, 9	AM
Reinforced Plate	0.6	6_Regular_Wave_Impact_010 – 014	10, 11, 12, 13, 14	AM

Table 8 Overview of different experiments including their water levels and gate type. The last column denotes the measurement device from which the data was taken: Accelerometers (AM) and/or Strain gauges (SG).

7.3 Identified modes

The merged datasets are analysed using the FDD method, from which several mode shapes and natural frequencies are retrieved. The unique mode shapes are then obtained via a MAC analysis, for which high values (close to one) mean high correspondence between two modes. First the dry modes of the Solid and Reinforced Plate are treated, after which the wet modes of both plates are elaborated.

7.3.1 Identified dry modes

As readily discussed in paragraph 7.1 the identified dry modes enable to execute different types of analyses. The modes that are detected are used for input of the SA model in paragraph 7.4.3 and 7.4.4. The modal shapes are obtained by interpolating the eigenvectors from the FDD analysis on a grid that represents the plate.

Solid Plate

The dry modes of the solid plate are obtained using the datasets *3_Dry_Modal_Analysis_008, 009 & 010* (see Table 8). The singular values show clear peaks, indicating modes at the corresponding frequencies. Figure 33 gives the singular value plot for dataset *3_Dry_Modal_Analysis_008*. The modes are checked on their uniqueness using the MAC matrix. A diagonal matrix gives an impression on the fact that all modes are unique.

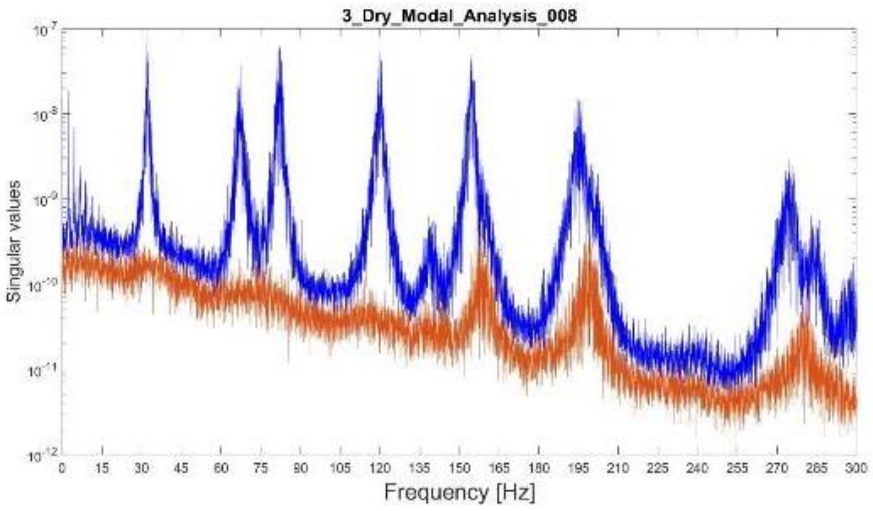

Figure 33 Singular Value Plot for dry modal analysis of the Solid Plate

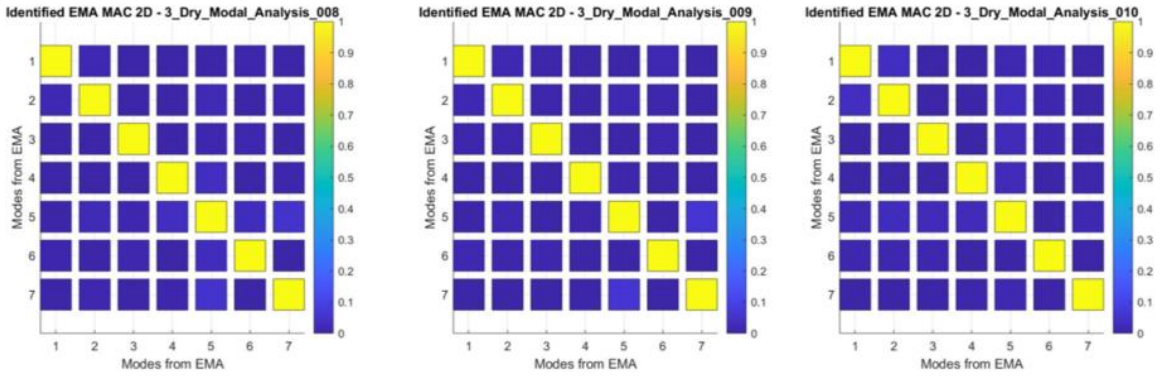

Figure 34 MAC matrices for identified dry modes of the Solid Plate. The bar at the right side of the diagrams explains the colour coding of the MAC values. Yellow depicts a MAC value of 1, blue a MAC value of 0.

Figure 34 gives the MAC matrices comparing the identified modes with each other. The matrices are showing a clear diagonal matrix for all datasets. All dry modes that are identified can be classified as unique. Table 9 gives the corresponding frequencies. Figure 35 gives an overview of the unique dry modes that are detected using a FDD analysis.

Data ID	**f_1 [Hz]**	**f_2 [Hz]**	**f_3 [Hz]**	**f_4 [Hz]**	**f_5 [Hz]**	**f_6 [Hz]**	**f_7 [Hz]**
008	32.3	67.4	82.0	119.7	139.2	154.3	195.5
009	32.2	67.2	82.3	119.8	138.8	154.7	195.1
010	32.2	67.3	81.7	119.8	140.2	154.2	195.2

Table 9 Natural Frequencies of the identified dry modes of the Solid Plate

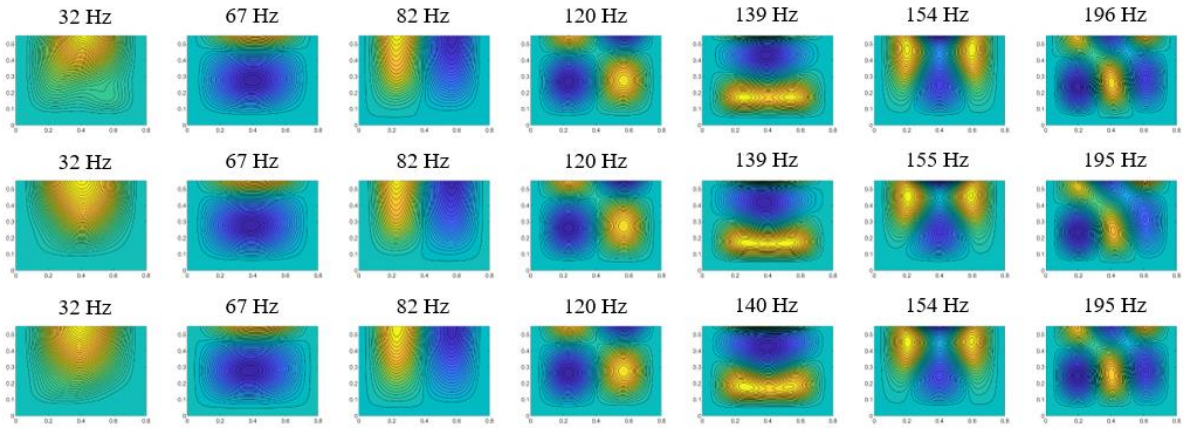

Figure 35 Dry mode shapes for Solid Plate. Top) 3_Dry_Modal_Analysis_001, middle) 3_Dry_Modal_Analysis_002, bottom) 3_Dry_Modal_Analysis_003.

Reinforced Plate

The Reinforced Plate makes use of the datasets *3_Dry_Modal_Analysis_033, 034 & 035*. Following the same reasoning as for the Solid Plate the Singular Value Plots and MAC matrices can be obtained (Figure 36 & Figure 37). Again, a diagonal matrix is observed, but with relatively larger non-diagonal MAC values for several modes. This might indicate that modes are unique but that experiments are not executed properly. Reasons for this might be found in the fact that stiffness and damping play a considerable role in the amplitudes of the accelerations and strains. Therefore, the datasets might be inefficient for analysis.

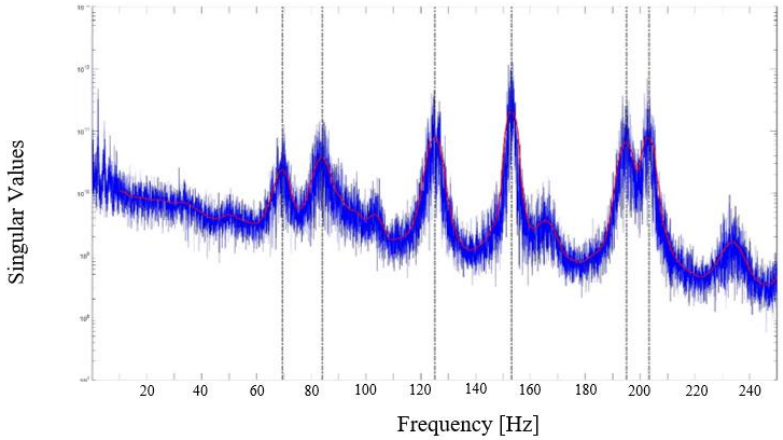

Figure 36 Singular value plot from which the natural frequencies are retrieved for the Reinforced Plate. Singular value plot retrieved from dataset 3_Dry_Modal_Analysis_033.

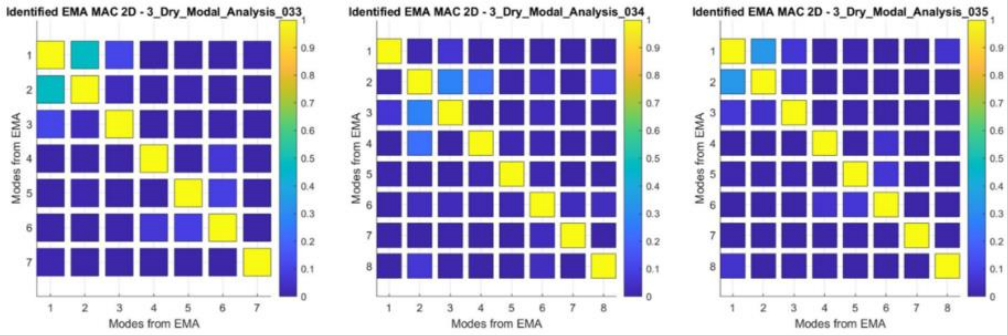

Figure 37 MAC matrices for identified dry modes of the Reinforced Plate. Yellow depicts a MAC value of 1, blue a MAC value of 0.

Data ID	f_1 [Hz]	f_2 [Hz]	f_3 [Hz]	f_4 [Hz]	f_5 [Hz]	f_6 [Hz]	f_7 [Hz]
033	69.48	83.95	125.11	153.05	165.63	195.09	203.29
034	69.56	84.15	124.72	153.02	165.98	195.11	202.83
035	69.63	83.77	124.92	153.10	165.34	195.02	202.73

Table 10 Natural Frequencies of the identified dry modes of the Reinforced Plate

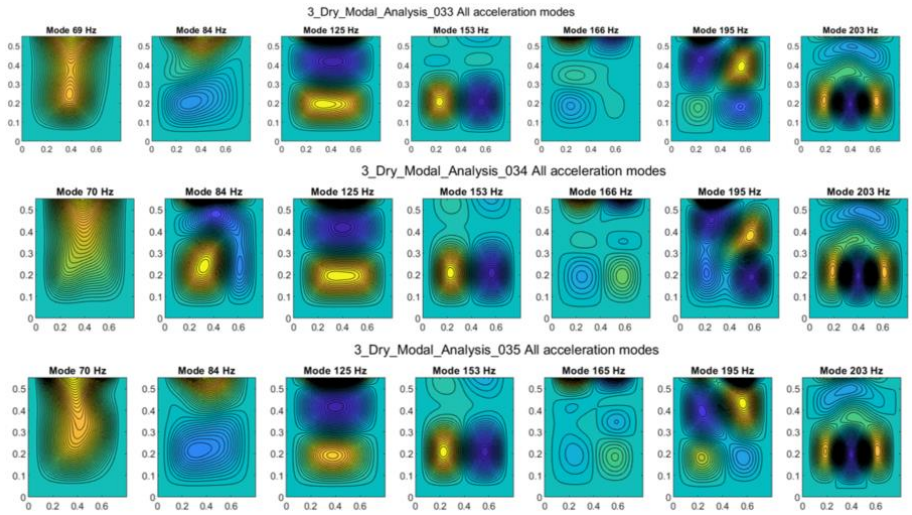

Figure 38 Overview of the dry mode shapes of the Reinforced Plate using a FDD analysis

7.3.2 **Identified wet modes**

The identified wet modes are considered while performing a validation of the SA model. They serve as input in the MAC analysis for different water levels in order to obtain a scientific base for comparison between the identified modes and the SA predicted modes.

Solid Plate

The datasets used for the wet modal analysis of the solid plate are subdivided into different water levels. Table 11 gives an overview of the merged datasets per water level. Again, the datasets are process in terms of zero mean averaging and detrend as described in §5.3. This procedure is done before the datasets where merged. For the water level of 0.6 meters only datasets 013 were available, since the other two experiments turned out to have failed.

Water level	Merged datasets
0.3 m	*5_Wet_Modal_Analysis_004 - 006*
0.4 m	*5_Wet_Modal_Analysis_007 - 009*
0.5 m	*5_Wet_Modal_Analysis_010 - 012*
0.56 m	*5_Wet_Modal_Analysis_016 - 018*
0.6 m	*5_Wet_Modal_Analysis_013*

Table 11 Datasets per water level for the wet modal analysis of the Solid Plate

The MAC matrices for the identified modes for different water levels are depicted in Figure 39. It can be clearly seen that for all water levels identical modes are detected since the MAC matrices show a clear diagonal pattern. The corresponding natural frequencies are listed in Table 12. An overview of the corresponding modes is presented in Figure 40.

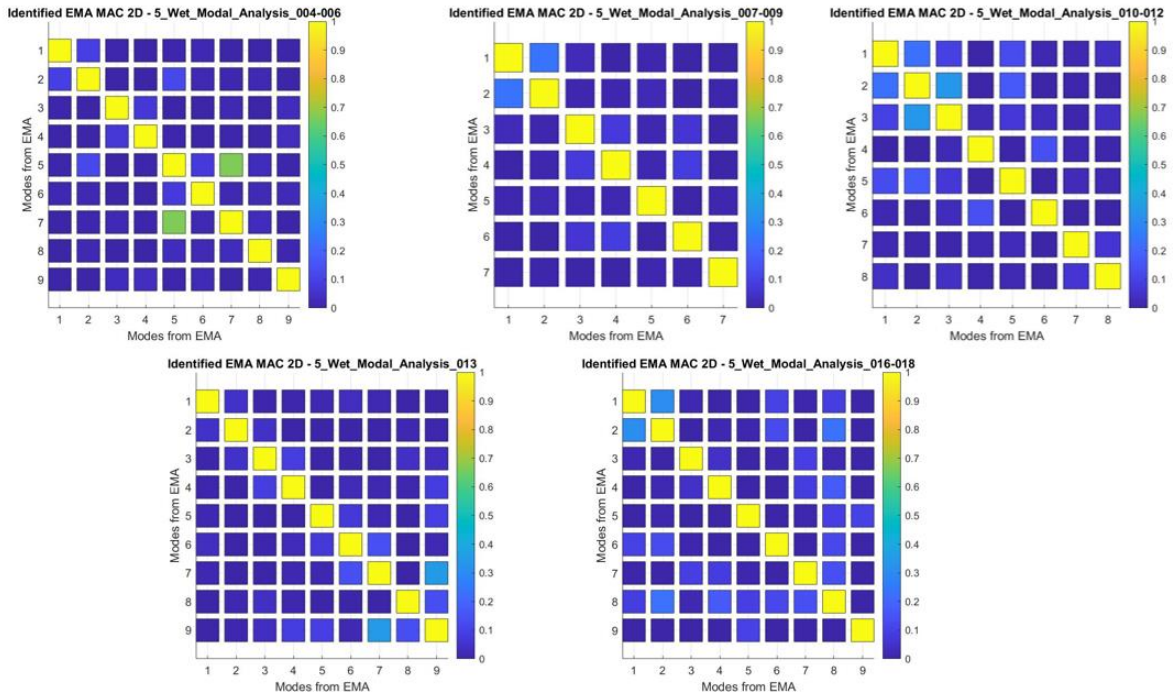

Figure 39 MAC matrices for wet modal analysis for different water levels at the Solid Plate. The modes detected are all unique modes.

Waterlevel	f_1 [Hz]	f_2 [Hz]	f_3 [Hz]	f_4 [Hz]	f_5 [Hz]	f_6 [Hz]	f_7 [Hz]	f_8[Hz]	f_9[Hz]
0.3 m	27.9	49.1	63.3	91	100	115.3	136.9	163.1	171.9
0.4 m	20.7	44.6	50.2	89.9	96.6	131.6	154.6		
0.5 m	15.9	42.2	45	78.5	86.5	124.6	135.2	188.8	
0.56 m	13.2	32	38.3	65.8	77	81.9	116.9	130.5	170.8
0.6 m	10.5	29.6	33.5	52.2	72.1	74.1	97.2	104.8	122.5

Table 12 Natural frequencies for identified wet modes for the Solid Plate

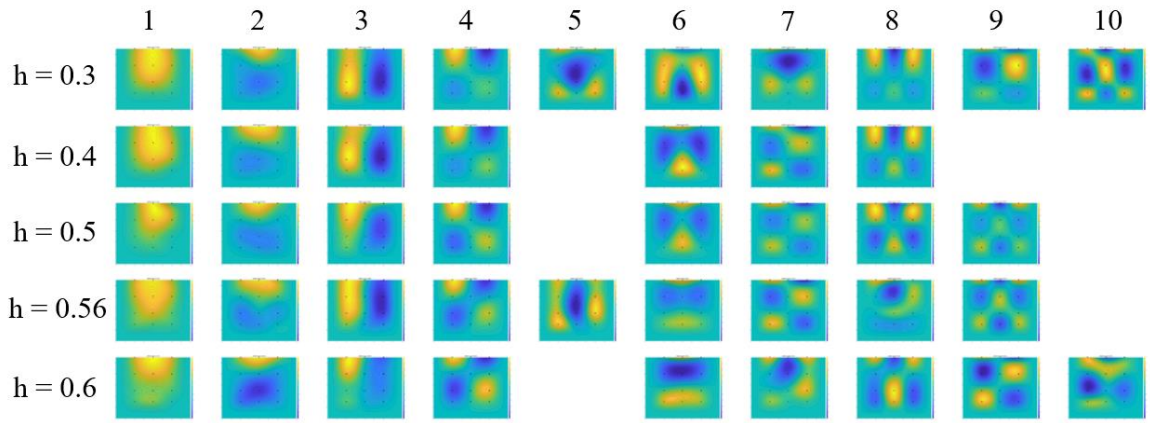

Figure 40 Mode shapes from accelerometers for the Solid Plate for different water levels

Reinforced Plate

The reinforced plate's wet modal analysis makes use of the regular wave impact datasets as well. The main reason for doing so is that the plate experiences high damping and relatively small excitation amplitudes. Hammering might therefore cause insufficient deflections, accelerations and/or strains. The datasets that are used are given in Table 13. For these datasets only the strain data is used.

Water level	Merged datasets
0.3 m	*5_Wet_Modal_Analysis_001 – 003*
0.4 m	*5_Wet_Modal_Analysis_008 – 010*
0.5 m	*5_Wet_Modal_Analysis_015 – 017*
0.56 m	*5_Wet_Modal_Analysis_019 – 021 & 025 – 027* *6_Regular_Wave_Impact_005 – 009*
0.6 m	*5_Wet_Modal_Analysis_028 – 030 & 034 – 036* *6_Regular_Wave_Impact_010 – 014*

Table 13 Datasets used for the Wet Modal Analysis for the Reinforced Plate.

The MAC matrices reveal that for multiple experiments modes are detected multiple times. Modes that are not unique are marked with a red circle. Removing one of the set of double modes from the datasets leaves the natural frequencies and mode shapes as given in Table 14 and Figure 42.

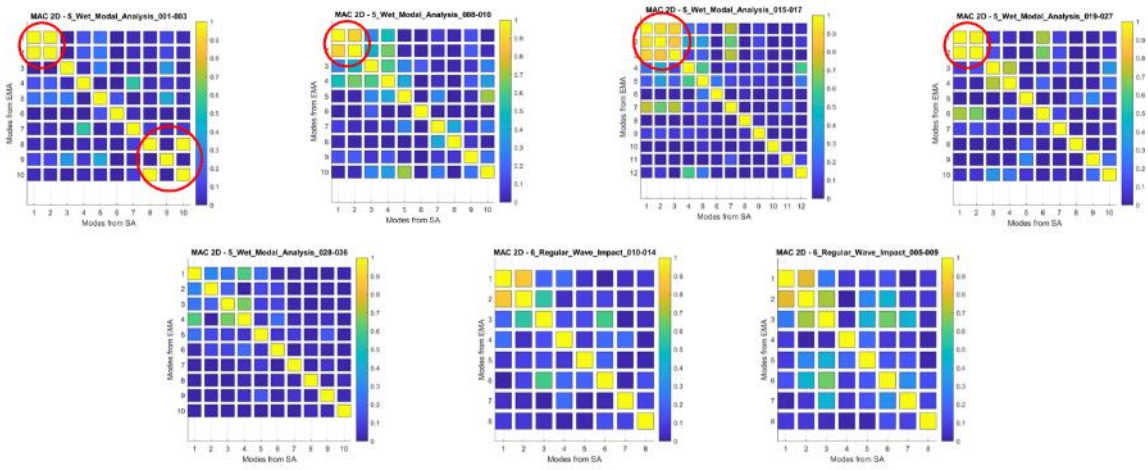

Figure 41 MAC matrices for Wet modes of the Reinforced Plate. Some modes are detected twice and will be removed from the set of modes.

Waterlevel	f_1 [Hz]	f_2 [Hz]	f_3 [Hz]	f_4 [Hz]	f_5 [Hz]	f_6 [Hz]	f_7 [Hz]	f_8[Hz]	f_9[Hz]
0.3 m	72.3	101.2	125.7	155.6	163.9	180.1	205.3	230.35	
0.4 m	32.8	40.2	55.5	66.2	87	125.8	146.8	174.2	187.8
0.5 m	26.1	50.4	52.5	88.3	112.9	122.7	131.1	162.2	
0.56 m	19.4	45.6	69.4	82.1	110	126	141.5	170.3	190
0.56 m (RWI)	16.5	21.5	30.7	51.1	80.5	90	100.7	115.1	
0.6 m	17.3	22.5	30	38.9	51.4	78.2	112.5	122.1	177
0.6 m (RWI)	13.5	22	30	52.5	81	100.8	115.7		

Table 14 Identified natural frequencies for Reinforced Plate after removing double identified modes. RWI = Regular Wave Impact.

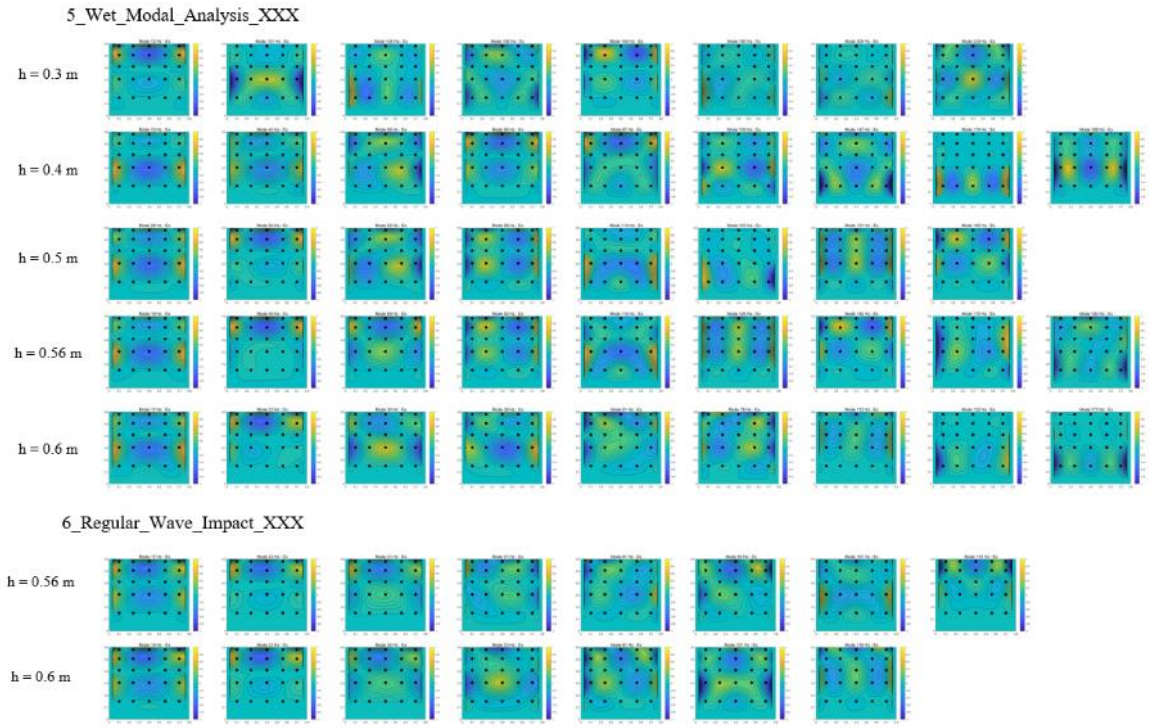

Figure 42 Overview of identified strain modes for the Reinforced Plate

7.4 Comparison SA and FDD modes

An important validation step for the semi-analytical model is to determine whether the dry modes that serve as an input are correct. Besides the dry modes, which can be adjusted for potential better SA results, the wet modes are validated as well. The wet modes are a result of the SA model and therefore directly influence the time series and maxima calculated by the model. This paragraph first elaborates the validation of the dry modes from which conclusion can be drafted regarding the correctness of the SA model input. Afterwards, the wet modes are validated for the case with the FEM modes as input (see §7.1). As a second analysis an adjusted set of FEM modes are used as input together with the corresponding natural frequencies. The identified FEM modes and their updated natural frequencies are used as input. A third analysis focusses on the influence of the boundary conditions. This analysis uses the modal shapes and corresponding frequencies that are found for the dry modal analysis as input for the SA model.

7.4.1 Dry modes

The procedure for validation of the input modes has the same structure as for the identified modes. First a MAC analysis is performed between the identified modes and FEM modes, which is concluded with a comparison between the corresponding natural frequencies.

Solid Plate

The MAC matrices depicted in Figure 43 give a clear view on the correspondence between the identified FDD and the FEM modes. Diagonal matrices are observed, indicating that the identified modes are the same as from the FEM software. This outcome indicates that the correct modes are used in the SA model.

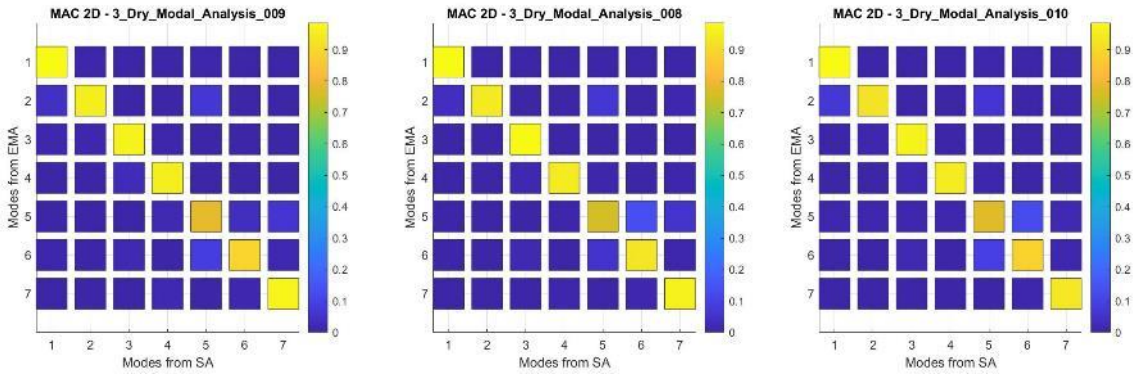

Figure 43 MAC matrices for identified dry FDD modes compared to the predicted SA mode. Clear correspondence between the two is observed.

A second validation step is to determine if the natural frequencies correspond to each other. Graph 2 gives an overview of the natural frequencies for the identified modes compared to the FEM modes. From this graph it can immediately be seen that the SA model consistently predicts about 5-10% higher natural frequencies. This might have several reasons:

1. The boundary conditions of the gate are not as expected. The gate was glued on a U-frame. This might have given complications about the fact that it could be that it was not completely clamped.
2. The material characteristics used in ANSYS differ from the one used in the experiments. Analysis shows a little decline of the natural frequencies, in the order of 1% - 2%.

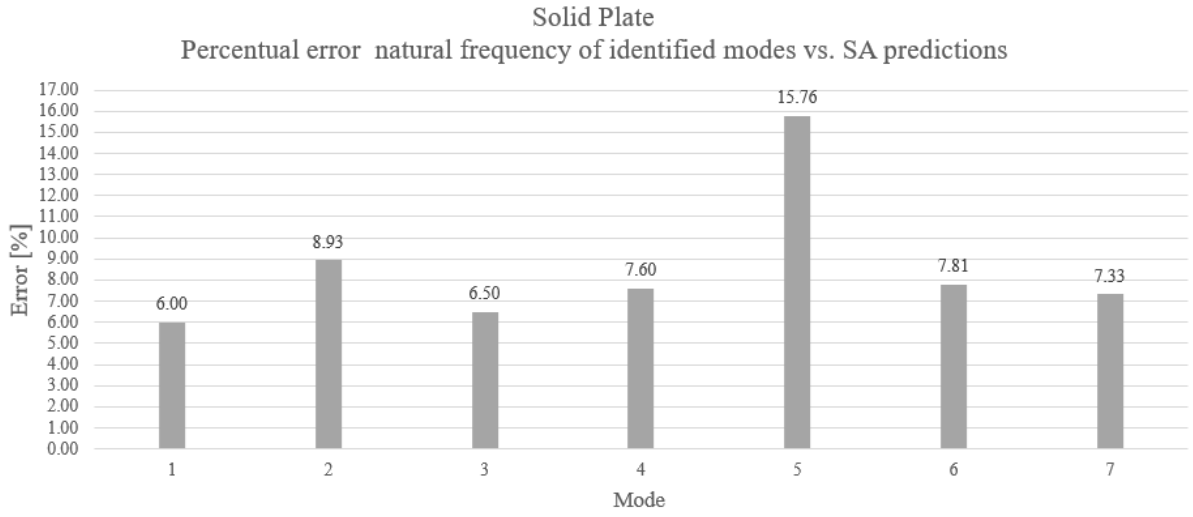

Graph 2 Overview of the natural frequencies percentual deviation. The FEM software consistently overshoots the natural frequencies compared with the experimental results.

Reinforced plate

The reinforced plate has the same approach as the solid plate. Figure 44 gives the results of the MAC analysis for the accelerometer data of the Reinforced Plate. The FEM modes are not identified in all cases. Modes 2 and 7 are poorly identified in all experiments, while mode 6 is not detected at all. These results might serve in an extra validation step for the wet modes, executed in §7.4.3 & §7.4.4. A new set of modes as input could probably give different results in the wet modal analysis of the SA model. Again, the FEM modes overshoot the natural frequencies consistently by approximately 10%, which again might be because of the boundary conditions that are not met.

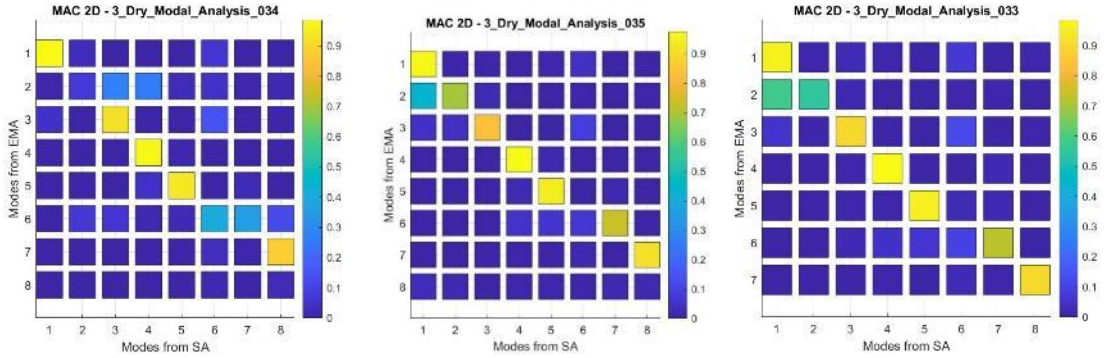

Figure 44 MAC matrices for the identified modes versus the FEM modes for the Reinforced Plate. Modes 1, 3, 4, 5 and 8 are identified consistently.

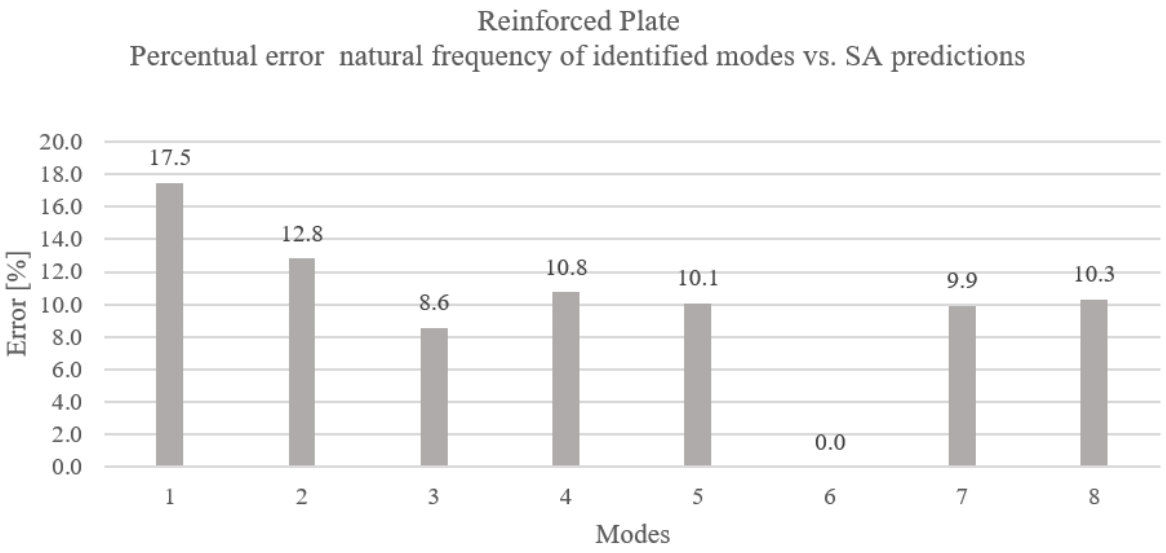

Graph 3 Percentual error of the natural frequencies of the identified and FEM modes for the Reinforced Plate. Mode 6 is not detected in all experiments.

7.4.2 **Wet modes – FEM input**

This analysis focusses on the validation of the SA model using the default FEM modes as input. These modes are generated by ANSYS and correspond to the intended procedure of the SA model. The analysed datasets for the Solid Plate only contain Wet Modal Analysis experiments. The Reinforced Plate also takes the Regular Wave Impact experiments into account.

Solid Plate

The Solid Plate identified wet modes are retrieved from the MAC analysis elaborated in §7.3.2 and are taken into the MAC analysis which compares the SA modes with the experimentally identified ones. The most important modes for the Solid Plate are modes 1 to 4. According to the SA model these modes have the largest contribution to the response of the plate. Table 15 gives an overview of the identified mode that matches the corresponding SA modes. This table also contains a row where the summation of the errors of the first four modes is given. It is clear that mode 5 is not detected for all water levels, only for water levels 0.56 and 0.6 m. Furthermore mode 3 is poorly detected for water level 0.5 m. The green dots show a MAC value higher than 0.75 while the orange dots indicate a value between 0.5 and 0.75.

Waterlevel	Mode 1	Mode 2	Mode 3	Mode 4	Mode 5	Error
0.3 m	1 [0.99] 🟢	2 [0.86] 🟢	3 [0.96] 🟢	4 [0.97] 🟢	-	3.1%
0.4 m	1 [0.99] 🟢	2 [0.94] 🟢	3 [0.92] 🟢	4 [0.97] 🟢	-	2.3%
0.5 m	1 [0.93] 🟢	2 [0.88] 🟢	3 [0.56] 🟠	4 [0.97] 🟢	-	6.0%
0.56 m	1 [0.96] 🟢	2 [0.77] 🟢	3 [0.95] 🟢	4 [0.90] 🟢	5 [0.87] 🟢	2.7%
0.6 m	1 [0.97] 🟢	2 [0.95] 🟢	3 [0.90] 🟢	4 [0.92] 🟢	6 [0.78] 🟢	4.7%

Table 15 Overview of the Identified modes that matches the SA predictions using dry FEM modes as input, corresponding to the MAC matrices with their value between brackets. The last column give the sum of the errors for the first three modes.

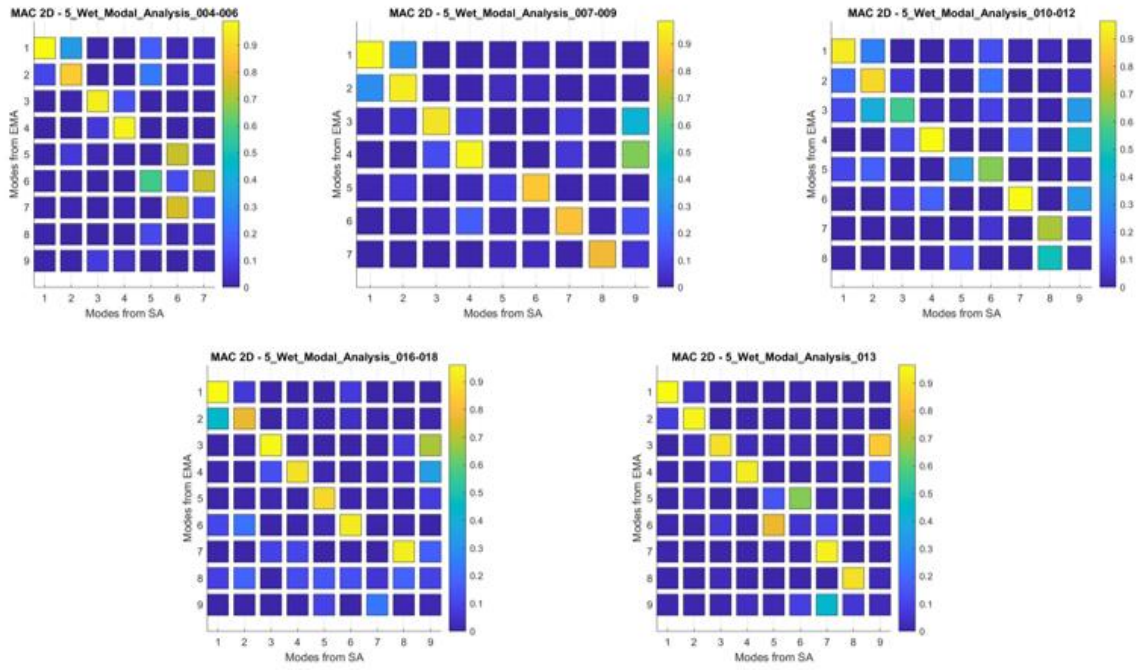

Figure 45 MAC matrices for comparing between the identified modes and the SA prediction using dry FEM modes as input.

The natural frequencies on their turn are analysed and presented in Graph 4. This graph gives the relative error in percentages of the identified modes compared to the SA modes. A negative values means a undershoot while a positive value represents an overshoot by the SA model.

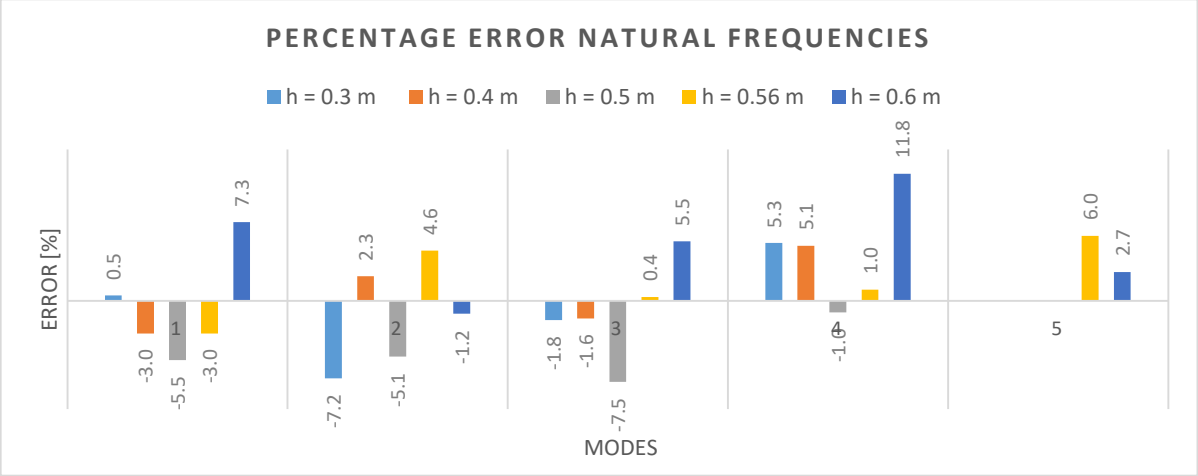

Graph 4 Relative error of identified modes compared with the SA prediction using dry FEM modes as input. Negative values mean an undershoot while positive values represent an overshoot of the SA model.

Reinforced Plate – Strain gauges

Based on the MAC matrices depicted in Figure 46, it can be directly concluded that there is a significant mismatch in the identified modes and the SA modes. A reason for this is the already mentioned amplitude of the deflection (see §6.2) of the gate for relatively small hammer impacts. In the case of a water level of 0.4, 0.5 and 0.6 meters the first three modes are found more or less with small MAC values. Table 16 gives an overview of the identified modes that belong to the SA modes together with their MAC value.

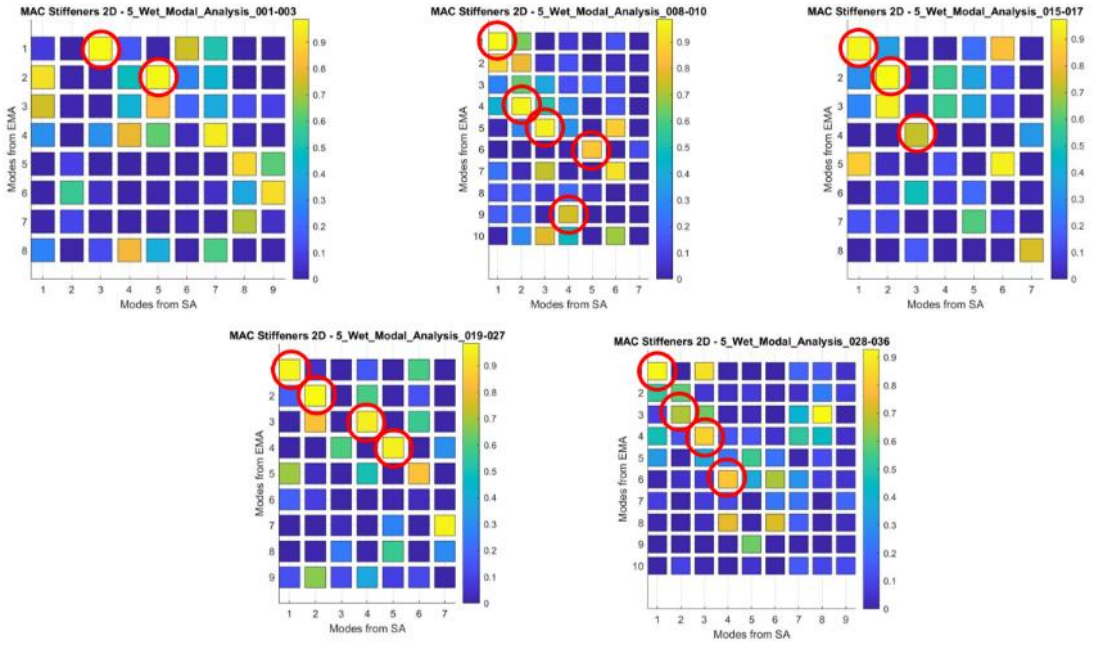

Figure 46 MAC matrices for Reinforced Plate wet modes of the SA model with dry FEM modes as input, compared to the identified wet modes of the experiments. Red circles indicate an identified mode that matches the SA mode

Waterlevel	Mode 1	Mode 2	Mode 3	Mode 4	Mode 5	Error
0.3 m		-	1 [0.99] 🟢		2 [0.97] 🟢	71.7%
0.4 m	1 [0.98] 🟢	4 [0.96] 🟢	5 [0.86] 🟢	9 [0.75] 🟠	6 [0.75] 🟠	6.5%
0.5 m	1 [0.96] 🟢	2 [0.97] 🟢	4 [0.59] 🟠	-	-	8.2%
0.56 m	1 [0.96] 🟢	2 [0.98] 🟢	-	3 [0.94] 🟢	4 [0.96] 🟢	43.3%
0.6 m	1 [0.93] 🟢	3 [0.67] 🟠	4 [0.83] 🟢	6 [0.80] 🟢	-	24.2%

Table 16 Overview of the Identified modes that matches the SA modes with dry FEM modes as input corresponding to the MAC matrices with their value between brackets. The last column denotes the average relative natural frequency error over the first three modes.

The corresponding natural frequencies are analysed, and the SA shows inconsistency for especially the higher water levels. In comparison to the Solid Plate the Reinforced Plate makes larger errors, especially large undershoots. It should be noted that mode 4 at a water level of 0.4 m is highly uncertain. Looking at the stiffeners of the system one can see similarities between the SA and identified mode, however when looking at the inner fields they differ.

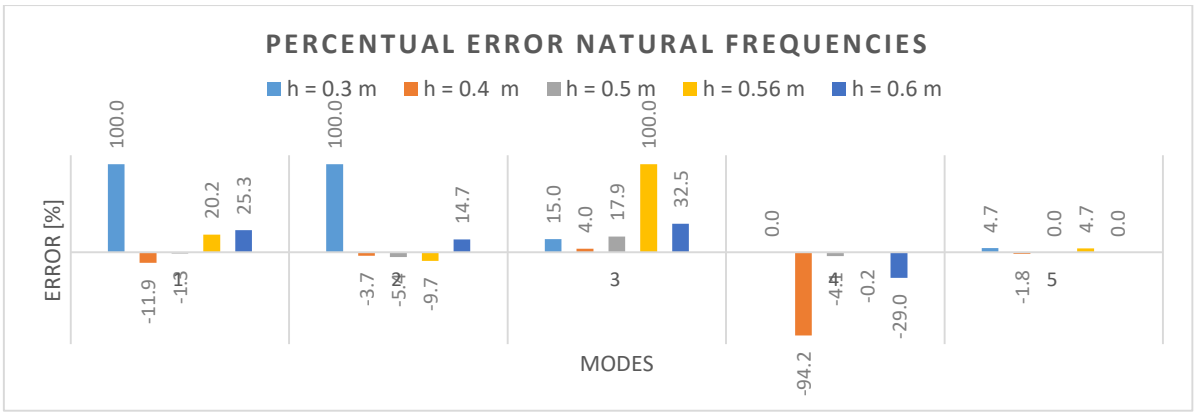

Graph 5 Percentual error of the identified natural frequency compared to the SA prediction. Negative value is an SA overshoot, positive value is an SA undershoot. The dry FEM modes are used for the SA model input.

Reinforced Plate – Accelerometers

To accomplish water levels with large errors in the identification of natural frequencies, the accelerometer data for these experiments is analysed. The identified modes and corresponding natural frequencies are added to the results of the strain gauges. The minimum error of the natural frequency is taken as best fit and is used in the results for the combined dataset.

The following water levels and datasets are considered:

- h = 0.4 meter - 5_Wet_Modal_Analysis_005-010
- h = 0.5 meter - 5_Wet_Modal_Analysis_012-017
- h = 0.56 meter - 5_Wet_Modal_Analysis_019-027
- h = 0.6 meter - 5_Wet_Modal_Analysis_028-036

The MAC matrices of the identified modes in comparison with the SA modes are given in Figure 47. Modes that are not detected with the strain gauge data, or that have large errors with the SA predictions, are identified by the accelerometer data. The natural frequencies of the identified modes that correspond to with the SA modes are given in Graph 6. The graph shows a decline in error for most modes. Interesting to see is that for water levels of 0.5 m and 0.56 m, the third mode is not identified. These modes have exactly the same shape. The strain gauge data gave large errors at this mode for h = 0.5 m while it was not identified for h = 0.56 m, which therefore might indicate that this mode is not correct.

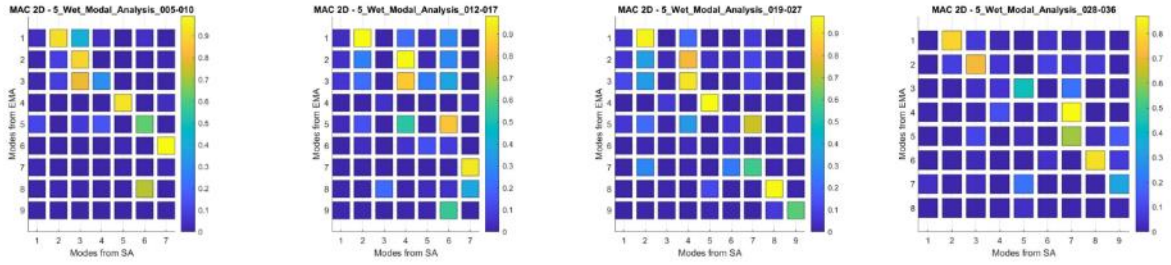

Figure 47 MAC matrices for Reinforced Plate accelerometer data with dry FEM modes as input.

Waterlevel	Mode 1	Mode 2	Mode 3	Mode 4	Mode 5
0.4 m	-	1	2	3 [Visual]	4
0.5 m	-	1	-	2	-
0.56 m	-	1	-	3	4
0.6 m	-	2	3	-	-

Table 17 Matching identified modes with the SA prediction. Mode 4 for h = 0.4 m is added based on visual approval. Dry FEM modes are used as input.

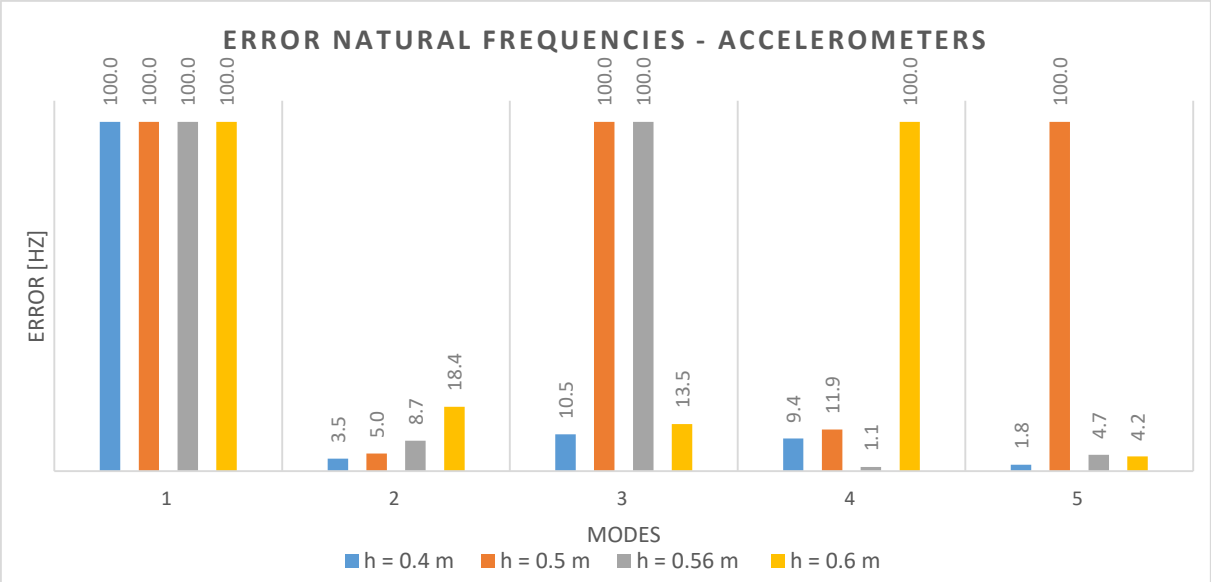

Graph 6 Absolute error of the identified natural frequency compared to the SA mode for the accelerometer data. Negative value is a SA overshoot, positive value is a SA undershoot.

Taking these results into account a total overview of identified modes with the smallest error can be made. Both the strain gauges and accelerometer datasets are taken into account in Graph 7. It can be observed that the errors are reduced significantly when the datasets are both taken into account. Table 18 gives the summation of errors of the first three modes of the strain and accelerometer dataset combined results.

Water level	0.4 m	0.5 m	0.56 m	0.6 m
Error	6.5%	16.7%	43%	17.8%

Table 18 Averaged relative natural frequency error of the first three modes both sensors of the Reinforced Plates using dry FEM modes as input for the SA model.

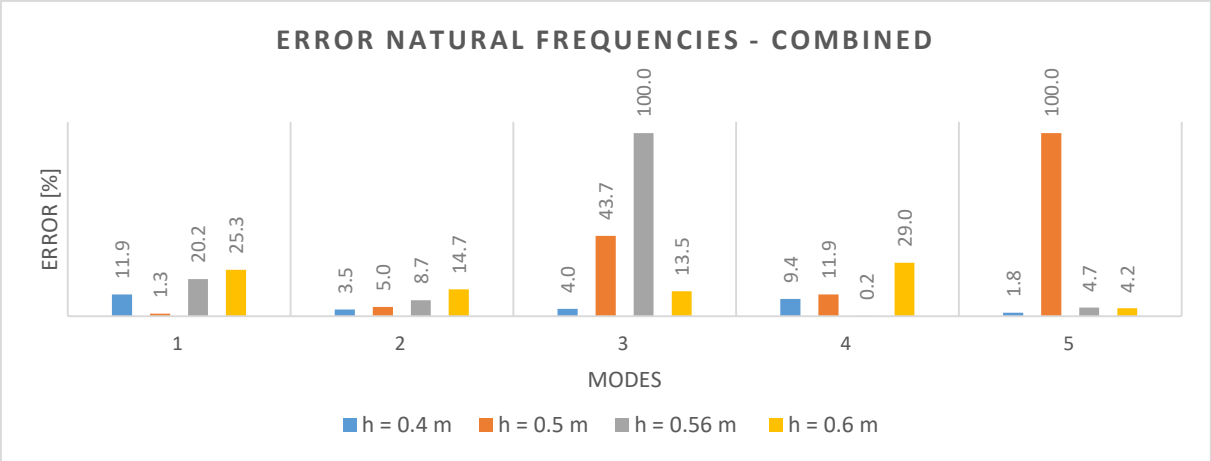

Graph 7 Relative error of the identified natural frequency compared to the SA predictions, using dry FEM modes as input, for the combined strain gauge and accelerometer data. Negative value is an SA overshoot, positive value is an SA undershoot.

Reinforced Plate – Regular Wave Impact

The MAC matrices show a clear identification of the first three modes for both the water level 0.56 and 0.6 meters. High MAC values are obtained for these modes when comparing them to

the SA modes. The absolute error between the SA model and the identified modes is relatively small for the smaller modes (7-10 Hz) while it tends to increase for the higher modes (+/- 16 Hz). Table 19 contains a row with the averaged relative error over the first three modes.

Waterlevel	Mode 1	Mode 2	Mode 3	Mode 4	Mode 5	Error
0.56 m	1 [0.77]	3 [0.82]	4 [0.72]	-	-	27.0 %
0.6 m	1 [0.82]	3 [0.95]	4 [0.78]	-	5 [0.83]	17.9 %

Table 19 Identified modes linked to the SA modes for the Regular Wave Impact experiments with dry FEM modes as input for the SA model.

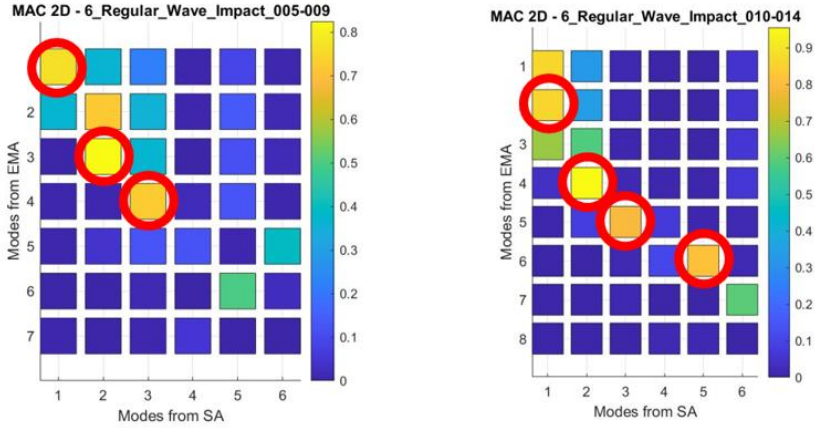

Figure 48 MAC matrices for the Regular Wave Impacts for the Reinforced Plate with FEM input. The first three modes are clearly identified.

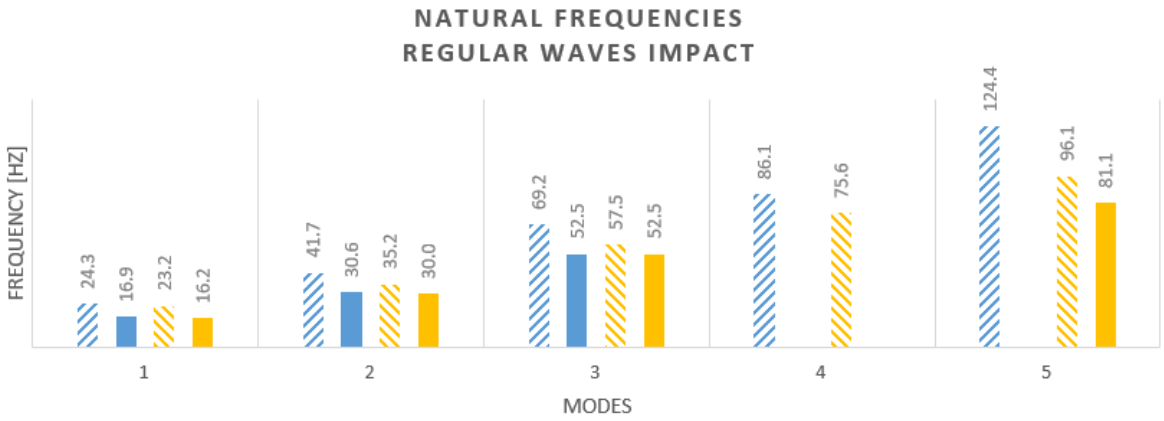

Graph 8 Relative error of the identified natural frequency for regular wave experiments compared to the SA mode with dry FEM modes as input. Negative value is an SA overshoot, positive value is an SA undershoot.

7.4.3 Wet modes - Adjusted set of FEM modes input

In order to investigate the influence of the input modes a set of adjusted FEM modes is used. The set contains the mode shapes from the FEM modes that are identified during the dry modal analysis experiments. The corresponding natural frequencies are updated using the results from the dry experiments.

Solid Plate

The input from the identified dry modes is limited to the natural frequencies that are found. The modes that are identified have a corresponding shape to the ones generated by the FEM software. The natural frequencies of the input modes are readily given in Table 9 in §7.4.1.

Data ID	f_1 [Hz]	f_2 [Hz]	f_3 [Hz]	f_4 [Hz]	f_5 [Hz]	f_6 [Hz]	f_7 [Hz]
008	32.4	67.5	82.0	119.7	136.2	154.5	195.2

Table 20 Identified modes and their natural frequencies of the Solid Plate. These serve as new input for the SA calculations.

The modes generated by the SA model did shift in both natural frequencies and shape, while changing the input modes. The natural frequencies turned out to be lower than for the case with the FEM input. In total more modes have been found, but a negative side effect is that the error with respect to the frequencies has grown. The overall natural frequencies of the SA model declined, which causes the increase of the deviation of the summation of errors of the first four modes.

Waterlevel	Mode 1	Mode 2	Mode 3	Mode 4	Mode 5	Error
0.3 m	1 [0.99]	2 [0.86]	3 [0.90]	4 [0.94]	5 [0.62]	9.2%
0.4 m	1 [0.99]	2 [0.95]	3 [0.90]	-	5 [0.68]	8.3%
0.5 m	1 [0.93]	2 [0.88]	3 [0.56]	5 [0.71]	-	14.3%
0.56 m	1 [0.96]	2 [0.78]	3 [0.95]	4 [0.86]	6 [0.64]	6.3%
0.6 m	1 [0.97]	2 [0.95]	3 [0.90]	4 [0.93]	5 [0.83]	4.8%

Table 21 Overview of the Identified modes that matches the SA modes, using an adjusted set of dry FEM modes as input, corresponding to the MAC matrices with their value between brackets. The last column gives the averaged relative natural frequency error over the first three modes

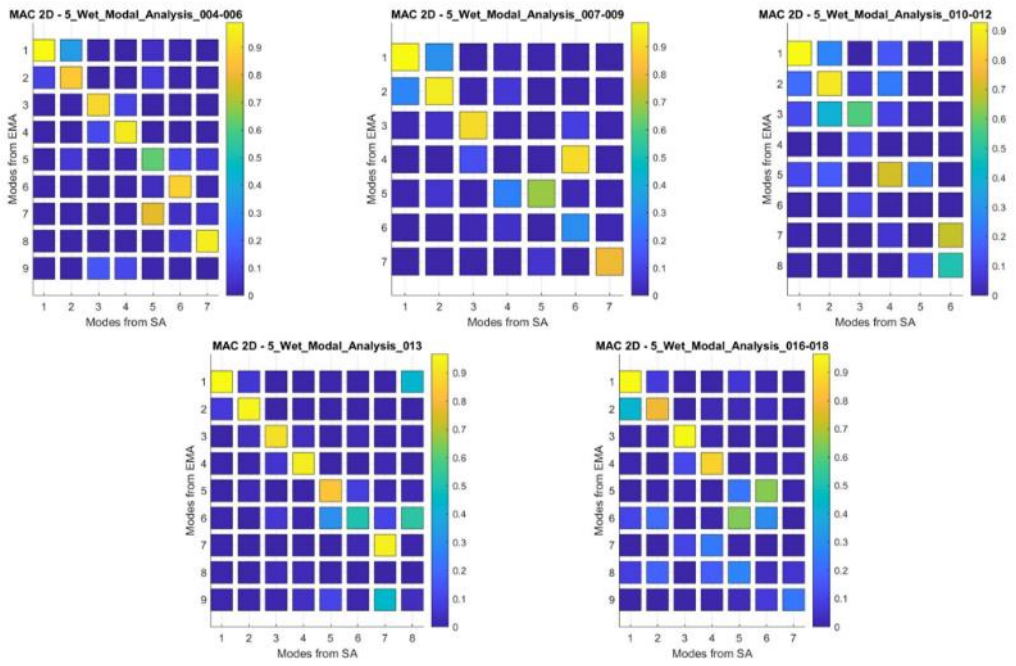

Figure 49 MAC matrices for Solid Plate wet modes of the SA model with adjusted set of dry FEM modes as input, compared to the identified wet modes of the experiments. Every matrix corresponds to a water level.

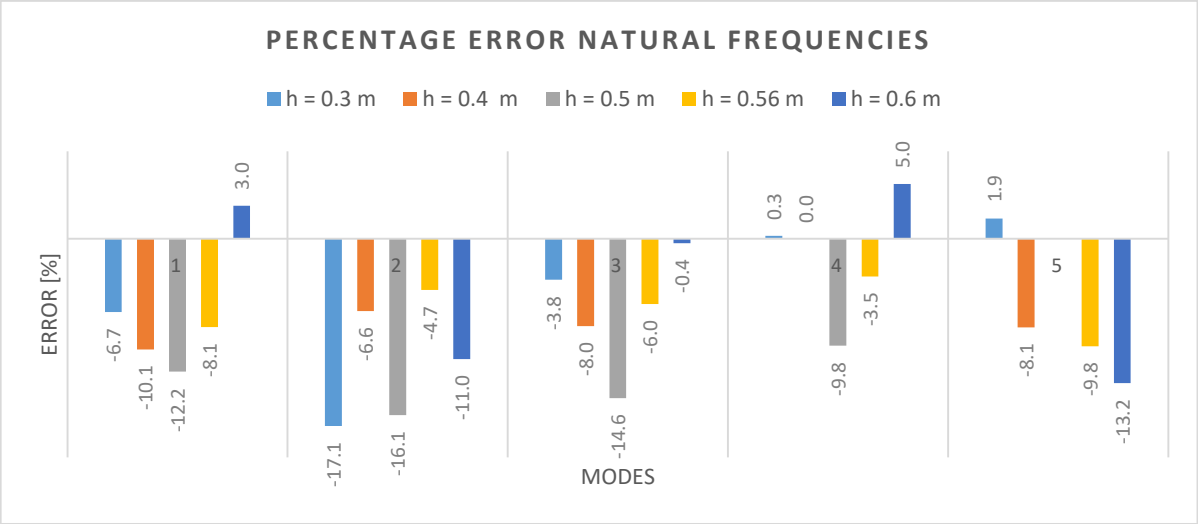

Graph 9 Relative error of identified modes compared with the SA modes using the adjusted set of dry FEM modes as input. Negative values mean an undershoot while positive values represent an overshoot of the SA model.

Reinforced Plate – Strain gauges

The scarcity of correct identified modes directly while using a total set of FEM modes as input, leads to use the identified dry modes in the analysis. In §7.4.1 it was observed that dry mode 6 was poorly identified. It will therefore be excluded from the input modes. Furthermore the natural frequencies of the dry modes will be adjusted to the values the where identified. The new values are listed in Table 22. It seems that the adjustment of the input didn't result in detecting other modes. Nevertheless, the modes that are detected have a rather high MAC value and can therefore incorporated in the analysis with high insurance. Table 23 gives an overview of the SA modes matched with the identified ones.

Mode	1	2	3	4	5	6	7
$\mathbf{f_n}$	69.6 Hz	83.9 Hz	124.9 Hz	153.1 Hz	165.7 Hz	195.1 Hz	203 Hz

Table 22 Identified modes and their natural frequencies of the Reinforced Plate. These serve as new input for the SA calculations.

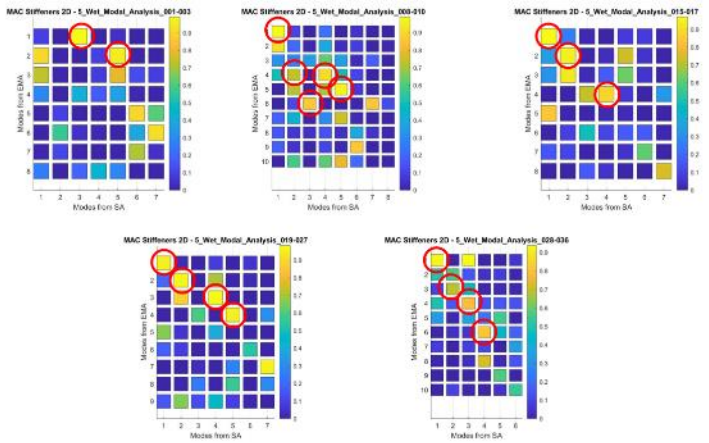

Figure 50 MAC matrices for Reinforced Plate wet modes of the SA model using the adjusted set of dry FEM modes as input, compared to the identified wet modes of the experiments. Red circles indicate a identified mode that matches the SA mode

Waterlevel	Mode 1	Mode 2	Mode 3	Mode 4	Mode 5	Error
0.3 m	-	-	1 [0.99]	-	2 [0.96]	67%
0.4 m	1 [0.99]	4 [0.72]	6 [0.86]	-	5 [0.97]	52.4%
0.5 m	1 [0.97]	2 [0.94]	-	4 [0.86]	-	45.7%
0.56 m	1 [0.95]	2 [0.97]	-	3 [0.96]	4 [0.95]	43.9%
0.6 m	1 [0.92]	3 [0.70]	4 [0.79]	6 [0.82]		13.4%

Table 23 Overview of the Identified Reinforced Plate modes that matches the SA modes, using the adjusted set of dry FEM modes as input, with their MAC value between brackets. The averaged natural frequency error of the first three modes is depicted in the last column.

Just like the case for the Solid Plate, again a decrease of the natural frequency of the SA modes is observed. This results in a shift downwards of the errors. Graph 10 gives an overview of these errors, for which the positive value became smaller and the negative values larger.

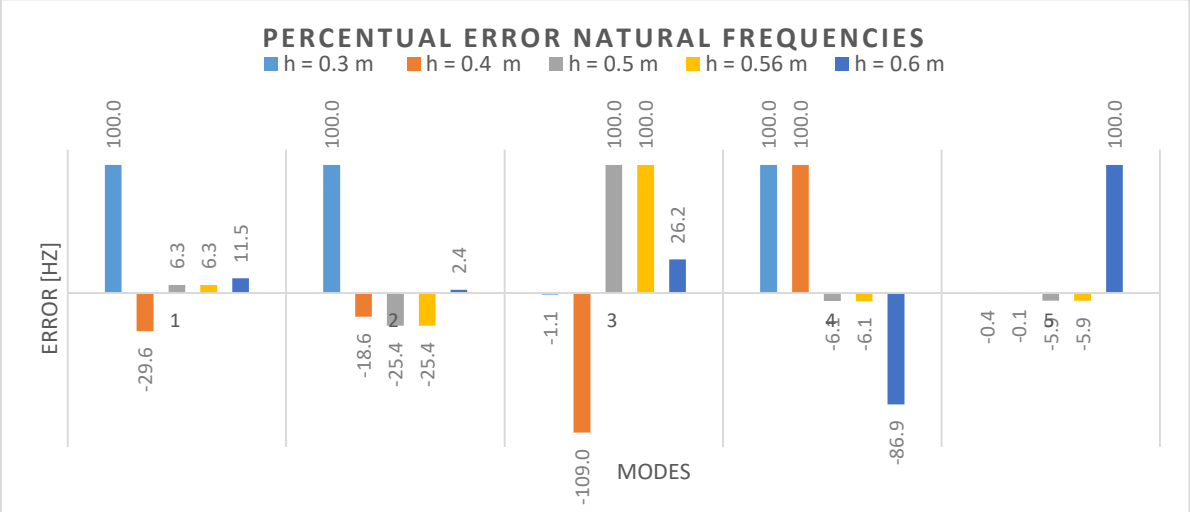

Graph 10 Error of the identified natural frequency compared to the SA mode. Negative value is an SA overshoot, positive value is an SA undershoot. The adjusted set of dry FEM modes are used as input for the SA model.

Reinforced Plate – Regular Wave Impact

Regarding the mode shapes, the adjustment of the modes for input did result in the same identification of modes. Both plates show high MAC values for the first three modes, which was the case for the situation where all FEM modes were used as input.

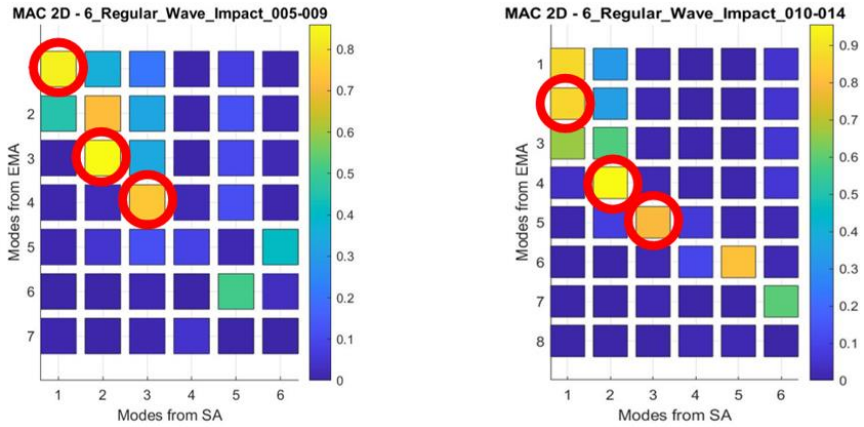

Figure 51 MAC matrices for the Regular Wave Impacts for the Reinforced Plate with adjusted set of dry FEM modes input.

Waterlevel	Mode 1	Mode 2	Mode 3	Mode 4	Mode 5	Error
0.56 m	1 [0.83]	3 [0.72]	4 [0.76]	-	-	12.6 %
0.6 m	1 [0.86]	3 [0.95]	4 [0.79]	-	-	6.6 %

Table 24 Identified modes compared linked to the corresponding SA prediction using the adjusted set of dry FEM modes as input. The averaged relative error over the first three modes is given in the last column.

The corresponding identified frequencies show a very well correspondence with the SA modes when the adjusted set of FEM modes are used as input. The absolute error for the first three modes, that were dominant, declined rapidly to a maximum of 6 Hz and 13.3 Hz.

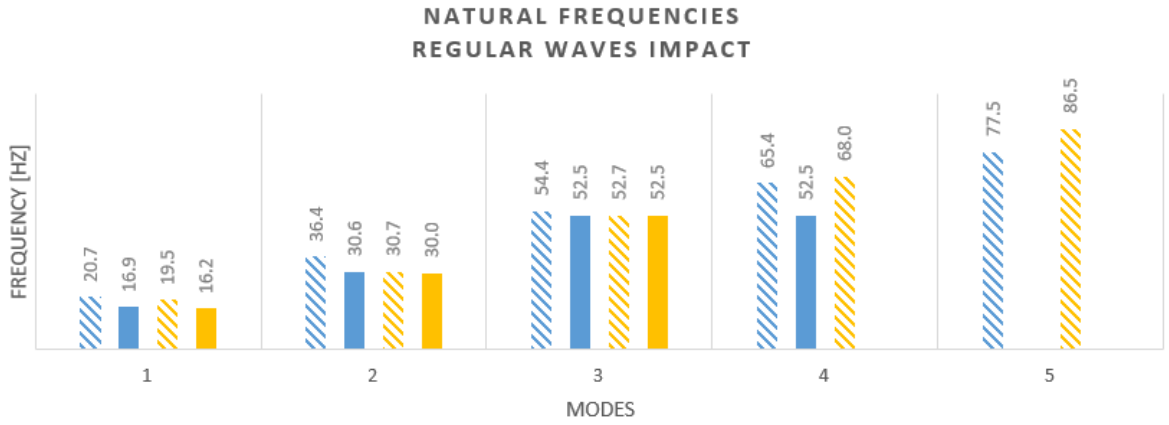

Graph 11 Natural frequencies of the SA model using the adjusted set of dry FEM modes as input and the identified natural frequencies for RWI experiments.

7.4.4 Dry FDD modes input – Influence of bounary conditions

In order to schematize the boundary conditions in the situation of the experiment the modal shapes from the dry modal analysis experiments are used as input. They replace the FEM modes that were used in the previous analyses.

Input modes

The mode shapes and corresponding natural frequencies that serve as input are obtained via the dry modal analysis. The dry modes from the following datasets are considered:

- Solid plate : 3_Dry_Modal_Analysis_008
- Reinforced plate : 3_Dry_Modal_Analysis_035

Figure 52 gives an overview of the modes of both datasets, while the natural frequencies are given in Table 25.

Plate	f_1	f_2	f_3	f_4	f_5	f_6	f_7
Solid	32.3 Hz	67.4 Hz	82.0 Hz	119.7 Hz	139.2 Hz	154.3 Hz	195.5 Hz
Reinforced	69.6 Hz	83.8 Hz	124.9 Hz	153.1 Hz	165.3 Hz	195.0 Hz	202.7 Hz

Table 25 Natural frequencies used for input of the SA model.

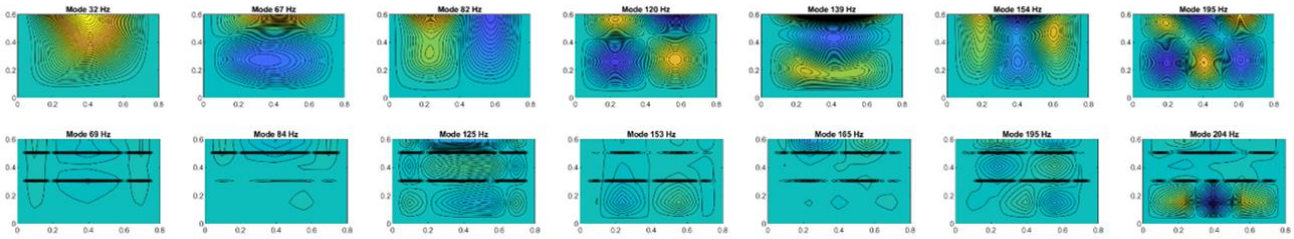

Figure 52 Modes used for input of the SA model. Top row: Dry modes for the Solid Plate, bottom row: Dry modes for the Reinforced Plate.

Solid Plate

The modes that predicted by the SA model are compared to the readily identified modes from datasets:

- h = 0.5 m : 5_Wet_Modal_Analysis_010 - 012
- h = 0.56 m : 5_Wet_Modal_Analysis_016 - 018
- h = 0.6 m : 5_Wet_Modal_Analysis_013

The MAC plots are given in Figure 53 clearly illustrating that in all cases the first four modes have been detected. The percentual error of the natural frequencies that of the SA prediction and the identified modes are plotted in Graph 12. The first mode has relatively large errors. This can be declared by the fact that these natural frequencies are low compared to the rest of the set. Small deviations lead to large percentual errors. The sum of the absolute error is given in Table 26 to quantify the results.

Water level	h = 0.5 m	h = 0.56 m	h = 0.6 m
Error	15.3%	11.0%	8.6%

Table 26 Averaged relative error over the first 3 natural frequencies for the Solid Plate with FDD mode shapes as input.

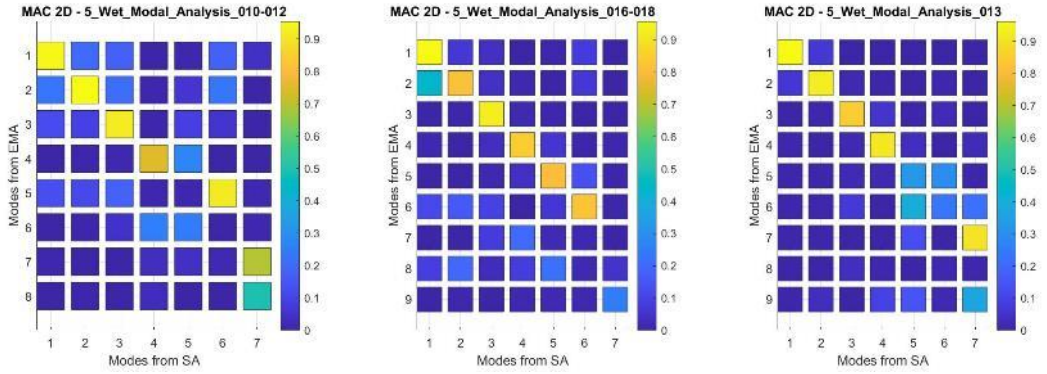

Figure 53 MAC matrices for the Solid Plate wet modes of the SA model with dry FDD mode shapes and frequencies as input.

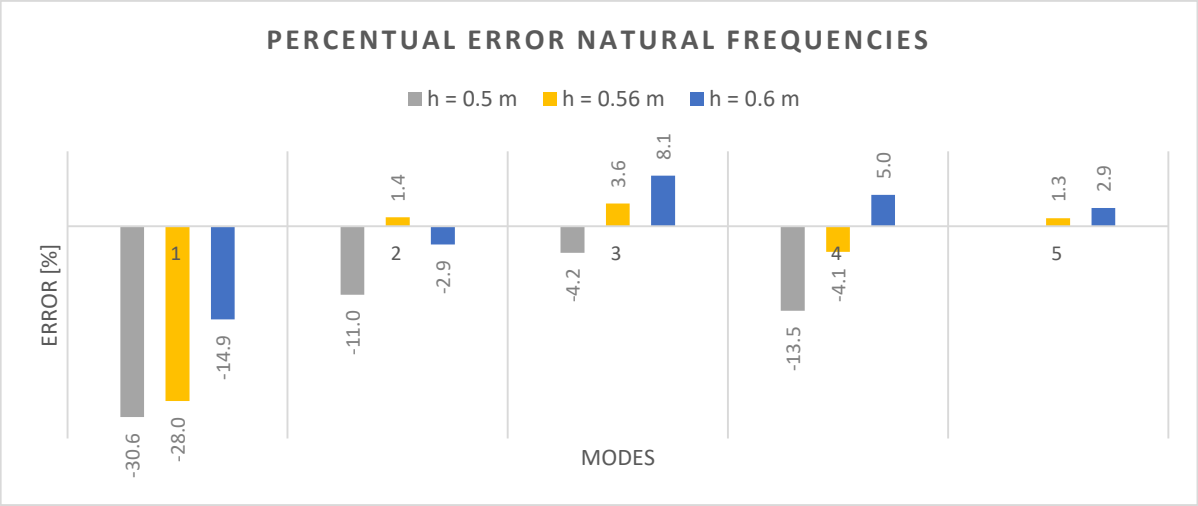

Graph 12 Percentual error of the wet modes of the Solid Plate with the dry FDD mode shapes as input for the SA model.

Reinforced Plate

The new predicted modes by the SA model are compared to the already identified modes of datasets:

- h = 0.5 m : 5_Wet_Modal_Analysis_015 – 017
- h = 0.56 m : 5_Wet_Modal_Analysis_019 – 021 & 025 – 027
- h = 0.6 m : 5_Wet_Modal_Analysis_028 – 030 & 034 – 036

The new input modes did not sort into the desired results. Figure 54 gives the MAC matrices for the different water levels. The MAC matrices reveal directly concluded that out of the first five modes only two are found. In the SA model prediction with FEM modes as input the first three modes were found consistently for these water levels.

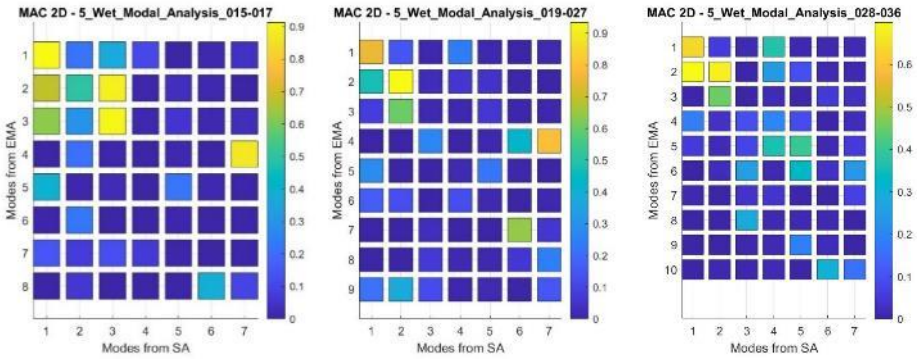

Figure 54 MAC matrices for the Reinforced Plate wet modes of the SA model with dry FDD mode shapes and frequencies as input.

The low resolution of identified modes does not give any reason to investigate the natural frequencies of the system. Conclusions regarding this approach can directly be drafted.

7.4.5 **Overview modal shapes**

This paragraph provides an overview of a selection of modal shapes that are obtained via the different analyses. The structure of the paragraph is such that every plate is treated separately. Solely visual overview are given.

Solid Plate

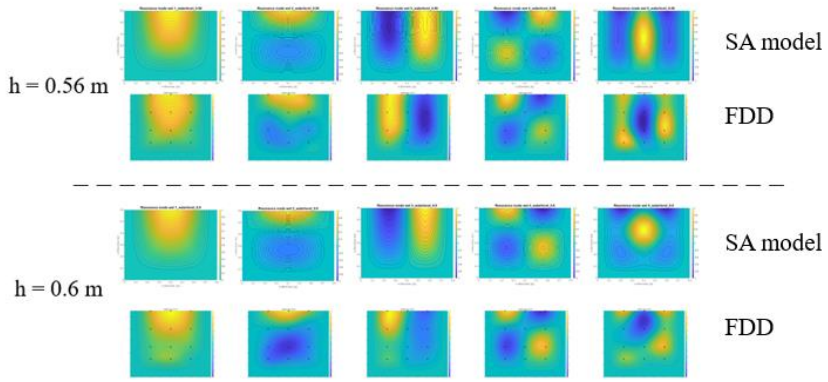

Figure 55 Solid Plate SA modes for FEM mode input (top row) and identified modes (bottom row)

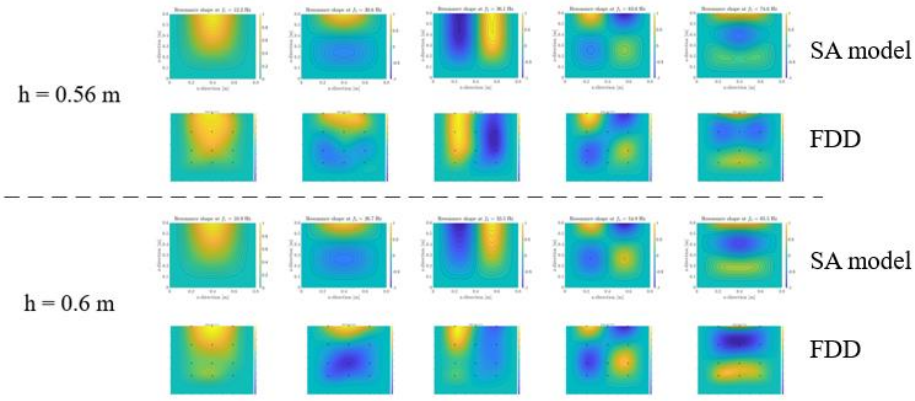

Figure 56 Solid Plate SA modes for the adjusted set of FEM mode input (top row) and identified modes (bottom row)

Reinforced Plate – Strain gauge

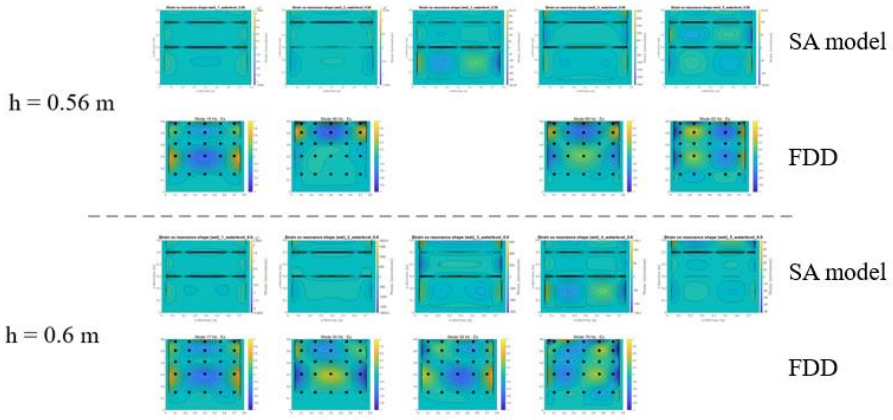

Figure 57 SA model predictions with FEM modes as input (top row) and the identified modes (bottom row) for the Wet Modal Analysis for the Reinforced Plate.

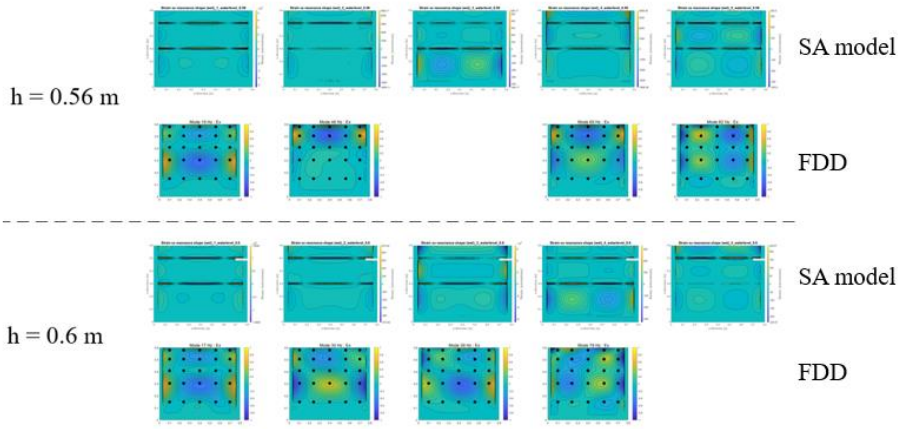

Figure 58 SA model predictions with the adjusted set of FEM modes as input (top row) and the identified modes (bottom row) for the Wet Modal Analysis for the Reinforced Plate. input.

Reinforced Plate – Regular wave impacts

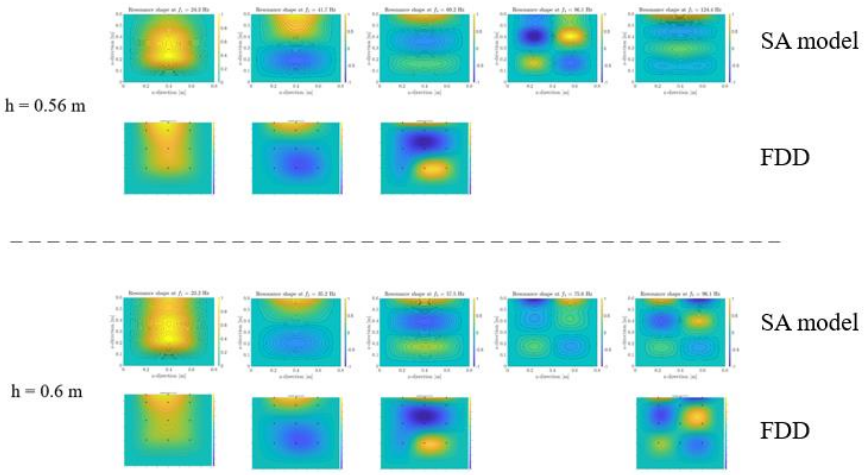

Figure 59 SA model predictions with FEM modes as input (top row) and the identified modes (bottom row) for the Regular Wave experiments for the Reinforced Plate..

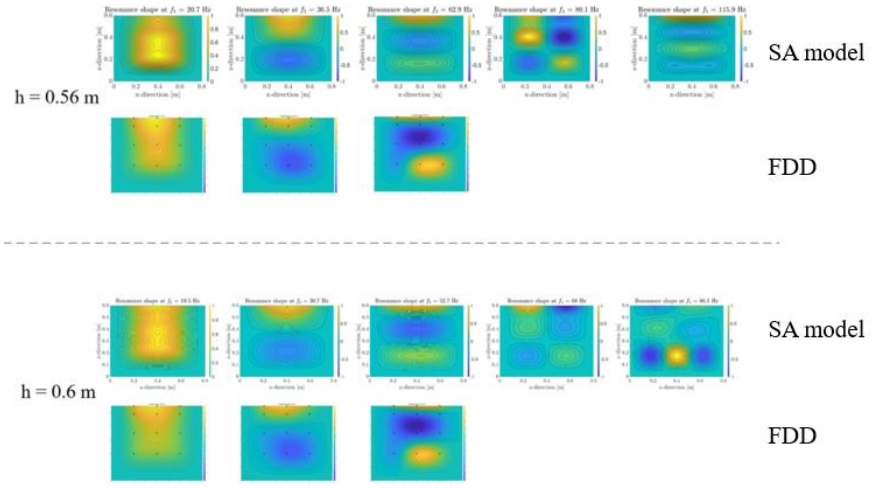

Figure 60 SA model predictions with adjusted set of FEM modes as input (top row) and the identified modes (bottom row) for the Regular Wave Impact experiments for the Reinforced plate.

7.5 Conclusion

This paragraph is intended to give an overview and summary of the results that were found during the analysis executed in the previous paragraphs.

7.5.1 Dry modes

The solid plate shows good correspondence in terms of the MAC values. It can be concluded that for the dry modes, all modes have been identified in the experiments.

The Reinforced Plate shows more deviation on this topic. Mode 6 is not identified at all while modes 2 and 7 are not consistently identified over all experiments.

The natural frequencies on their turn show the same behaviour for both gates. The FEM modes are consistently overshooting the identified FDD frequencies. Especially the Reinforced Plates shows large percentual deviations for the first two modes. The Solid Plate is more or less constant in its overshoot. Values range between the 7 and 16 percent for both gates.

Reasons for the overshoot can be twofold. Firstly, the errors for the Reinforced Plate can be mainly due to the boundary conditions. The gates are glued on a steel U-frame. This glue turned out to be not completely applied on the full contact area between the plate and the U-frame. This might indicate that the gate is not completely clamped. Furthermore, the steel characteristics of the material that was used in the experiments might deviate from the ones used in the FEM modes. This might lead to smaller values for the natural frequencies, which then move slowly towards the ones found in the experiments. The fact that not all modes are found for the Reinforced Plate can be clarified by damping. The single hammer impact experiments reveal that the damping for the Reinforced Plate is approximately 23% higher than for the Solid Plate. This might cause the vibrations to damp out early, so that the FDD analysis cannot detect them sufficiently. This is the reason why Regular Wave Impact tests are used for the wet modal analysis.

7.5.2 Solid Plate – Wet modes

On first basis the mode shapes were found correctly while using the standard FEM modes as an input for the SA model. Mode 1 is dominating the response and was consistently found for all water levels, together with modes 2 and 3. At larger water levels (0.56 and 0.6 m) all modes that were predicted by the SA model were found. The average natural frequency errors of the first three modes varied between 2% and 6%, which are relatively low percentages.

Using the adjusted set of FEM modes as input for the SA model did not result in more identified modes. All cases showed the first three modes, which was the case for the FEM input as well. The natural frequencies that were predicted by the SA model declined rapidly, leading to an increase of the absolute error when compared to the identified modes. Table 27 gives an overview of the average errors of the natural frequencies of the first three modes. The maximum error grew to 14%. Interesting to see is that lower modes now also experience this order of magnitude when it comes to the absolute error.

Input	h = 0.3 m	h = 0.4 m	h = 0.5 m	h = 0.56 m	h = 0.6 m
FEM	3.1%	2.3%	6.0%	2.1%	4.7%
Adj. FEM	9.2%	8.3%	14.3%	6.3%	4.8%

Table 27 Overview of the averaged natural frequency error of the first three modes for the Solid Plate with different input modes.

7.5.3 Reinforced Plate – Wet modes

The wet modal analysis did not give the desired results for the Reinforced Plate. Larger water levels gave a sufficient result in terms of identified modes. Four of the first five modes were found for all water levels, except 0.3 m and 0.56 m. The natural frequencies on their turn where consistently low for the first two modes. The third mode however showed a large natural frequency error with a maximum of 32%. The averaged natural frequency errors of the first three modes for all water levels were observed in a range between 6% and 43%.

Using the adjusted set of FEM modes as input for the SA model resulted in a somewhat similar result, the same modes were identified. MAC values turned out to be somewhat higher which indicates a better mode correspondence. This was limited to only a few modes. The natural frequencies showed the same behaviour as for the Solid Plate. The value of the SA frequencies decreased, which in some cases led to an increase in the error. Table 28 gives an overview of the averaged natural frequency error and the corresponding water level.

Taking the accelerometers into account and subsequently combining the results, give an improvement in terms of mode detection and errors of the natural frequency. All modes are found, except mode three for h = 0.56 m. The situation where all first three modes are identified shows a drastic decline of the error in natural frequencies. This was the case of h = 0.3, 0.4 and 0.6 m. The other water levels show large errors due to the failure in identification of the third mode.

Input	h = 0.4 m	h = 0.5 m	h = 0.56 m	h = 0.6 m
FEM	6.5%	16.7%	43%	17.8%
Adj. FEM	52.4%	45.7%	43.9%	13.4%
Combined	6.5%	16.7%	43%	17.8%

Table 28 Overview of the averaged natural frequency error of the first three modes for the Reinforced Plate with different input mode.

It was already expected that the Wet Modal Analysis for the Reinforced Plate was difficult to execute. The high damping values of the plate ensure that large forces are needed to make the FDD analysis to work. This is difficult to achieve with a smaller hammer.

7.5.4 Reinforced Plate – Regular Wave Impact modes

The expectation was that the Regular Wave Impact experiments would give a better result in terms of identified modes. The first three modes were expected to be dominant in these experiments. It can be concluded that for the situation with the original FEM modes as input for the SA model, the first three modes were detected for both water levels. High MAC values (>0.8) proof that the identified modes had good correspondence with the predicted SA modes.

The natural frequencies again experienced an overshoot by the SA model. Water level of 0.6 m experienced some good predictions, except for the first mode which was almost twice as high compared to the identified one.

Using the identified dry FEM modes as input for the SA calculations, the first three modes were found. The cumulative error with respect to the natural frequencies declined on his turn as well. Smaller natural frequencies for the dry modes established this decline.

Input	h = 0.56 m	h = 0.6 m
FEM	27%	17.9%
Adj. FEM	12.6%	6.6%

Table 29 Overview of the averaged natural frequency error of the first three modes for the Reinforced Plate with different input modes.

7.5.5 Dry FDD modes – Influence of boundary conditions

The Solid Plate showed a limited decrease in the natural frequency error for a water level of 0.6 m. The other water levels showed an increase. It can therefore be concluded that the overall performance declined. The original situation with the FEM modes as input still perform best when looking at the natural frequencies. Regarding the identification of modes, the inclusion of different boundary conditions showed a more accurate identification of the modes. More modes were detected for a water level of 0.5 m, while the other water levels showed equal results with respect to the FEM modes as input.

The Reinforced Plate did not give the desired result. It showed that including the real time boundary conditions were lacking performance. Solely mode 1 & 2 were identified for the larger water levels. This might have several reasons which will be discussed in the discussion in chapter 8.

8 Discussion

The discussion treats the potential errors that have been made during the experiments, which could have influenced the results. This chapter treats potential flaws of the experiments, semi-analytical model and the approach of the analyses that could have influenced the results. The chapter is structured such that first the potential flaws in the experiments are treated. After this paragraph the topics treated are taken as input to elaborate the influence on the validation of the semi-analytical model. The last paragraph proposes an improvements for the experiments to obtain more reliable and accurate results.

8.1 Experiments

The semi-analytical model revealed a large deviation in terms of performance between the Solid Plate and Reinforced Plate. The Solid Plate turned out to be more precise in its match between the SA predictions and identified modes, while the Reinforced Plate showed large errors and unidentified modes. The reasons for this will be treated in the following paragraphs. Since only the Reinforced Plate showed large deviations from the expected outcome, this plate will be discussed in this paragraph.

8.1.1 Calibration of FEM model

In the performed analyses an adjusted set of FEM modes was taken into consideration. Modes that were not detected were assumed to have no play in the response of the gate and were removed from the set of input modes. This could have introduced large errors. In case of not identifying a mode with an experimental modal analysis, cannot imply that a mode is not there. It might well be the case that given certain circumstances it is just missed. Nevertheless this method was chosen as an alternative to calibrate the FEM modes.

Calibration of the FEM model using the results of the experimental modal analysis could have given a model that perfectly reflects the boundary conditions. This was out of scope for this thesis. Nevertheless it might increase the performance of the SA model. Dry modes that represent the real situation are found to be key, when smaller errors are induced in this part the SA model is able to give better predictions for the wet modes (§9.1.3). Calibration of the FEM model may exists of material properties and boundary conditions. Both lead to an influence in the natural frequency.

8.1.2 Loose components of Reinforced Plate

While reinstalling the Reinforced plate for extra additional experiments, it was observed that the stiffeners had come loose from the steel plate. This was also observed for the Solid Plate before the experiments started. This plate however was repaired for the planned experiments and did not fail anymore. Regarding the Reinforced Plate, it was missed and had not been noticed until the plate was reinstalled again. It is therefore not sure when this process of loosening started.

The gates were applied on a steel U-frame by gluing the contact area between the two components. It is well known that applying glue on a steel-steel interface is a rather difficult procedure. The glue must be of high quality and must be applied on the full contact area. Consulting the constructor of the gates afterwards learned that this was not the case. The glue was only partly applied on the contact area.

It is not likely that components come of relatively slowly, since glue is a brittle material. Nevertheless parts of the contact area might have been partly loose during the experiments. Locations where less glue was present might have failed. This should have been identified by using the identified dry modes of the dry modal experiments as input. Doing so for the Reinforced Plate did not give the desired result and still large mismatches were observed. Therefore, it can be assumed that after the dry modal analysis experiments the gate have gotten loose during the submerged experiments.

8.1.3 Inclination and fixation of Accelerometers

During the wave experiments of the Reinforced Plate it was observed that the accelerometers had a large inclination angle after installation. This might have happened for some accelerometers, leading to potentially unreliable calibration for this measurement device.

Another feature that might have taken place is the loosening of the accelerometers. It was observed during the experiments that accelerometers got loose. This resulted in the inclination in the first place but this feature leads to vibrations of the device that do not correspond to the vibrations of the plate. This leads to unreliable acceleration data as well. The spectral density plots of the accelerometers were compared with the strain gauges and nothing extraordinary was observed. The limited frequency band was 500 Hz, so in case of higher frequencies of the loose accelerometers it cannot be concluded based on the data whether the accelerometers where fixed on the plate.

The dry modes that have been identified with the acceleration data show good correspondence with the FEM modes. It is therefore likely that during the wave and wet modal experiments the accelerometers slowly got loose from the plate, resulting in potentially unreliable data. Especially larger water levels might be prone for this. The sequence of tests was first a wet modal experiment where after wave tests were executed.

8.1.4 Effect of large damping Reinforced Plate

The damping ratio in the Reinforced Plate was approximately 20% higher than for the Solid Plate in dry conditions. High damping in systems mean small amplitudes of the response. This can lead to dynamic behaviour that is difficult to measure. The accelerations were in the order 20 m/s^2 for both plates while the strains were 50 – 150 microstrain for the Solid Plate and only 5 – 30 microstrain for the horizontal strains on the front plate of the Reinforced Plate. The vertical strains had larger magnitudes but were not measured due to large local peaks which were difficult to capture (see §6.4). The strains at the stiffeners were in the same order as for

the Solid Plate. Since only the stiffeners showed proper values for the strains, the number of measurement devices was limited which induces errors for these types of complex gates.

Besides the initial amplitude of the response the increase in damping also generates a fast decay of the response. The strains and acceleration damp out quite quickly, 0.1 s for the Reinforced Plate versus 0.5 s for the Solid Plate. The Frequency Domain Decomposition thrives best by many observed cycles of every mode. Due to the fast damping of these cycles it might have been the case that hammering was not hard or long enough for this plate. This was perfectly illustrated by using the wave impact datasets that generate a larger impact force, thus also larger amplitudes and more cycles per impact. The modes with most energy were detected for this situation.

Brincker et al. (2003) state that the minimal time length of a dataset is dependent on the damping and natural frequencies of the structure, as well as the number of segments one opts to choose. Increasing the damping and lowering the natural frequency leads to an increase of desired data length. This is in line with the results that were found.

Nevertheless there is no reason to assume that the SA model's prediction is worse for situations with large damping. The damping of the plate solely affects the performance of the experimental modal analysis and thus the validation of the model. The SA model predicts the same order of magnitude for modal damping over the first three modes of the reinforced plate. Furthermore it was observed that for larger wave impacts the model did not had any difficulties for predicting the modal shapes. Real life structures have larger damping than the plates that were investigated. On the other hand larger impulses excite the structure so the two balance each other.

8.2 Semi-analytical model

The validation of the modal calculations of the semi-analytical model is the main goal of this research. Different types of analyses were performed to obtain a valuable conclusion on this part. The measurements and analysis were executed in order to validate the modal shapes and the natural frequencies of both the reinforced and solid plate. Given the fact that the final output of the semi-analytical model is to predict the maximum displacement and stress of a submerged slender gate with an overhang, still additional research has to be done to come up with a full validation of the model.

The semi-analytical uses dry mode shapes as input for the calculations. Any flaw or difference in these modes that deviate from reality induces errors in the calculations. The model was validated using different experiments for a solid plate and a reinforced plate. Analyses showed that for the solid plate the modal shapes and corresponding natural frequencies were predicted correctly.

8.2.1 Input modes

The semi-analytical predictions of the reinforced plate showed a consistent overshoot of the dry natural frequencies, while the modal shapes turned out to have a high correlation when compared with the experimental data. Reasons for an overshoot in the dry natural frequencies of the reinforced plate can be explained using the previous paragraphs. Most likely the boundary conditions that were assumed in the finite element method, did not reflect the reality. Loosing or partly clamping of the front plate from the U-frame results in a more simply support boundary conditions, inducing lower natural frequencies. The boundary conditions might therefore reflect a partially clamped plate. This pattern was observed during the wave experiments. Adjusting the natural frequencies of the dry input modes resulted in a smaller error of the semi-analytical predictions. The modal shapes turned out to have more or less the same correlation, meaning that the prediction of the semi-analytical model is sufficient on this part. It was observed that, especially for the reinforced plate, more accurate dry natural frequencies result in a better performance of the semi-analytical predictions of the wet natural frequencies. The latter could have been obtained by calibration of the finite element software model. This would have enabled more realistic dry modes that serve as input for the semi-analytical model, resulting in more reliable validation results. It was observed that for the input of the identified dry natural frequencies (Adjusted FEM input) the relative averaged error over the first three natural frequencies dropped from:

- Water level of 0.56 m : 27 % (FEM input) to 12.6 % (Adjusted FEM input)
- Water level of 0.60 m : 17.9 % (FEM input) to 6.6 % (Adjusted FEM input)

8.2.2 Extrapolation of results to other plates

Incorporating stiffeners on a front plate complicates calculations when compared to gates that exists of a front plate alone. Based on the result and relative simple calculations of the solid plate, it can be assumed that the results of the analyses can be extrapolated to a wide series of solid plate geometries. The more complicated geometries (reinforced plates) cannot be assigned the same conclusion based on this research. Although the semi-analytical predictions for the reinforced plate under consideration are in line with the experimental results, more research should be done to conclude the same for even more complicated geometries. §8.3 gives handhelds for improving the experiments. To obtain a 100% validation of the semi-analytical model it is also needed to do research on more gate geometries that have multiple stiffeners in different directions as well.

8.3 Lessons learned - Improvement of analyses

Based on the previous paragraphs some lessons learned for the execution of experiments and analyses can be drafted. Given the large number of potential errors during the experiments of the Reinforced Plate, it is recommended to repeat the experiments for this plate and for more complex geometries. The results showed proper matching between the identified modes and the

predicted SA modes. Nevertheless, the results were not as good as for the Solid Plate. This might have multiple important reasons:

1. Insufficient bonding between the U-frame and plate was likely to influence the dynamic properties and boundary condition because the stiffeners and plate to slowly detached from the U-frame. Although this cannot be said with 100% certainty.
2. Calibration of the FEM model in order to obtain dry modes that have a small error with the reality.
3. Increase in complexity of the semi-analytical calculations resulting in less accurate predictions.

Furthermore the execution of the wet modal analysis revealed some flaws. Most important is that the duration of the experiments was too short. A minimal number of cycles for every modes was not reached. Especially the accelerometers showed the influence of damping in the experiments, leading to a less reliable validation of the semi-analytical model during the wet modal experiments. Longer duration of experiments will fix this issue. In addition harder hits will result in the same remedy.

9 Conclusion & Recommendation

The conclusion starts by repeating the main research question of this thesis, where after a brief overview of the executed analyses is given. This is followed by the most relevant results. Based on these results both an overall conclusion and recommendations will be given. Conclusions are based on the results of the experimental modal analysis of the different experiments that were executed.

9.1 Conclusion

This thesis was performed in order to validate a new semi-analytical (SA) model by Tieleman et al. (2020). This model was developed to determine the dynamic behaviour of flood gates with an overhang that are subjected to standing waves. The model was yet to be validated with modal and wave experiments, which were not carried out before. This research focused on the validation of the modal prediction of the model and whether it holds for general geometries of flood gates.

9.1.1 Recap experiments and analyses

Multiple experiments were executed in order to retrieve a solid validation of the semi-analytical model. First of all dry modal experiments served as a basis for the validation of the input modes for the semi-analytical model. The SA model uses the dry modes of the system in order to perform calculations for the submerged modes and corresponding time series. These experiments revealed the dry natural frequencies and mode shapes of each plate (solid and reinforced). This analysis resulted in a set of identified modes shapes and corresponding natural frequencies. These were gathered in an adjusted set of finite element method (FEM) modes in order to reflect the real boundary conditions of the plates. The default situation, in which the modes generated by FEM software were used as input, was analysed as well.

Wet modal experiments were executed to compare the semi-analytical prediction with the identified mode shapes and frequencies in order to validate the model for the solid plate. The reinforced plate used the experiments that consists of the regular wave impacts. They served the same goal as for the solid plate.

Furthermore the number of identified modes and their modal assurance criterion (MAC) value was a measure for quantifying the performance of the SA model.

9.1.2 Conclusion Solid Plate

The analyses of the Solid Plate showed that the first four wet modes were identified. The SA model predicted that the first mode was dominant and that the second and third had little contribution to the total response of the plate. The first mode was consistently found with MAC values in the order of 0.95, which gives reason to believe the SA prediction was correct. The other modes had MAC values in the order of 0.8 – 0.99, indicating a solid prediction of the SA

model in terms of mode shapes. Using an adjusted set of FEM modes as input did not result in an increase of the results. The SA model is capable of predicting the right wet modal shapes for the solid plate using a set of dry FEM modes as input.

Table 30 Averaged MAC values of the first three modes of the Solid Plate with different input modes.

	Water level	Dry	h = 0.4 m	h = 0.5 m	h = 0.56 m	h = 0.6 m
MAC values	**FEM input**	0.95	0.95	0.79	0.90	0.94
	Adjusted FEM mode input	-	0.95	0.79	0.90	0.94

The error of the natural frequencies where small for the wet modes, based on the relative averaged value of the first three modes. This indicates that the SA model performs the right calculations and that it is able to come up with solid predictions. When observing the averaged natural frequency errors of different modes over the water levels, it shows that the natural frequency error in dry modes directly influences the error of the wet modes. It is observed that the ratio between the two is rather constant with a value of 0.5 - 0.6. This implies that the relative error is approximately halved for the wet modes when compared to the dry modes.

Table 31 Averaged relative error in natural frequencies made by the SA model over the first three modes of the Solid Plate.

	Water level	**Dry**	**h = 0.4 m**	**h = 0.5 m**	**h = 0.56 m**	**h = 0.6 m**
F_n	**FEM input**	7.1%	2.3%	6%	2.7%	4.7%
	Adjusted FEM mode input	0%	8.3%	14.3%	6.3%	4.8%

Table 32 Error of the natural frequencies of the dry modes and wet modes (averaged) and the ratio between the two for the first four modes of the Solid Plate for FEM modes as input.

Error per mode	**Mode 1**	**Mode 2**	**Mode 3**	**Mode 4**
Dry	6 %	8.9 %	6.5 %	7.6 %
Averaged error wet modes	3.9 %	4.1 %	3.3 %	4.9 %
Ratio error Dry/wet	0.6	0.5	0.5	0.6

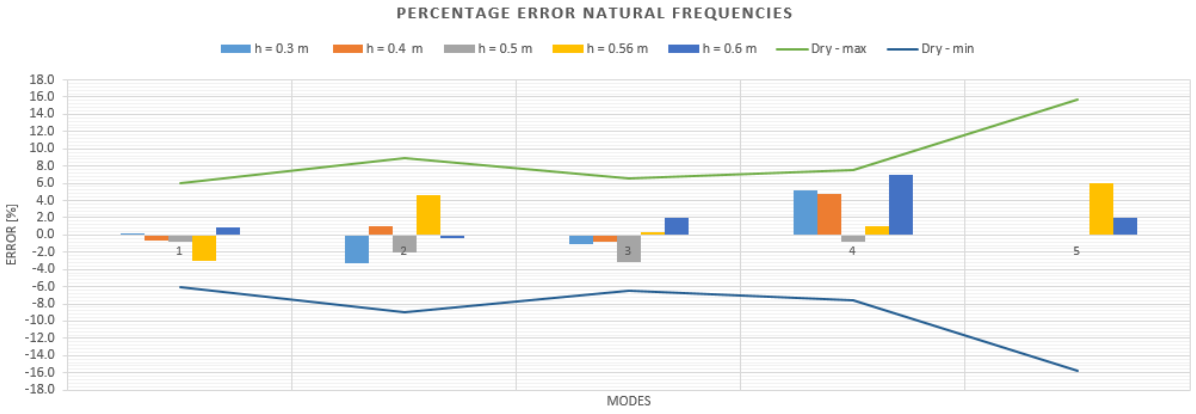

Graph 13 Error in terms of percentages per mode per water level. The lines indicate upper and lower bounds of the error of the dry modes. The SA model stays in this range, indicating proper predictions.

9.1.3 Conclusion Reinforced Plate

The Reinforced Plate was analysed using the Regular Wave Impact experiments. The SA model predicted that the first three modes were dominant in the response of the plate. This was observed in the results of the experiments, where the first three modes were consistently found. MAC values varied between 0.77 and 0.95 indicating a proper correlation between the identified and the predicted modes in terms of shape. The SA model is able to predict the correct mode shapes as well as the modes that dominate the response.

Table 33 Averaged MAC values of the first three modes of the Reinforced Plate with different input modes.

	Water level	Dry	h = 0.56 m	h = 0.6 m
MAC values	**FEM input**	0.77	0.77	0.85
	Adjusted FEM mode input	-	0.77	0.87

The averaged error of the natural frequencies for the first three wet modes turned out to be lower when compared to the averaged frequency error of the dry modes. The percentage was declined from 38% to 27% for a water level of 0.56 meters and 17.9% for 0.6 meters. Using adjusted set of FEM modes resulted in lower averaged errors for the natural frequencies. Averaged values of 12.6% for a water level of 0.56 meters and 6.6% for 0.6 meters where observed.

Looking at the relative natural frequency error of the individual modes averaged over the water levels, larger natural frequency errors of the input modes resulted in larger natural frequency errors of the predicted wet modes. Overall a ratio between the dry mode error and the wet mode error between 1.6 and 1.9 was found. The induced relative error of the natural frequencies for the dry modes declines over the higher modes. The same is shown for the wet modes that are predicted by the SA model. This trend is clearly visible in Graph 14. This concludes that a smaller natural frequency error of the FEM modes that serve as input, result in a smaller error in the prediction of the SA model.

Table 34 Cumulative error of the absolute error in natural frequencies by the SA model over the first three modes of the Reinforced Plate.

Error per water level	**Water level**	Dry	h = 0.56 m	h = 0.6 m
Natural frequencies	**FEM input**	38%	27%	17.9%
	Adjusted FEM mode input	0%	12.6%	6.6%

Table 35 Relative natural frequency error of the dry modes and wet modes (averaged) and the ratio between the two for the first three modes of the Reinforced Plate using dry FEM modes as input.

Error per mode	**Mode 1**	**Mode 2**	**Mode 3**
Dry	17.5 %	12.8 %	8.6 %
Averaged error wet modes	30.1 %	20.6 %	16.4 %
Ratio error Wet/Dry	1.7	1.6	1.9

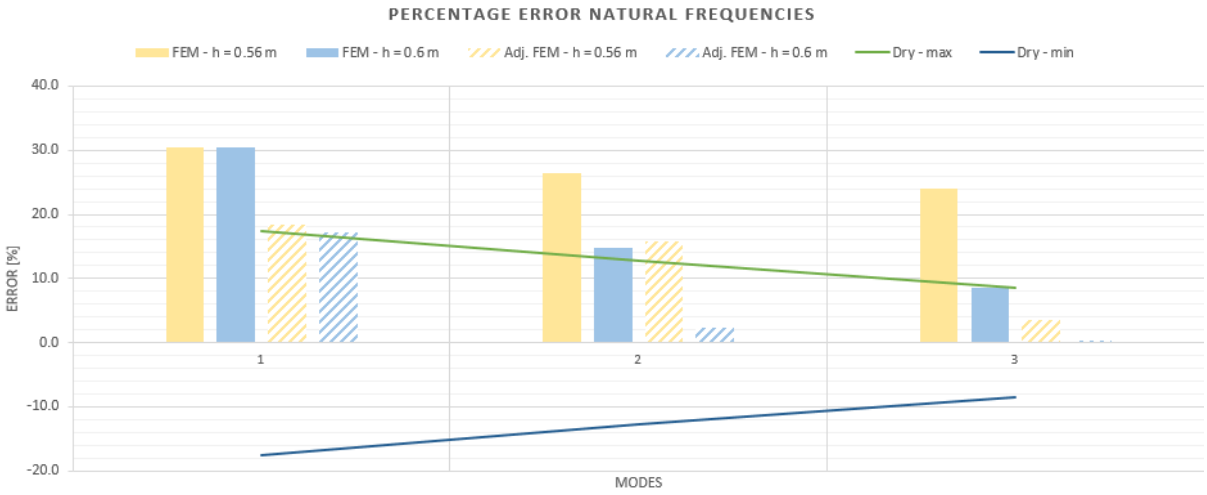

Graph 14 Reinforced plate natural frequency error in terms of percentages per mode per water level. The lines indicate upper and lower bounds of the error of the dry modes. The SA model is out of bounds, indicating wrong predictions.

9.1.4 Overall conclusion

The semi-analytical model is able to predict dynamic characteristics of submerged gates. Simpler gate geometries such as the Solid Plate are predicted correctly in terms of both natural frequencies as well as mode shapes. It was observed that for this gate type the MAC values where sufficiently high (order of 0.9) indicating high correlation between the modal shapes and the predicted ones from the SA model. Furthermore the default input modes, generated by FEM software, gave errors in the order of 2% - 7%. Using the adjusted set of FEM modes resulted in an increase in the relative error. It was observed that the error rose to 5% - 14%. Taking both into account leads to the conclusion that the SA model is capable of predicting the dynamic quantities of the Solid Plate, representing simple gate geometries.

The Reinforced Plate is lacking correct predictions in terms of natural frequencies. Large deviations were observed for lower modes. Errors in the order of 18% - 27% were observed for analyses with the default FEM input modes. Using the adjusted set of FEM modes as input resulted in a decrease of errors in the natural frequencies. Relative errors dropped to approximately 7% - 12%. The MAC values were predicted correctly for both analyses and had magnitudes in the order of 0.8, indicating well correspondence and proper mode shape prediction.

Analyses of the individual modes revealed that modes with a large error of the input modes, give larger errors in the modes calculated by the SA model. This trend was observed for both the Solid Plate and the Reinforced Plate. A ratio between the relative wet mode errors and the relative dry mode errors of 0.5 was observed for the Solid Plate. The Reinforced Plate had a ratio of approximately 1.7 – 1.9.

Overall it can be concluded that the SA model was able to predict the right modal shapes of both plates. The natural frequencies were predicted with high precision for the solid plate, indicating a proper performance of the SA model for these gate types. The reinforced plate showed larger errors in terms of natural frequencies. Situations where the dry input modes are

representing the one of the gate under consideration resulted in smaller natural frequency errors. Therefore it is crucial that for this gate type, the dry modes reflect the real life situation, resulting in small errors of natural frequencies.

9.2 Recommendations

The SA model turned out to have high performance of the predictions for the Solid Plate. Due to the relative larger errors in natural frequencies of the reinforced plate the same cannot directly be concluded for more complex gate geometries. Therefore it is recommended to perform more experiments with these types of gates. Especially gates with multiple stiffeners in different directions should be examined, since most gates have this kind of geometry.

To be concise, it is recommended to redo the experiments for complex gate geometries taking the following into account:

1. Proper attachment of the gate on the U-frame by means of glueing the full contact area.
2. Proper attachment of the stiffeners on the gate by means of glueing the full contact area.
3. Level out and fix the accelerometers properly so that they have a small inclination angle and follow the plate's surface.
4. Wet modal analysis experiments should have sufficient vibration cycles of every mode, which can be achieved by longer experiments or larger impulses on the plate.
5. Proper calibration of the FEM model.

Taking these points into consideration will increase the reliability of the results. Therefore, the reliability of the validation of the semi-analytical model is increased. The modes that served as input for the SA model were based on clamped edges of the plate and clamped fixation of the stiffeners. Taking the first two recommendations into account this will be ensured. To ensure that proper representation of the real modes is achieved, the FEM model should be calibrated. This avoids unnecessary errors in the SA prediction.

Furthermore the threshold for a minimum duration of the wet modal analysis datasets might not have been met. Taking point 4 in consideration will ensure a proper length of the data. This was already observed when using the Regular Wave Impact experiments, which lasted longer.

10 References

Almeida, E De, Hofland, B., & Jonkman, S. J. (2019). Wave Impact Pressure-Impulse on Vertical Structures with Overhangs. In N. Goseberg & T. Schlurmann (Eds.), *Coastal Structures Conference* (pp. 86–96). Hannover, Germany: Bundesanstalt für Wasserbau. https://doi.org/10.18451/978-3-939230-64-9_010

Almeida, Ermano De, & Hofland, B. (2020). Validation of pressure-impulse theory for standing wave impact loading on vertical hydraulic structures with short overhangs. *Coastal Engineering*, *159*(103702). https://doi.org/10.1016/j.coastaleng.2020.103702

Avitabile, P. (2001). Experimental Modal Analysis (A Simple Non-Mathematical Presentation). *Sound & Vibration*, *35*(1). Retrieved from http://www.sandv.com/downloads/0101avit.pdf

Bagnold, R. A. (1939). Interim Report on Wave-Pressure Research. *Journal of the Institution of Civil Engineers*, *12*, 200–226.

Bredmose, H., Peregrine, D. H., & Bullock, G. N. (2009). Violent breaking wave impacts. Part 2: Modelling the effect of air. *Journal of Fluid Mechanics*, *641*, 389–430. https://doi.org/10.1017/S0022112009991571

Brincker, R., Ventura, C., & Andersen, P. (2003). Why output-only modal testing is a desirable tool for a wide range of practical applications. In *Proceedings of the International Modal Analysis Conference (IMAC) 21: A Conference on Structural Dynamics* (pp. 265–272). The Hyatt Orlando, Kissimmee, Florida: Society for Experimental Mechanics.

Brincker, R., Ventura, C. E., & Andersen, P. (2001). Damping Estimation by Frequency Domain Decomposition. In *Proceedings of IMAC 19: A Conference on Structural Dynamics* (pp. 698–703). Kissimmee, Florida: Proceedings of IMAC 19.

Brincker, R., & Zhang, L. (2009). Frequency Domain Decomposition Revisited. In C. Gentile, F. Benedettini, R. Brincker, & N. Moller (Eds.), *Proceedings of the 3rd International Operational Modal Analysis conference - IOMAC* (p. 615). Starrylink Editrice.

Brincker, R., Zhang, L., & Andersen, P. (2001). Modal identification of output-only systems using frequency domain decomposition. *Smart Materials and Structures*, *10*(3), 441–445. https://doi.org/10.1088/0964-1726/10/3/303

Chen, X., Hofland, B., Molenaar, W., Capel, A., & Van Gent, M. R. A. (2019). Use of impulses to determine the reaction force of a hydraulic structure with an overhang due to wave impact. *Coastal Engineering*, *147*(June 2018), 75–88. https://doi.org/10.1016/j.coastaleng.2019.02.003

Cooker, M. J., & Peregrine, D. H. (1995). Pressure-impulse theory for liquid impact problems. *Journal of Fluid Mechanics*, *297*, 193–214. https://doi.org/10.1017/S0022112095003053

Cunha, Á., & Caetano, E. (2006). Experimental Modal Analysis of Civil Engineering Structures. *Sound and Vibration*, (June), 12–20. Retrieved from http://www.sandv.com/home.html

Cuomo, G., Allsop, W., Bruce, T., & Pearson, J. (2010). Breaking wave loads at vertical seawalls and breakwaters. *Coastal Engineering*, *57*(4), 424–439. https://doi.org/10.1016/j.coastaleng.2009.11.005

Ewins, D. J. (1984). *Modal Testing: Theory, Practice and Application* (Revised). Taunton, Somerset: Research Studies Press LTD.

Felber, A. J. (1993). *Development of a hybrid bridge evaluation system (PhD. Thesis)*. University of British Columbia. https://doi.org/10.14288/1.0050403

Goda, Y. (1974). New Wave Pressure Formulae for Composite Breakwaters. *Proc. 14Th. Asce Coastal Engng. Conf. (Copenhagen, Denmark)*, *3*((JUNE 24-28, 1974)), 1702–1720. https://doi.org/10.1061/9780872621138.103

Hartsuijker, C. (2001). *Toegepaste mechanica; Deel 2 Spanningen, Vevormingen, Verplaatsingen* (5th ed.). Den Haag: Academic Service.

Hattori, M., & Tsujioka, N. (1996). Dynamic response of vertical elastic walls to breaking wave impact. In B. Edge (Ed.), *Coastal Engineering* (pp. 2456–2569). Orlando, Florida. Retrieved from https://doi.org/10.1061/%0A9780784402429.190

Hofland, B., Kaminski, M. L., & Wolters, G. (2010). Large scale wave impacts on a vertical wall. *Proceedings of the Coastal Engineering Conference*.

Katsikadelis, J. T. (2020). Chapter 9 - Analysis in the frequency domain. In J. T. Katsikadelis (Ed.), *Dynamic Analysis of Structures* (pp. 299–322). Academic Press. Retrieved from https://doi.org/10.1016/B978-0-12-818643-5.00009-1

Kolkman, P. A., & Jongeling, T. H. G. (1996a). *Dynamisch gedrag van waterbouwkundige constructies - Deel A: Constructies in stroming*. (Van Hassel Van Everdingen & Partners, Ed.). Delft. https://doi.org/10.1017/CBO9781107415324.004

Kolkman, P. A., & Jongeling, T. H. G. (1996b). *Dynamisch Gedrag van Waterbouwkundige Constructies - Deel B Constructies in Golven*. (Van Hasselt Van Everdingen & Partners, Ed.). Delft. Retrieved from https://puc.overheid.nl/rijkswaterstaat/doc/PUC_27394_31/

Lay, D. C. (2012). *Linear Algebra and its application*. (D. Lynch, W. Hoffmann, C. Celano, C. Bemelmans, B. Rawnsley, K. Wernholm, & T. Ambush, Eds.) (4th ed.). Boston: Addisson-Wesley.

Little, J. A., & Mann, B. P. (2019). Optimizing logarithmic decrement damping estimation through uncertainty propagation. *Journal of Sound and Vibration*, *457*, 368–376. https://doi.org/10.1016/j.jsv.2019.05.040

Lourens, E. (2020). System identification and modal testing. Retrieved March 18, 2021, from https://brightspace.tudelft.nl/d2l/le/content/320787/viewContent/1922011/View

Maia, N. M. M., & Silva, J. M. M. (2001). Modal analysis identification techniques. *The Royal Society*, *359*(1778), 29–40. Retrieved from https://www.jstor.org/stable/3066392

Metrikine, A. V. (n.d.). *Dynamics, Slender Structures and an Introduction to Continuum Mechanics CT 4145*. Delft.

Naderpour, H., & Fakharian, P. (2016). A Synthesis of Peak Picking Method and Wavelet Packet Transform for Structural Modal Identification. *Journal of Civil Engineering*, *20*(7), 2859–2867. https://doi.org/10.1007/s12205-016-0523-4

Ogno, M. G. L. (2013). *Identifying structural parameters of an Offshore Wind Turbine using Operational Modal Analysis (Msc. Thesis)*. University of Technology Delft. Retrieved from http://resolver.tudelft.nl/uuid:3fc31f79-e00a-4e34-98f4-9400d293602b

Pastor, M., Binda, M., & Harčarik, T. (2012). Modal Assurance Criterion. *Procedia Engineering*, *48*, 543–548. https://doi.org/10.1016/j.proeng.2012.09.551

Ranieri, C., & Fabbrocino, G. (2014). *Operational Modal Analysis of Civil Engineering Structures: An Introduction and Guide for Applications* (1st ed.). New York: Springer.

https://doi.org/10.1007/978-1-4939-0767-0

Schwarz, B. J., & Richardson, M. H. (1999). Experimental Modal Analysis. In *CSI Reliability Week, Orlando, FL* (pp. 1–12). Jamestown, California.

Spijkers, J. M. J., Vrouwenvelder, A. W. C. M., & Klaver, E. C. (2005). *Structural Dynamics CT 4140. Part 1: Structural Vibrations*. Delft: Delft University of Technology.

Tieleman, O. C., Hofland, B., Tsouvalas, A., Almeida, E. De, & Jonkman, S. N. (2020). *A fluid-structure interaction model for assessing the safety of flood gate vibrations due to wave impacts*. Submitted to Coastal Engineering Journal.

Tieleman, O. C., Tsouvalas, A., Hofland, B., Peng, Y., & Jonkman, S. N. (2019). A three dimensional semi-analytical model for the prediction of gate vibrations immersed in fluid. *Marine Structures*, *65*(December 2018), 134–153. https://doi.org/10.1016/j.marstruc.2018.12.007

Tsouvalas, A., & Metrikine, A. V. (2014). A three-dimensional vibroacoustic model for the prediction of underwater noise from offshore pile driving. *Journal of Sound and Vibration*, *333*(8), 2283–2311. https://doi.org/10.1016/j.jsv.2013.11.045

Zimmerman, A. T., Shiraishi, M., Swartz, R. A., & Lynch, J. P. (2008). Automated Modal Parameter Estimation by Parallel Processing within Wireless Monitoring Systems. *Journal of Infrastructure Systems*, *14*(1), 102–113. https://doi.org/10.1061/(asce)1076-0342(2008)14:1(102)

Appendices

A. Linear Algebra Tools

Dynamic equations can be brought back to a set of linear equations most of the time. Since the problems can be described in a set of equations one can apply linear algebra on the problems for possible dynamic solutions. Two linear algebra tools that are important are the Eigen decomposition and the singular value decomposition(SVD). Both techniques lead to a set of Eigenvalues and Eigenvectors. In the modal analysis these have a dynamical meaning and are known to be the natural frequencies and mode shapes of a system.

The set of equations that one works with are known as the EOM and originate from Newtons' second law F = ma. The EOMs most of the time have the simple form as given in eq. 40 (without damping) and eq. 41 (with damping).

$$F = m\ddot{x} + kx \tag{40}$$

$$F = m\ddot{x} + c\dot{x} + kx \tag{41}$$

In case of an MDOF system several degrees of freedom make that more EOMs are needed to describe the systems motion. The number of EOMs and degree of freedoms is in balance. The form of the EOMs can be either obtained via Finite Element software, Displacement method or the Lagrange method (Spijkers et al., 2005). Eventually an EOM for a MDOF system looks like the one given in eq. *42*. The M, C and K denotations are matrices that represent the mass, damping and stiffness terms for every DOF (Spijkers et al., 2005).

$$\boldsymbol{F} = \boldsymbol{M}\bar{\ddot{x}} + \boldsymbol{C}\bar{\dot{x}} + \boldsymbol{K}\bar{x} \tag{42}$$

Eigenvalue problem

Spijkers et al. (2005) elaborate that the Eigenvalue problem starts by solving the homogeneous solution of eq. *42*, which leads to eq. *43* in the case of no damping. The only non-trivial solution of this set of equations leads to the natural frequency of the system. This has a non-trivial solution if the determinant of the system is zero. Equation *44* gives an example.

$$\boldsymbol{M}\bar{\ddot{x}} + \boldsymbol{K}\bar{x} = 0 \rightarrow -\omega^2\boldsymbol{M} + \boldsymbol{K} = 0 \tag{43}$$

$$\det(-\omega^2\boldsymbol{M} + \boldsymbol{K}) = 0 \tag{44}$$

In case of a n x n matrix a Eigen decomposition can be executed. Eigenvalues are found by means of setting the determinant of A-λI to zero(Lay, 2012). Solving the corresponding equation leads to a set of Eigenvalues. The corresponding Eigenvectors are given by the relation Aλ = λx, in which x is the Eigenvector corresponding to the Eigenvalue under consideration.

Singular Value Decomposition

When a matrix has not the same amount of rows as columns, it can be denoted as a m x n matrix. In this case Eigen decomposition is not possible. Singular value decomposition is a powerful tool to obtain the natural frequencies of a system (singular values) and the mode shapes(left singular vector). Lay (2012) gives a detailed explanation on this topic. The reader is referred to his book.

B. Experimental Modal Analysis – Frequency Domain Decomposition

This appendix addresses more in detailed information about the FDD and on the algorithm implementation in this thesis. First of all the workflow for validation of implementation is given where after the algorithm itself is presented. The algorithm is given in a workflow as well to maintain the oversight.

Validation of implementation of Frequency Domain Decomposition algorithm

Validation of the implementation of the Frequency Domain Decomposition of Brincker, Zhang, et al. (2001) is based on synthetic data obtained from the semi-analytical model for Tieleman et al (2019). The workflow of the validation technique is given in Figure 61. Based on different outputs of the semi-analytical model the mode detection algorithm can be compared to the desired output from the semi-analytical model. The different input parameters should be chosen such that the different types of analysis in the semi-analytical model examine the same situation. Both the Reinforced and Solid plate are checked on their implementation for different situations, which are known to be:

- Eccentric forcing : Trigger of symmetric and asymmetrical modes
- Centric forcing : Trigger of symmetric modes only
- Various water levels
- Dry conditions
- Different values of damping
- Different measurement frequencies

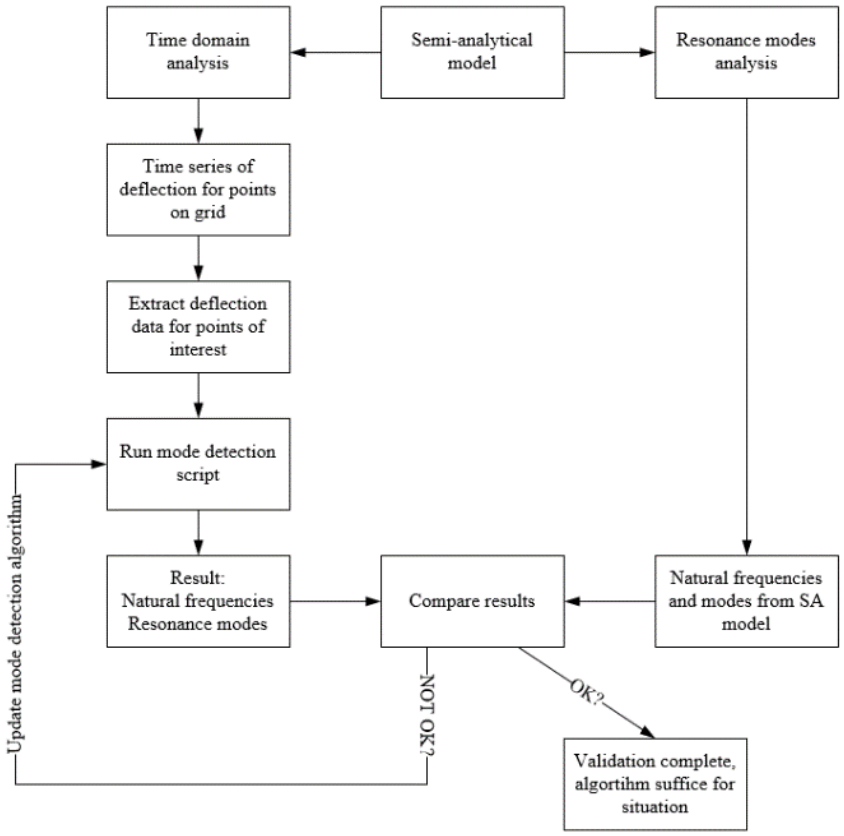

Figure 61 Workflow for EMA algorithm implementation validation

Frequency Domain Decomposition algorithm

The algorithm is based on the theory of Brincker, Zhang, et al. (2001) and Brincker & Zhang (2009) is specially developed for structures with modes that are close to each other. According to §6.1.1 it can be seen that the structures under investigation have potentially nearby modes. The algorithm consists of several steps that must be performed, these are listed below. The steps are elaborated in a workflow(Figure 62) with additional clarification on several subjects.

- Generate experimental data
- Sort data into matrix
- Specify settings such as measurement frequency, number of data points and number of segments
- Perform segmentation on data set if set is merged from multiple sets
- Perform a Fast Fourier Transform for every data point and segmented data set
- Create a spectral density matrix
- Perform a singular value decomposition in order to obtain the singular values and left singular vectors

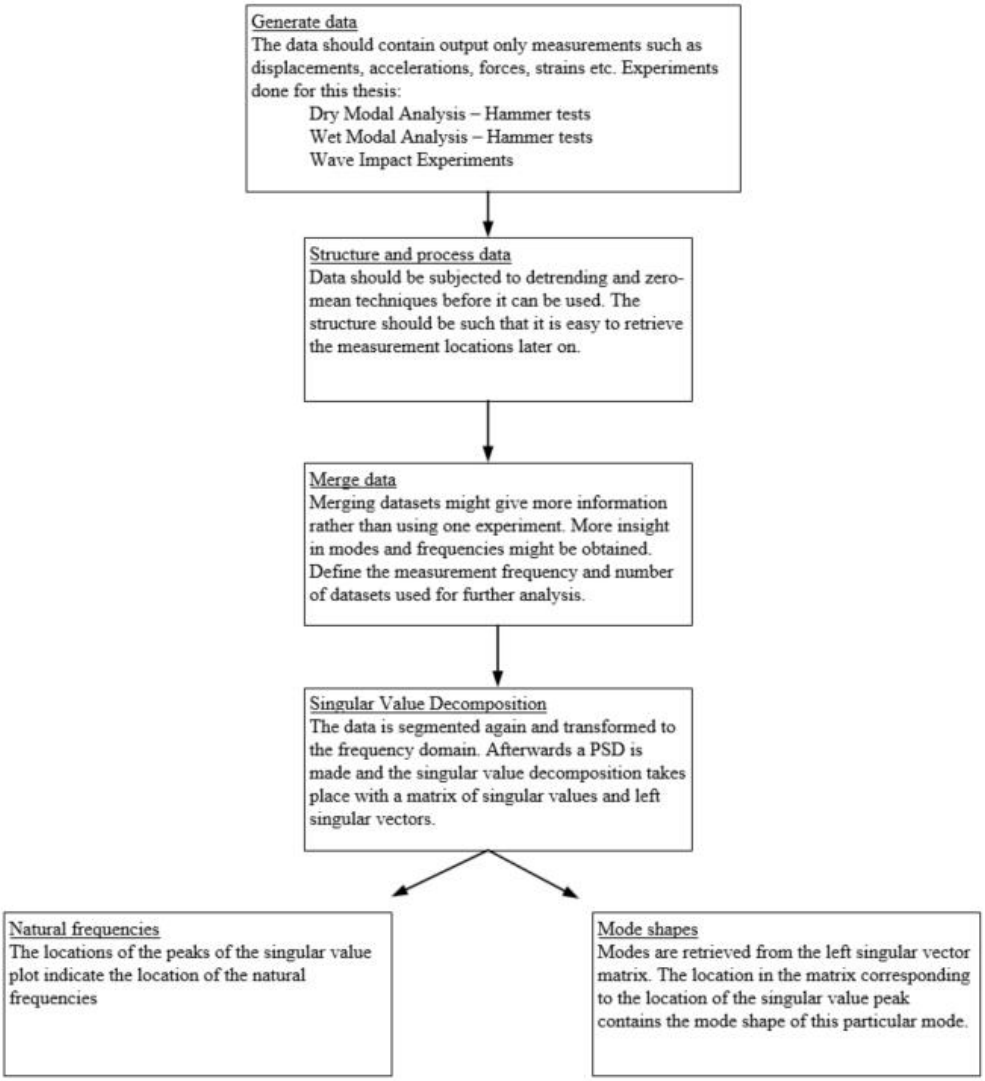

Figure 62 Schematic workflow of the Frequency Domain Decomposition approach.

C. Problem formulation semi-analytical model (Tieleman et al, 2019)

Tieleman et al (2019) derived a semi-analytical to predict gate vibrations in a fluid. This appendix will treat their reasoning and derivation of the problem, the information given is based on the work of Tieleman et al. (2019). The problem is split up in a structural part and a fluid part, which are each treated separately where after a coupling is made using interface conditions. Figure 63 gives an overview of the examined problem.

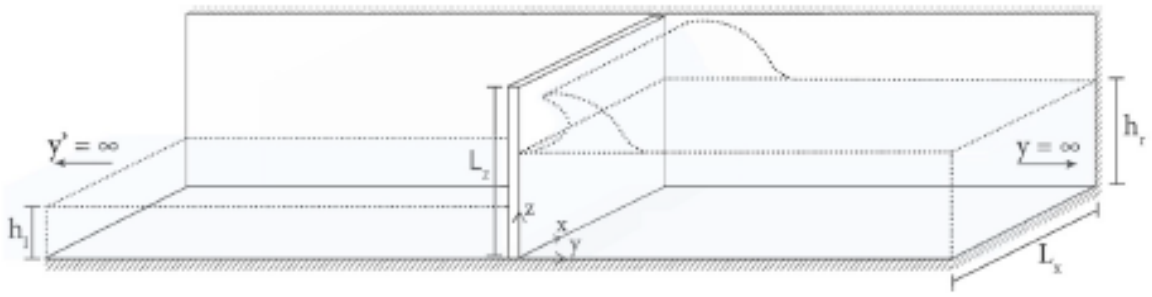

Figure 63 Problem under consideration (Tieleman et al, 2019)

The derivation is based on the assumption that the vertical thin plate is homogeneous and isotropic. The result is a 3-dimensional solution for the bending gate vibrations. the corresponding equations of motion for both the structure and the fluid can be found in chapter 2.3.1.

Tieleman et al(2019) use the technique of separation of variables for both the structural and fluid part for both the x- and z-direction. This leads to the following expansions in the frequency domain.

$$\tilde{w} = \sum_{m=1}^{\infty}\sum_{k=1}^{\infty} A_{km} W_{x,k}(x) W_{z,m}(z) \tag{45}$$

$$\tilde{\phi}(x,y,z) = \sum_{m=1}^{\infty}\sum_{k=1}^{\infty} B_{pr} \Phi_{pr}(x,z) e^{-ik_{y,pr}y} \tag{46}$$

The goal is now to rewrite the fluid modal shapes in terms of the structural modal shapes using the interface conditions at the gate-fluid interface. Tieleman et al(2019) eventually obtain a solution for both the water pressures in the fluid volume as well as the deflections of the gate. The solution for the deflections considers the amplitude matrix, which needs to be multiplied by the structural modes to obtain a real solution. The amplitude matrix is determined via equation 47.

$$\sum_{k=1}^{\infty}\sum_{m=1}^{\infty}\left[\rho_s(\omega_{km}^2 - \omega^2)\delta_{kl}\delta_{mn}\Gamma_{ln} - L_{km,ln} + R_{km,ln}\right]A_{ln} = F_{ln} \tag{47}$$

In which the variables are expressed by the following equations.

$$L_{km,ln} = i\omega^2 \rho_f \sum_{p=1}^{\infty} \sum_{r=1}^{\infty} \frac{Q_{km,pr} Q_{ln,pr}}{k_{y,pr} \Delta_{pr}} \quad 48$$

$$R_{km,ln} = i\omega^2 \rho_f \sum_{p=1}^{\infty} \sum_{r=1}^{\infty} \frac{Q_{km,pr} Q_{ln,pr}}{k_{y,pr} \Delta_{pr}} \quad 49$$

$$F_{ln} = \iint \tilde{f}_e\,(x, z, \omega) W_{ln}(x, z)\, dx\, dz \quad 50$$

$$Q_{km,pr} = \iint W_{mk}(x, z) \Phi_{pr}(x, z)\, dx\, dz \quad 51$$

$$Q_{ln,pr} = \iint W_{ln}(x, z) \Phi_{pr}(x, z)\, dx\, dz \quad 52$$

Figure 13 gives a roadmap to obtain a solution that fully depends on the structural modes only.

Structural problem

The structural problem is dominated by the EOM and its boundary conditions.

$$\rho \frac{\partial^2 w}{\partial t^2} + D \left[\frac{\partial^4 w}{\partial x^4} + \frac{\partial^4 w}{\partial x^2 \partial z^2} + \frac{\partial^4 w}{\partial z^4} \right] = -f_l + f_r + f_p \quad 53$$

In which D is the uniform bending rigidity and f_l, f_r and f_p are the time signals of the external forces.

Assuming a simply supported structure the following boundary conditions are defined.

$$w(x = 0, z) \;=\; M_{xx}(x = 0, z) \;=\; w(x = L_x, z) \;=\; M_{xx}\,(x = L_x\,, z) \;=\; 0 \quad 54$$

$$w(x, z = 0) \;=\; M_{xx}(x, z = 0) \;=\; w(x, z = L_z) \;=\; V_{zy}\,(x\,, z = L_z) \;=\; 0 \quad 55$$

The equation of motion can be rewritten in the frequency domain. The formulation is given in equation 43.

$$-\rho\omega^2 \tilde{w}(x, z, \omega) + D \left[\frac{\partial^4 \tilde{w}}{\partial x^4} + \frac{\partial^4 \tilde{w}}{\partial x^2 \partial y^2} + \frac{\partial^4 \tilde{w}}{\partial z^4} \right] = -\tilde{f}_l + \tilde{f}_r + \tilde{f}_p \quad 56$$

Fluid problem

the fluid problem is dominated by the equations of motion given in equations 57- 59 and are based on the fact that the fluid experiences high Reynolds numbers.

$$\nabla^2\phi(x,y,z,t) - \frac{1}{c_p^2}\frac{\partial^2\phi}{\partial t^2} = 0 \quad (57)$$

$$p(x,y,z,t) = -\rho_f \frac{\partial\phi}{\partial t} \quad (58)$$

$$v(x,y,z,t) = \nabla\phi(x,y,z,t) \quad (59)$$

The problem may be solved by introducing a set of boundary conditions, and is coupled with the structural problem by means of an interface condition.

$$\left.\frac{\partial\phi}{\partial x}\right|_{x=0} = \left.\frac{\partial\phi}{\partial x}\right|_{x=L_x} = \left.\frac{\partial\phi}{\partial z}\right|_{z=0} = 0 \quad (60)$$

$$\frac{\partial^2\phi}{\partial t^2} + g\frac{\partial\phi}{\partial z} = 0 \quad (61)$$

$$\left.\frac{\partial\phi}{\partial y}\right|_{y=0} = \frac{\partial w}{\partial t} \quad (62)$$

The equations of motion can be rewritten in the frequency domain. This holds for the boundary conditions as well. The formulations are given in equations 63-68.

$$\nabla^2\tilde{\phi}(x,y,z,\omega) - k_f^2\tilde{\phi}(x,y,z,\omega) = 0\ ;\ k_f^2 = \frac{\omega^2}{c_p^2} \quad (63)$$

$$\tilde{p}(x,y,z,\omega) = -\rho_f i\omega\tilde{\phi}(x,y,z,\omega) \quad (64)$$

$$\tilde{v}(x,y,z,\omega) = \nabla\tilde{\phi}(x,y,z,\omega) \quad (65)$$

$$\left.\frac{\partial\tilde{\phi}}{\partial x}\right|_{x=0} = \left.\frac{\partial\tilde{\phi}}{\partial x}\right|_{x=L_x} = \left.\frac{\partial\tilde{\phi}}{\partial z}\right|_{z=0} = 0 \quad (66)$$

$$\left.\frac{\omega^2}{g}\tilde{\phi}\right|_{z=h} = \left.\frac{\partial\tilde{\phi}}{\partial z}\right|_{z=h} \quad (67)$$

$$\left.\frac{\partial\tilde{\phi}}{\partial y}\right|_{y=0} = i\omega\tilde{w} \quad (68)$$

D. Semi-analytical modes and natural frequencies

This appendix gives an overview of all natural frequencies and mode shapes of the different gates based on the results of the semi-analytical model. Modes in the dry and wet, for different water levels, are generated by the semi-analytical model and serve as a basis for the validation of the model. The modes are compared to the outcome of the FDD of the experimental data where after they are classified in either detected or not detected. Depending on the result additional steps on the settings or input of the semi-analytical model can be taken for further research.

Natural frequencies Solid plate

	f_1	f_2	f_3	f_4	f_5	f_6	f_7
Dry	34.5	74.1	87.7	129.5	162.3	167.6	210.6
Wet 0.3 m	28.0	45.8	62.2	96.1	112.9	116.5	124
Wet 0.4 m	20.1	45.5	49	94.7	95	100.6	143.7
Wet 0.5 m	15.1	40.1	41.9	77.7	86.6	92.7	139.1
Wet 0.56 m	12.6	33.6	38.1	66.4	81.7	88.6	120.9
Wet 0.6 m	11.4	29.3	35.6	59.1	76.2	79.1	105.8

Table 36 Natural frequencies for different situations of Solid Plate

Natural frequencies Reinforced plate

	f_1	f_2	f_3	f_4	f_5	f_6	f_7
Dry	84.3	95.3	136.6	171.5	184.2	209.1	216.5
Wet 0.3 m	43.4	71.2	85.5	99.9	110.9	170	184.2
Wet 0.4 m	29.3	63.9	90.6	96.6	123.5	157	187.5
Wet 0.5 m	25.8	47.8	61.4	84.7	96.5	127.3	182.5
Wet 0.56 m	26	47.8	61.6	79	91.4	96.3	133
Wet 0.6 m	23.1	35.1	57.6	60.6	76.1	95.4	96.4

Table 37 Natural frequencies for different situations of Reinforced Plate

Mode shapes Solid Plate

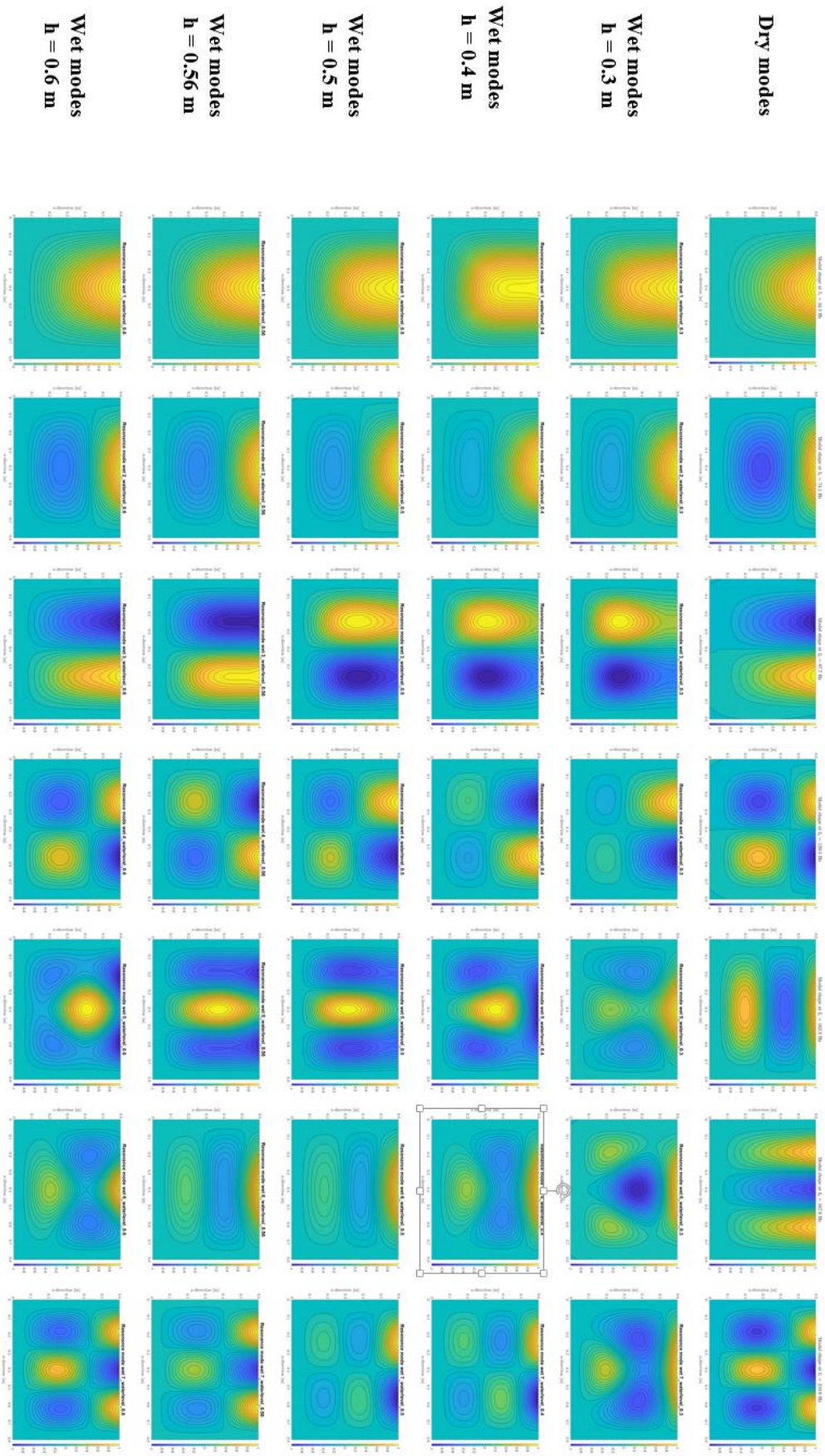

Mode shapes Reinforced Plate

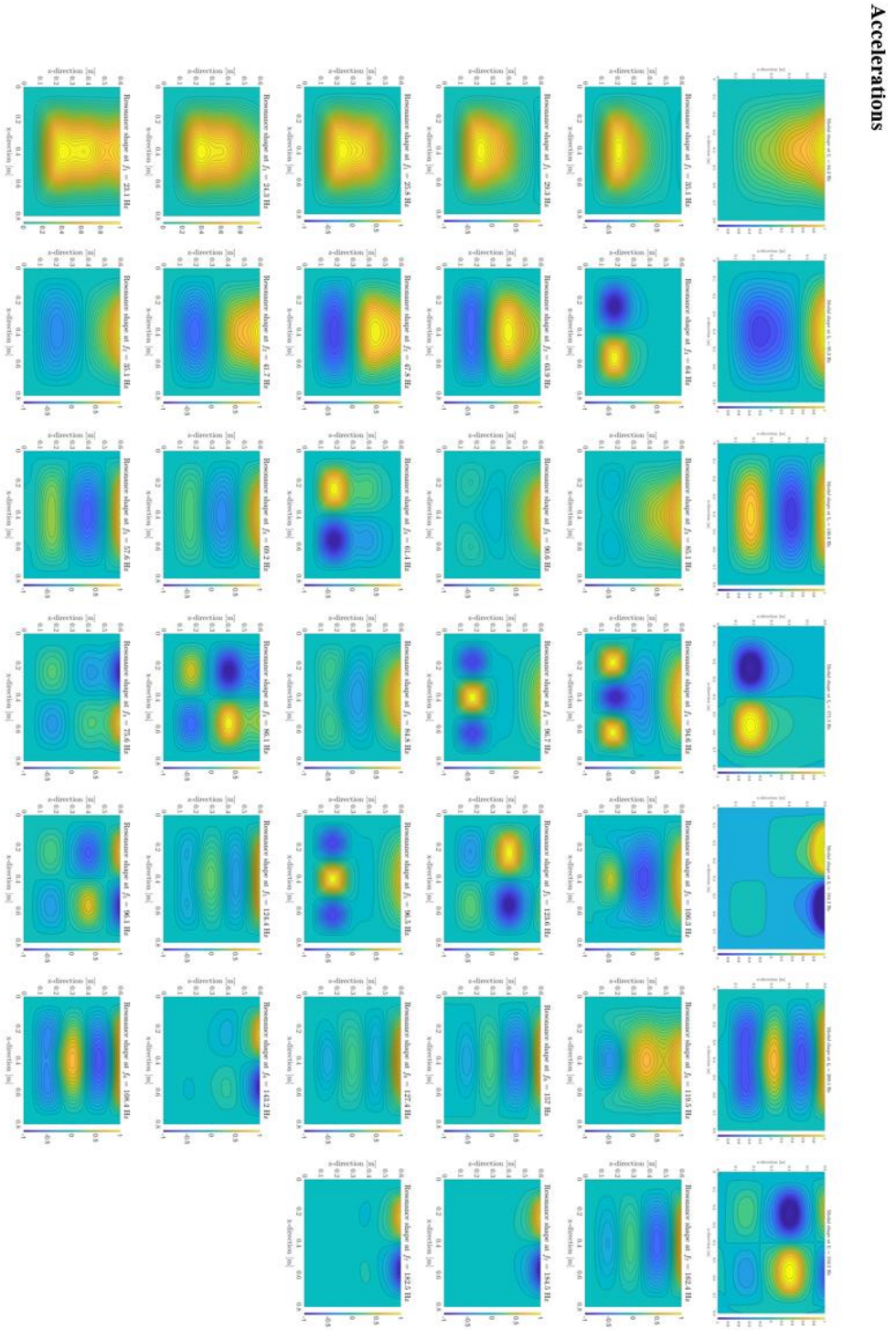

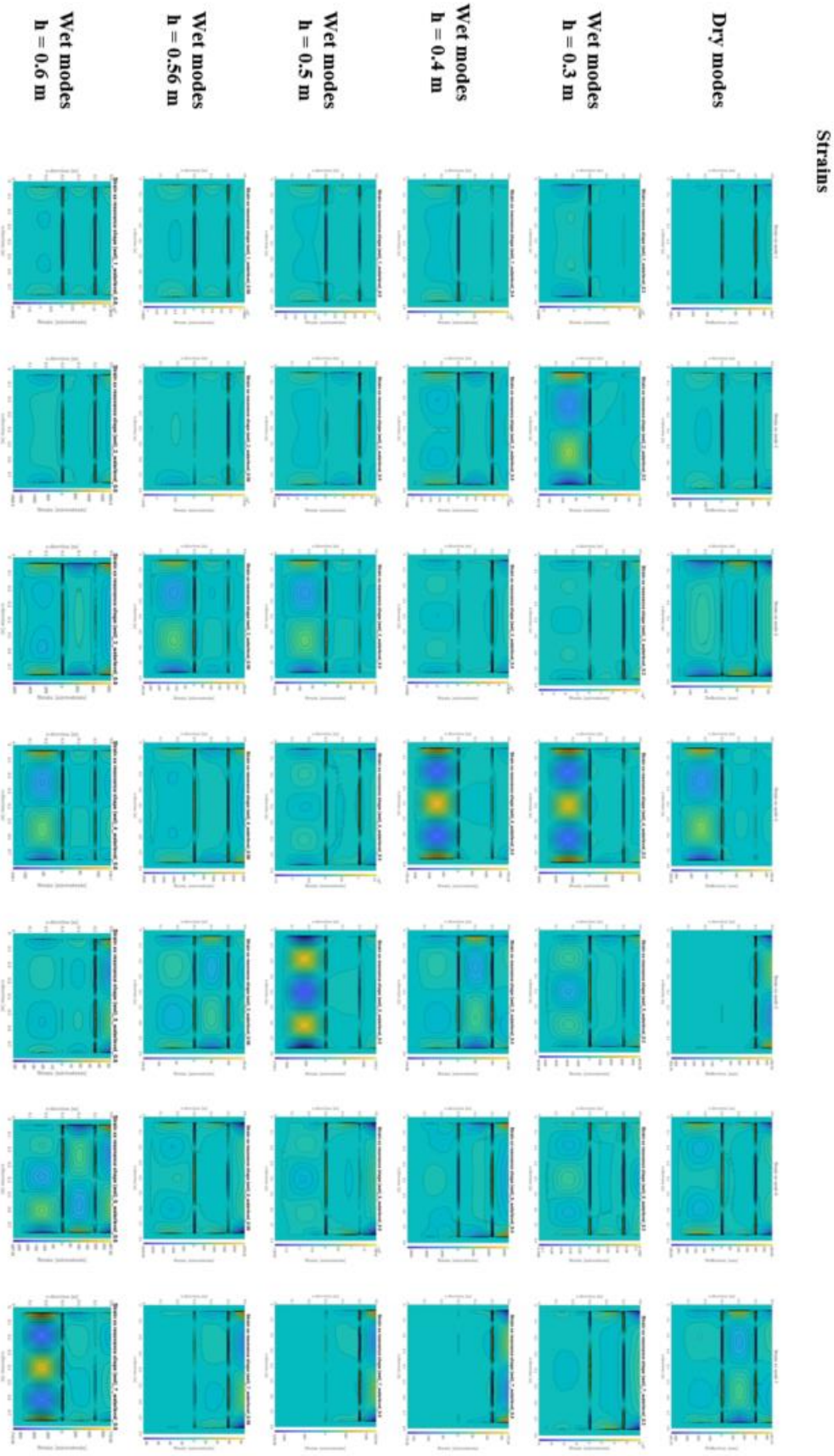
Strains
Dry modes
Wet modes h = 0.3 m
Wet modes h = 0.4 m
Wet modes h = 0.5 m
Wet modes h = 0.56 m
Wet modes h = 0.6 m

E. Experiments - overview

This appendix contains an overview of all experiments that are executed. The experiments are divided in 5 categories:

1. Dry modal analysis
2. Dry hammer impacts
3. Wet modal analysis
4. Regular wave impacts
5. Irregular wave impacts

Solid Plate

#	Test ID	Test name	Forcing method	Measurement frequency	Waterlevel
3	001	Dry modal analysis	Random hammer impacts	5000	-
3	002	Dry modal analysis	Random hammer impacts	5000	-
3	003	Dry modal analysis	Random hammer impacts	5000	-
3	004	Dry modal analysis	Random hammer impacts	5000	-
3	005	Dry modal analysis	Random hammer impacts	5000	-
3	006	Dry modal analysis	Random hammer impacts	5000	-
3	007	Dry modal analysis	Random hammer impacts	5000	-
3	008	Dry modal analysis	Random hammer impacts	5000	-
3	009	Dry modal analysis	Random hammer impacts	5000	-
3	010	Dry modal analysis	Random hammer impacts	5000	-
4	001	Dry hammer impact	Single hammer impacts loc 0-6	5000	
4	002	Dry hammer impact	Single hammer impacts loc 0-7	5000	
4	003	Dry hammer impact	Single hammer impacts loc 0-8	5000	
4	004	Dry hammer impact	Single hammer impacts loc 0-8	5000	
4	005	Dry hammer impact	Single hammer impacts loc 0-8	5000	
4	006	Dry hammer impact	Single hammer impacts loc 0-8	5000	
4	007	Dry hammer impact	Single hammer impacts loc 0-8	5000	
4	008	Dry hammer impact	Single hammer impacts loc 0-8	5000	
4	009	Dry hammer impact	Single hammer impacts loc 0-8	5000	
4	010	Dry hammer impact	Single hammer impacts loc 0-8	5000	
4	011	Dry hammer impact	Single hammer impacts loc 0-8	5000	
4	012	Dry hammer impact	Single hammer impacts loc 0-8	5000	
4	013	Dry hammer impact	Single hammer impacts loc 0-8	5000	
5	001	Wet modal analysis	Random hammer impacts	5000	0.304
5	002	Wet modal analysis	Random hammer impacts	5000	0.304
5	003	Wet modal analysis	Random hammer impacts	5000	0.304
5	004	Wet modal analysis	Random hammer impacts	5000	0.304
5	005	Wet modal analysis	Random hammer impacts	5000	0.304
5	006	Wet modal analysis	Random hammer impacts	5000	0.304
5	007	Wet modal analysis	Random hammer impacts	5000	0.401

5	008	Wet modal analysis	Random hammer impacts	5000	0.401
5	009	Wet modal analysis	Random hammer impacts	5000	0.401
5	010	Wet modal analysis	Random hammer impacts	5000	0.500
5	011	Wet modal analysis	Random hammer impacts	5000	0.500
5	012	Wet modal analysis	Random hammer impacts	5000	0.500
5	013	Wet modal analysis	Random hammer impacts	5000	0.600
5	014	Wet modal analysis	Random hammer impacts	5000	0.600
5	015	Wet modal analysis	Random hammer impacts	5000	0.600
5	016	Wet modal analysis	Random hammer impacts	5000	0.560
5	017	Wet modal analysis	Random hammer impacts	5000	0.560
5	018	Wet modal analysis	Random hammer impacts	5000	0.560
5	019	Wet modal analysis	Random hammer impacts	5000	0.600
5	020	Wet modal analysis	Random hammer impacts	5000	0.600
5	021	Wet modal analysis	Random hammer impacts	5000	0.600
5	022	Wet modal analysis	Random hammer impacts	5000	0.631
5	023	Wet modal analysis	Random hammer impacts	5000	0.631
5	024	Wet modal analysis	Random hammer impacts	5000	0.631
6	001	Regular wave impact	Regular waves	10000	0.600
6	002	Regular wave impact	Regular waves	10000	0.600
6	003	Regular wave impact	Regular waves	10000	0.600
6	004	Regular wave impact	Regular waves	10000	0.600
6	005	Regular wave impact	Regular waves	10000	0.600
6	006	Regular wave impact	Regular waves	10000	0.560
6	007	Regular wave impact	Regular waves	10000	0.560
6	008	Regular wave impact	Regular waves	10000	0.560
6	009	Regular wave impact	Regular waves	10000	0.560
6	010	Regular wave impact	Regular waves	10000	0.560
6	011	Regular wave impact	Regular waves	10000	0.630
6	012	Regular wave impact	Regular waves	10000	0.630
6	013	Regular wave impact	Regular waves	10000	0.630
6	014	Regular wave impact	Regular waves	10000	0.630
7	001	Irregular wave impact	Irregular wave spectrum	10000	0.600
7	002	Irregular wave impact	Irregular wave spectrum	10000	0.600
7	003	Irregular wave impact	Irregular wave spectrum	10000	0.600
7	004	Irregular wave impact	Irregular wave spectrum	10000	0.599
7	005	Irregular wave impact	Irregular wave spectrum	10000	0.599
7	006	Irregular wave impact	Irregular wave spectrum	10000	0,600

7	007	Irregular wave impact	Irregular wave spectrum	10000	0.560
7	008	Irregular wave impact	Irregular wave spectrum	10000	0.630

Reinforced plate

#	Test ID	Test name	Activity	Measurement frequency	Waterlevel
3	033	Dry modal analysis	Final - with tape all sides	5000	
3	034	Dry modal analysis	Final - with tape all sides	5000	
3	035	Dry modal analysis	Final - with tape all sides	5000	
3	036	Dry modal analysis	Final - with tape all sides	5000	
3	037	Dry modal analysis	Final - with tape all sides	5000	
4	001	Dry hammer impact	Outside flume - Loc 0	1000	
4	002	Dry hammer impact	Outside flume - Loc 1	1000	-
4	003	Dry hammer impact	Outside flume - Loc 2	1000	-
4	004	Dry hammer impact	Outside flume - Loc 3	1000	-
4	005	Dry hammer impact	Outside flume - Loc 4	1000	-
4	006	Dry hammer impact	Outside flume - Loc 5	1000	-
4	007	Dry hammer impact	Outside flume - Loc 6	1000	-
4	008	Dry hammer impact	Outside flume - Loc 7	1000	-
4	009	Dry hammer impact	Outside flume - Loc 8	1000	-
4	-	Dry hammer impact	In flume - tape test - tape all sides - loc 0	1000	-
4	010	Dry hammer impact	In flume - tape test - tape all sides - Loc 1	1000	-
4	011	Dry hammer impact	In flume - tape test - tape all sides - Loc 2	1000	-
4	012	Dry hammer impact	In flume - tape test - tape all sides - Loc 3	1000	-
4	013	Dry hammer impact	In flume - tape test - tape all sides - Loc 4	1000	-
4	014	Dry hammer impact	In flume - tape test - tape all sides - Loc 5	1000	-
4	015	Dry hammer impact	In flume - tape test - tape all sides - Loc 6	1000	-
4	016	Dry hammer impact	In flume - tape test - tape all sides - Loc 7	1000	-
4	017	Dry hammer impact	In flume - tape test - tape all sides - Loc 8	1000	-
4	-	Dry hammer impact	In flume - tape test - no tape - loc 0	1000	-
4	018	Dry hammer impact	In flume - tape test - no tape - Loc 1	1000	-

4	019	Dry hammer impact	In flume - tape test - no tape - loc 2	1000	-
4	020	Dry hammer impact	In flume - tape test - no tape - loc 3	1000	-
4	021	Dry hammer impact	In flume - tape test - no tape - loc 4	1000	-
4	022	Dry hammer impact	In flume - tape test - no tape - loc 5	1000	-
4	023	Dry hammer impact	In flume - tape test - no tape - loc 6	1000	-
4	024	Dry hammer impact	In flume - tape test - no tape - loc 7	1000	-
4	025	Dry hammer impact	In flume - tape test - no tape - loc 8	1000	-
4	028	Dry hammer impact	Final - with tape - loc 0	5000	-
4	029	Dry hammer impact	Final - with tape - loc 1	5000	
4	030	Dry hammer impact	Final - with tape - loc 2	5000	
4	031	Dry hammer impact	Final - with tape - loc 3	5000	
4	032	Dry hammer impact	Final - with tape - loc 5	5000	
4	033	Dry hammer impact	Final - with tape - loc 6	5000	
4	034	Dry hammer impact	Final - with tape - loc 7	5000	
4	035	Dry hammer impact	Final - with tape - loc 8	5000	
4	036	Dry hammer impact	Final - with tape - loc 4	5000	
5	001	Wet modal analysis	h = 0.3 Hammer front	5000	0.302
5	002	Wet modal analysis	h = 0.3 Hammer front	5000	0.302
5	003	Wet modal analysis	h = 0.3 Hammer front	5000	0.302
5	004	Wet modal analysis	h = 0.3 Hammer back	5000	0.302
5	005	Wet modal analysis	h = 0.4 Hammer front	5000	0.403
5	006	Wet modal analysis	h = 0.4 Hammer front	5000	0.403
5	007	Wet modal analysis	h = 0.4 Hammer front	5000	0.403
5	008	Wet modal analysis	h = 0.4 Hammer front through water	5000	0.403
5	009	Wet modal analysis	h = 0.4 Hammer front through water	5000	0.403
5	010	Wet modal analysis	h = 0.4 Hammer front through water	5000	0.403
5	011	Wet modal analysis	h = 0.4 Hammer back	5000	0.403
5	012	Wet modal analysis	h = 0.5 Hammer front	5000	0.504
5	013	Wet modal analysis	h = 0.5 Hammer front	5000	0.504
5	014	Wet modal analysis	h = 0.5 Hammer front	5000	0.504
5	015	Wet modal analysis	h = 0.5 Hammer front through water	5000	0.504
5	016	Wet modal analysis	h = 0.5 Hammer front through water	5000	0.504
5	017	Wet modal analysis	h = 0.5 Hammer front through water	5000	0.504
5	018	Wet modal analysis	h = 0.5 Hammer back	5000	0.504
5	019	Wet modal analysis	h = 0.56 Hammer front through water	5000	0.56
5	020	Wet modal analysis	h = 0.56 Hammer front through water	5000	0.56
5	021	Wet modal analysis	h = 0.56 Hammer front through water	5000	0.56
5	022	Wet modal analysis	h = 0.56 Hammer back	5000	0.56
5	023	Wet modal analysis	h = 0.56 Hammer back	5000	0.56
5	024	Wet modal analysis	h = 0.56 Hammer back	5000	0.56
5	025	Wet modal analysis	h = 0.56 Hammer front through water lower	5000	0.56
5	026	Wet modal analysis	h = 0.56 Hammer front through water lower	5000	0.56

5	027	Wet modal analysis	h = 0.56 Hammer front through water lower	5000	0.56
5	028	Wet modal analysis	h = 0.6 Hammer front through water	5000	0.6
5	029	Wet modal analysis	h = 0.6 Hammer front through water	5000	0.6
5	030	Wet modal analysis	h = 0.6 Hammer front through water	5000	0.6
5	031	Wet modal analysis	h = 0.63 Hammer front through water	5000	0.63
5	032	Wet modal analysis	h = 0.63 Hammer front through water	5000	0.63
5	033	Wet modal analysis	h = 0.63 Hammer front through water	5000	0.63
5	034	Wet modal analysis	h = 0.6 Hammer front through water	5000	0,599
5	035	Wet modal analysis	h = 0.6 Hammer front through water	5000	0,599
5	036	Wet modal analysis	h = 0.6 Hammer front through water	5000	0,599
5	037	Wet modal analysis	h = 0.3 Hammer front only dry	5000	0.301
5	038	Wet modal analysis	h = 0.3 Hammer front dry and through water	5000	0.301
5	039	Wet modal analysis	h = 0.4 Hammer front dry only	5000	0.402
5	040	Wet modal analysis	h = 0.4 Hammer front through water and dry	5000	0.402
5	041	Wet modal analysis	h = 0.5 Hammer front through water	5000	0.502
5	042	Wet modal analysis	h = 0.56 Hammer front through water	5000	0.559
5	043	Wet modal analysis	h = 0.6 Hammer front through water	5000	0.599
5	044	Wet modal analysis	h = 0.6 Hammer front through water	5000	0.599
5	045	Wet modal analysis	h = 0.63 Hammer front through water	5000	0.631
6	001	Regular wave impact	Leakage test - mechanical fit	50000	0.6
6	002	Regular wave impact	Leakage test - tape - h 0,62	5000	0.62
6	003	Regular wave impact	Leakage test - tape - h 0,6	5000	0.6
6	004	Regular wave impact	AS56R	5000	0.56
6	005	Regular wave impact	AS56R	10000	0.559
6	006	Regular wave impact	BS56R	10000	0.559
6	007	Regular wave impact	CS56R	10000	0.559
6	008	Regular wave impact	DS56R	10000	0.559
6	009	Regular wave impact	ES56R	10000	0.559
6	010	Regular wave impact	AS60R	10000	0.6
6	011	Regular wave impact	BS60R	10000	0.6
6	012	Regular wave impact	CS60R	10000	0.6
6	013	Regular wave impact	DS60R	10000	0.6
6	014	Regular wave impact	ES60R	10000	0.6
6	016	Regular wave impact	BS63R	10000	0.63
6	017	Regular wave impact	CS63R	10000	0.63
6	018	Regular wave impact	DS63R	10000	0.63
6	019	Regular wave impact	ES63R	10000	0.63
6	020	Regular wave impact	CS60R - redone 125x	10000	0.6
6	021	Regular wave impact	ES60R - redone 125x	10000	0.6
7	002	Irregular wave impact	AS56I	10000	0.56
7	003	Irregular wave impact	AS60I	10000	0.6

7	004	Irregular wave impact	AS63I	10000	0.56
7	005	Irregular wave impact	BS60I	10000	0.6
7	006	Irregular wave impact	CS60I frozen computer	10000	0.6
7	007	Irregular wave impact	CS60I	10000	0,599
7	008	Irregular wave impact	DS60I	10000	0,599
7	009	Irregular wave impact	ES60I	10000	0,599
7	010	Irregular wave impact	BS60I - redone 125x	10000	0.6
7	011	Irregular wave impact	AS60I - redone 125x	10000	0.6

F. Identified modes

All modes that are identified during the different experiments are given in this appendix. These modes have been part of the modal analysis in chapter 7. First the dry modes for both plates are given, afterwards the modes from the Wet Modal Analysis experiments are visualized. Finally the identified modes for the Regular Wave Impacts are listed. The wet modes are divided in sections containing the FEM and FDD input. FDD input refers to the identified dry FEM modes using the FDD method. The plots contain two rows for each water level. The top row represents the SA predictions while the bottom row depicts the identified mode shapes.

Dry modes – Solid Plate

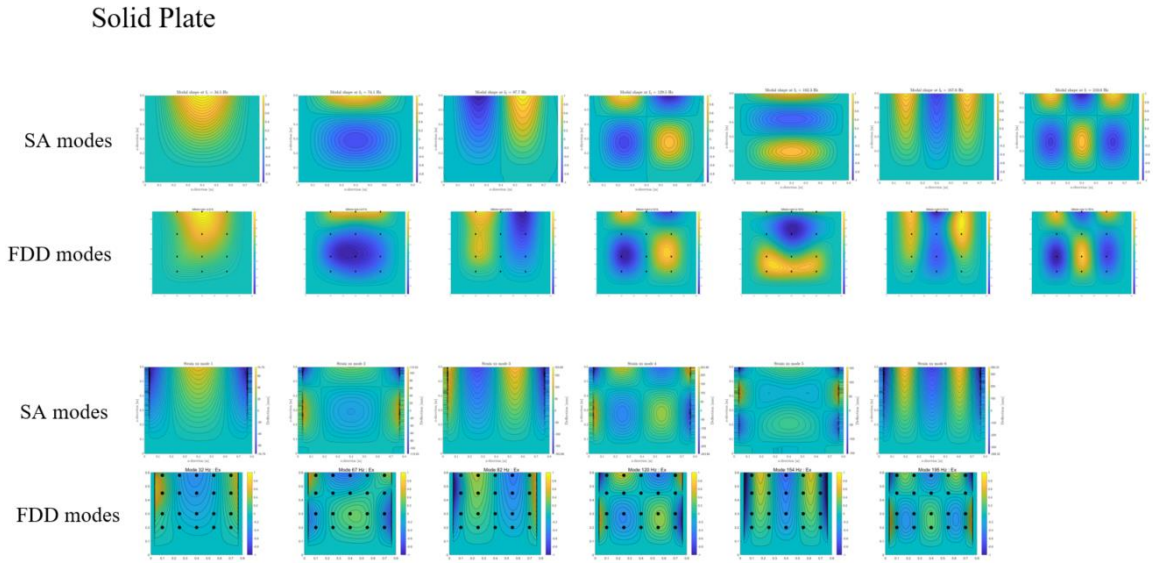

Dry modes – Reinforced Plate

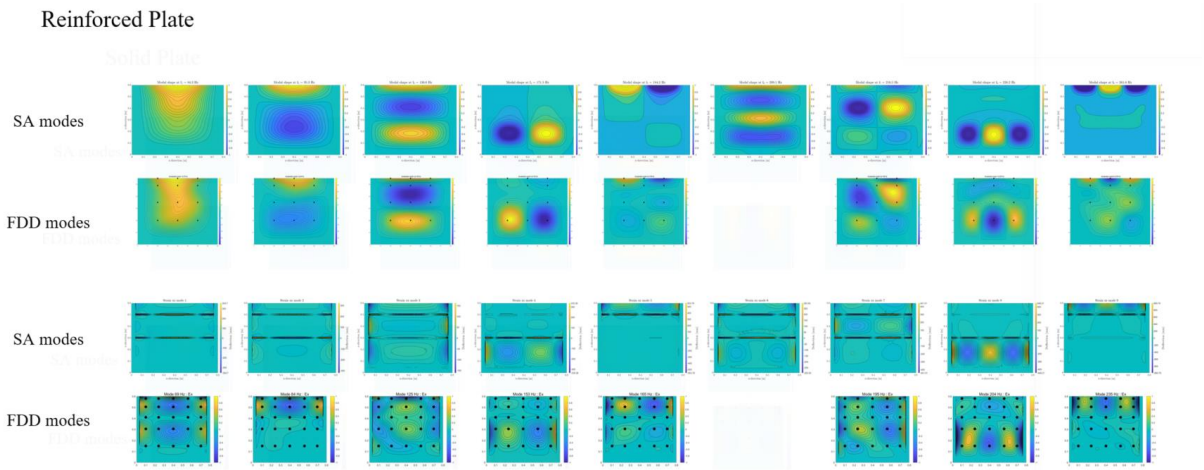

Wet modes – Solid Plate

A division is made between modes that are generated with FEM modes as input and with FDD modes as input. The figures below give both overviews of SA modes and the corresponding

identified mode. The top rows are the SA predictions while the bottom rows are the identified mode shapes.

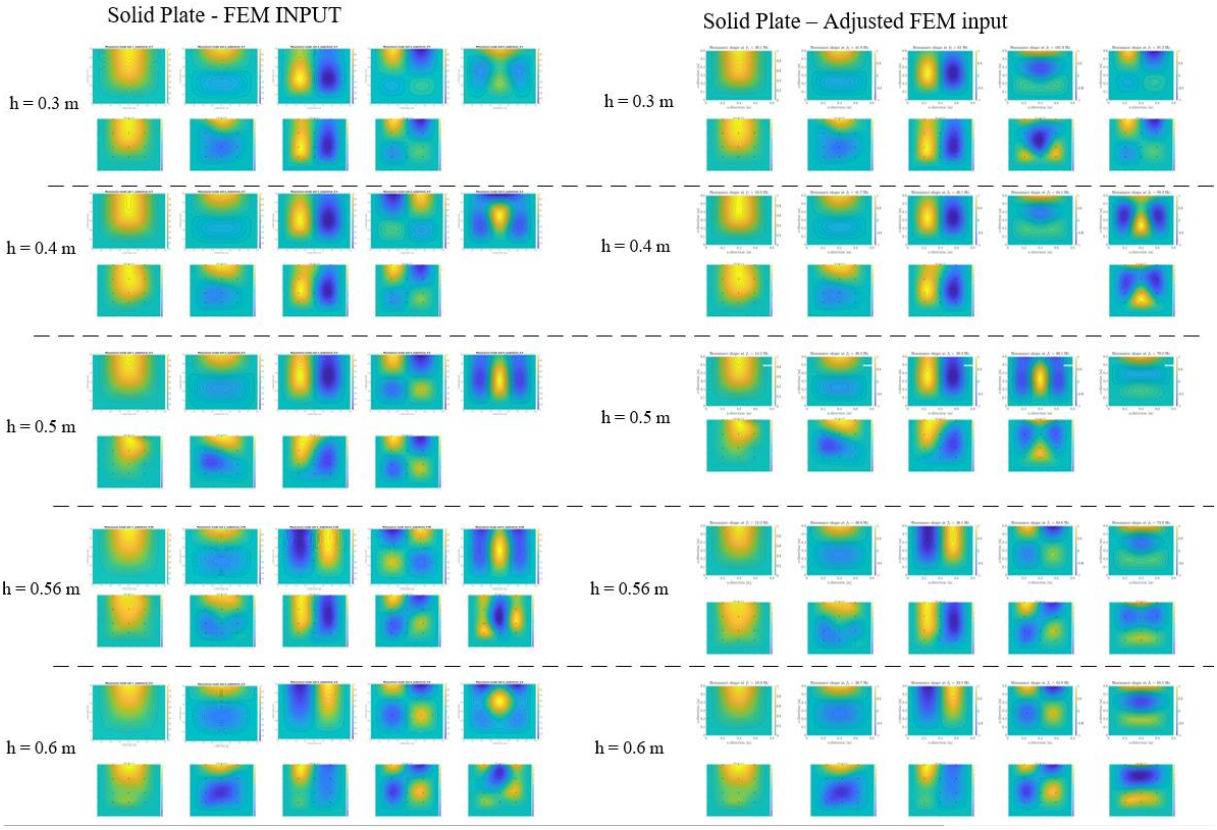

Wet modes – Reinforced Plate

The Reinforced Plate makes used of the strain gauge data. Small amplitudes made it difficult to use the accelerometers. Strain gauges are more precise. The figures below give both overviews of SA modes and the corresponding identified mode. The top rows are the SA predictions while the bottom rows are the identified mode shapes.

FEM input

h = 0.3 m

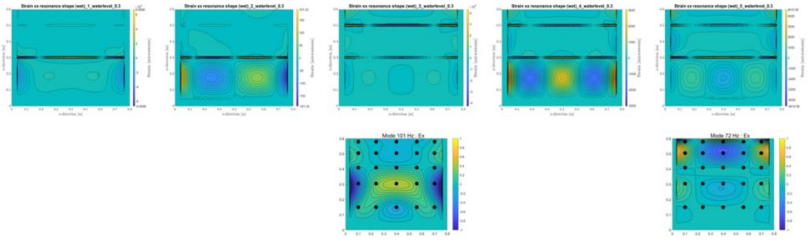

h = 0.4 m

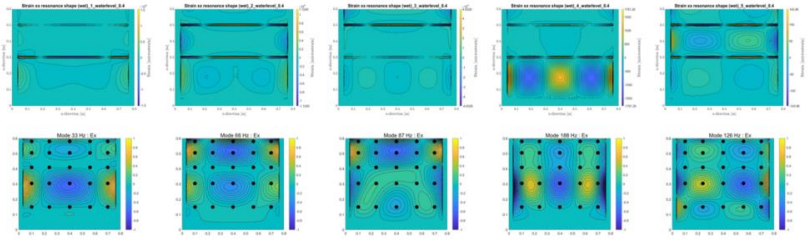

h = 0.5 m

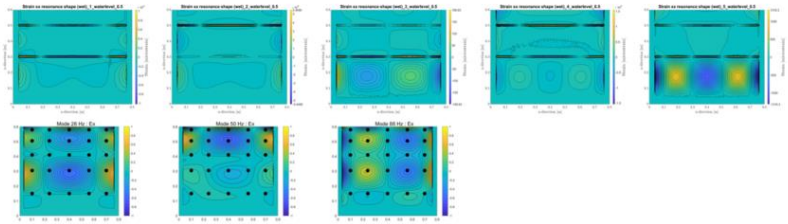

h = 0.56 m

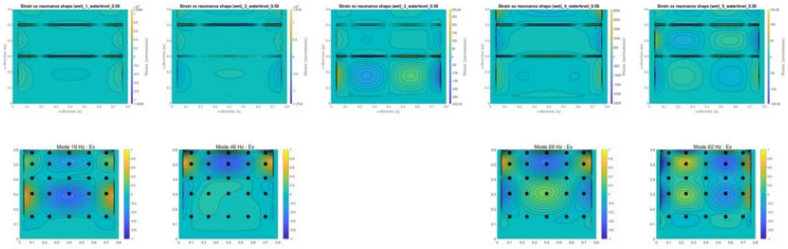

h = 0.6 m

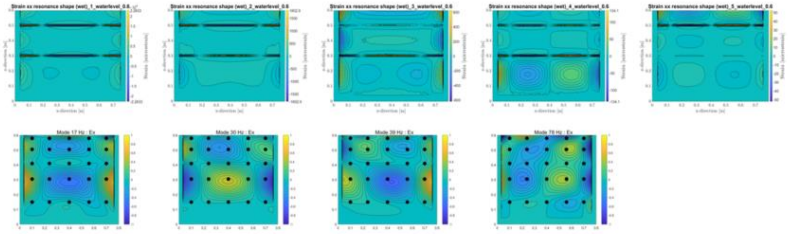

Identified dry FEM input

h = 0.3 m

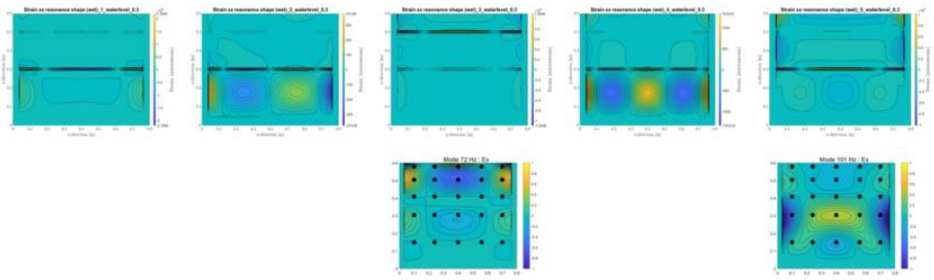

h = 0.4 m

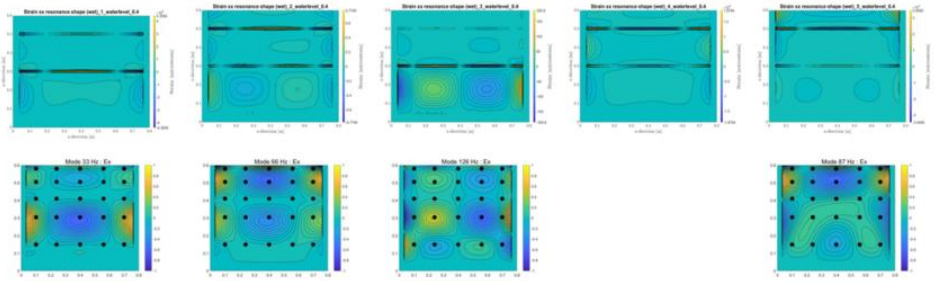

h = 0.5 m

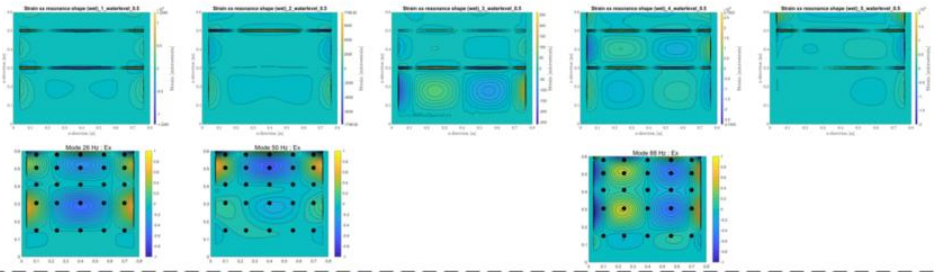

h = 0.56 m

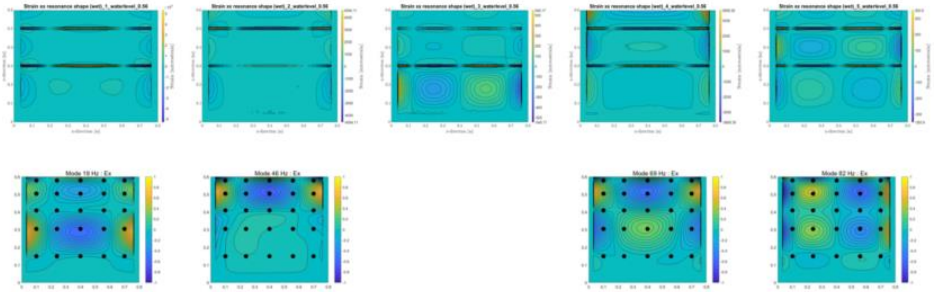

h = 0.6 m

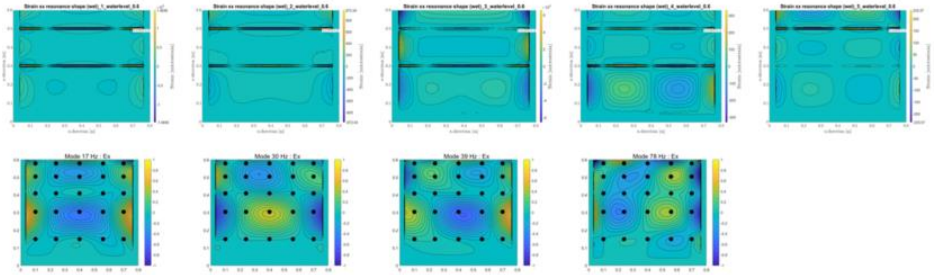

Regular Wave Impact – Reinforced Plate

FEM Input

h = 0.56 m

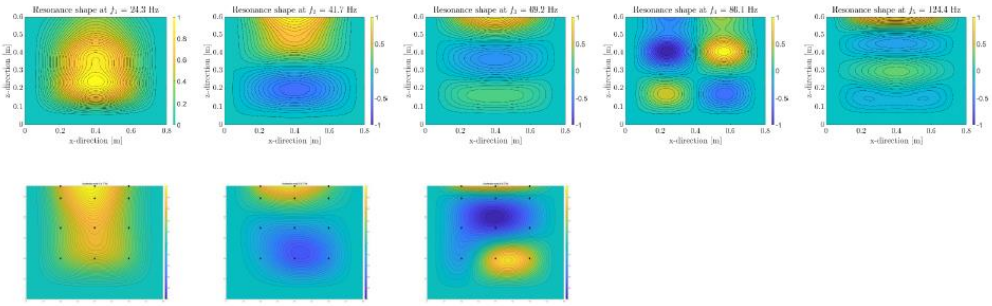

---

h = 0.6 m

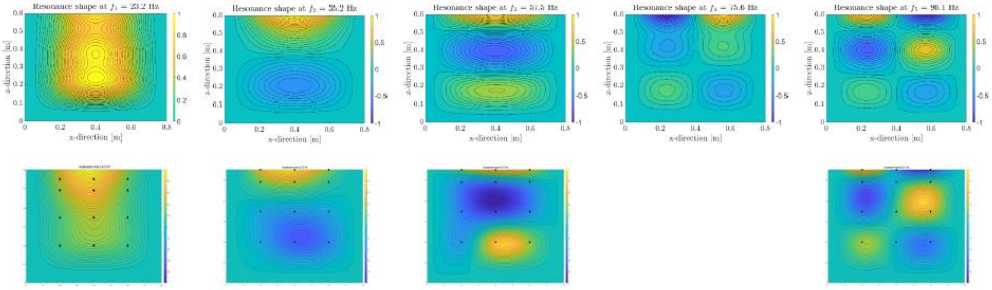

Adjusted FEM Input

h = 0.56 m

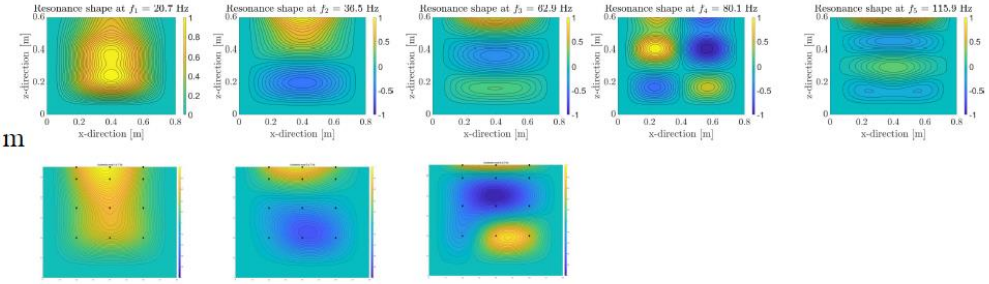

---

h = 0.6 m